Diavik Waste Rock Project: Geochemical and mineralogical investigations of waste-rock weathering

by

Stacey E. S. Hannam

A thesis

presented to the University of Waterloo

in fulfillment of the

thesis requirement for the degree of

Master of Science

in

Earth Sciences

Waterloo, Ontario, Canada, 2012

AUTHOR'S DECLARATION

I hereby declare that I am the sole author of this thesis. This is a true copy of the thesis, including any required final revisions, as accepted by my examiners.

I understand that my thesis may be made electronically available to the public.

Abstract

The oxidation of sulfide minerals in mine waste rock has the potential to generate acidity and contribute sulfate, metals and other trace constituents to drainage. The rate and extent to which this process occurs are dependent upon climactic conditions and the overall hydrologic, geochemical and physical properties of the waste rock. A laboratory and field-based study is currently being conducted at the Diavik Diamond Mine in the Northwest Territories, Canada, which is investigating the evolution of waste rock exposed to subaerial conditions in the continuous permafrost region. Over the course of the mine life, Diavik is expected to generate a stock pile up to 120 Mt of low-sulfide waste-rock composed primarily of granite and granite pegmatite with smaller amounts of biotite schist which occurs as xenoliths, and trace contributions from diabase dykes. Waste rock is segregated based on sulfur content into Type I (< 0.04 wt % S), Type II (0.04-0.08 wt % S) and Type III (> 0.08 wt % S) rock. The Diavik Waste Rock Research Project includes four 2 m by 2 m lysimeter experiments, two each constructed with Type I and Type III waste rock. Also constructed were two well-instrumented, 15 m high test scale waste-rock piles, one composed of Type I and one composed of Type III uncovered waste rock, and one covered test pile based on a reclamation concept which consists of a Type III waste rock core, a 1.5 m glacial till layer, and a 3 m layer of Type I waste rock. In addition, instrumentation was installed in four locations of the operational waste-rock stockpile. The geochemical differences between the Type I and Type III lysimeters and test piles is discussed to compare

the non-acid generating Type I waste rock with the potentially acid-generating Type III. The effluent from the Covered test pile retained the character of the Type III waste-rock core over the course of observation producing slightly acidic drainage, possibly due to a zone of unfrozen till on the crest as a result of heat trace within the test pile. Observations from the geochemistry of the Type III waste rock will also be compared to mineralogical analysis from Type III samples collected during installation of instruments in the full scale waste-rock stockpile. Due to the low concentration of sulfide minerals, advanced techniques such as SEM and synchrotron-based analyses were employed for in-depth characterization of initial sulfide-oxidation products. SEM images and elemental mapping reveal development of reaction rims on many pyrrhotite grains, but lower instances of weathering of pyrite. Distinct zonation of weathering trends between depths within the stockpile was also absent. These observations indicate that the waste rock is in the early weathering stages may not yet be affected by the formation of permafrost. These observations act as a baseline for future studies. Correlations between the mineralogical and geochemical analyses, in addition to future monitoring and continuation of these studies, will assist in understanding the evolution of waste rock stored in a permafrost environment.

Acknowledgements

I would like to thank my supervisor, Dr. David Blowes, for his support and guidance throughout this project, and my committee members, Dr. Carol Ptacek, Dr. Rich Amos, and Dr. Dogan Paktunc for their valuable contributions and assistance. Thanks also to Dr. Leslie Smith from the University of British Columbia and Dr. David Sego from the University of Alberta.

I would like to express my gratitude to the previous graduate students, co-op students and employees involved in the construction phase of this project. Thanks to Lianna Smith, Gord Macdonald and the employees at Diavik for their support of the Test Piles project, supervision and guidance while on site. Thanks to Jeff Bain for his vast contribution both in the field and at the University. I appreciate the support of my fellow graduate students: Brenda Bailey for her assistance, experience and comprehensive guidance in field and laboratory geochemistry; Nate Fretz, for his help on site and hydrogeology knowledge, and Sean Sinclair for his enthusiasm to continue the geochemical studies. My sincerest appreciation to Laura Groza, Joy Hu, Corina McDonald, Julia Jameison-Hanes at the University of Waterloo for their technical and analytical expertise. Thanks to Dr. Blair Gibson and Dr. Matt Lindsay for their tireless hours spent at, and traveling to, the APS, and assistance in data interpretation. This project would not have been possible without the support from the hard-working co-op students, both in the field and at the University of Waterloo.

This research is part of the Diavik Waste Rock Project; a joint research project by the University of Waterloo, the University of British Columbia and the University of Alberta. Funding for this research was provided by Diavik Diamond Mines Inc., the Natural Science and Engineering Research Council of Canada (NSERC) Collaborative Research and Development (CRD) program, a Canadian Foundation for Innovation (CFI) Innovation Fund Award, the Mine Environment Neutral Drainage (MEND) Program, the International Network for Acid Prevention (INAP), and Northern Scientific Training Program. Use of the Advanced Photon Source was supported by the U. S. Department of Energy, Office of Science, Office of Basic Energy Sciences, under Contract No. DE-AC02-06CH11357.

Table of Contents

List of Figures

List of Tables

Chapter 1

Introduction

1.1 Introduction

Mine tailings and waste rock have the potential to produce environmental impacts if not properly managed (Blowes & Jambor 1990; Nordstrom & Alpers 1999; Moncur et al. 2005). Much of the environmental concern arises from exposing sulfide minerals to oxidizing conditions by fragmenting and moving rock, Oxidation of sulfide minerals generates acidity and releases dissolved Fe and SO_4^{2-} to effluent water. The subsequent pH decrease in pore water releases additional metals from sulfide minerals and other minerals. The oxidation of the common sulfide minerals pyrite and pyrrhotite under atmospheric conditions can be described as follows:

Pyrite: $$FeS_2 + \frac{7}{2}O_2 + H_2O \rightarrow Fe^{2+} + 2SO_4^{2-} + 2H^+$$

Pyrrhotite: $$Fe_{(1-x)}S_{(s)} + \left(2 - \frac{1}{2}x\right)O_2 + xH_2O \rightarrow (1-x)Fe^{2+} + SO_4^{2-} + 2xH^+$$

Determining the rate and extent of potential oxidation in mine wastes is thus important for management and remediation planning.

Sulfide oxidation in mine tailings has been well characterized (Blowes & Jambor 1990; Al et al. 1997; Moncur et al. 2005; Gunsinger et al. 2006), but fewer studies have been conducted exploring the processes within mine waste rock (Ritchie 1994; Stromberg &

Banwart 1999; Lefebvre et al. 2001; Sracek et al. 2006). Waste rock is rock of non-economical grade that is removed in order to access ore and can amass in large quantities, especially during open-pit mining. Unlike mine tailings, waste rock is often heterogeneous in grain size and sulfide content (Ritchie 1994). Internal structures and stratigraphy can be created when waste rock is dumped and compacted by haul-truck traffic (Nichol et al. 2005), which makes the flow regime within waste-rock piles difficult to characterize. Infiltrating water has a greater potential to follow preferential flowpaths within heterogeneous waste rock, which limits the ability to predict the rate and extent of water-rock interaction and mineral weathering (Nichol et al. 2005; Smith & Beckie 2003).

Much of the mineral weathering within waste-rock piles occurs within the fine-grained matrix material where water flows at a slower rate, increasing contact time with the more reactive material (Stockwell et al. 2006). When macropore flow occurs through the larger grain-size material, water-rock interaction is limited and solute concentrations within effluent water are lower. These factors, combined with the often large scale of waste-rock dumps, pose challenges when attempting to predict the extent of possible environmental impacts. Studies have been conducted attempting to determine and characterize the contribution from macropore and matrix flow pathways and thus predict the potential quality of effluent waters over time. The difficulties encountered in characterization of the various sites illustrate the need for continued studies into heterogeneous waste-rock responses to subaerial weathering. Examining the geochemistry and internal mineralogical weathering

over time combined with studies of flow regimes can provide more insight into the behaviour of mine waste rock (Sracek et al. 2006).

The research study conducted at the Diavik Diamond Mine (Diavik) (Figure 1) is unique among waste-rock studies in that it is being conducted in the continuous permafrost region of the Northwest Territories, Canada. Assessing the potential impacts of long-term waste-rock storage on surface poses different challenges due to the sensitive receiving environment at this remote mining location. The extreme cold temperatures prevalent in the continuous permafrost region add complexity to the flow regimes within waste rock as flow pathways thaw and become active at different times. Extreme temperatures and the potential for development of permafrost at depth within a waste-rock stockpile also have an effect on the rate of sulfide oxidation and potential for oxidation products to be transported. The comprehensive waste rock study being conducted at Diavik began with construction of the test site in 2005 (Smith et al. 2012a) and will continue to be monitored past 2015.

1.1.1 Site description

Diavik is located 300 km northeast of Yellowknife, Northwest Territories, Canada, in the continuous permafrost region. The mean annual air temperature from 1998 to 2007 was -9.1 °C with maximum averages of 27 °C in July, and minimum averages of -44 °C in January/February (Environment Canada, 2012). Average precipitation in the area for this time period was 280 mm, approximately 60% of which falls as snow (Environment Canada, 2012). The mine infrastructure is located on a 20 km^2 island within Lac de Gras. The

infrastructure consists of two open pits and underground workings to mine three diamondiferous kimberlite pipes. The kimberlite ore is surrounded by Archean country rock which is composed primarily of granite and granite pegmatite (approximately 89%). The remaining fractions are made up of biotite schist (approximately 10%), which occurs as xenoliths within the granite, and diabase dykes that crosscut the area (approximately 1%) (Jambor 1997). The rock has low sulfur content and low neutralization potential. Sulfide minerals occur primarily as trace quantities of pyrite in the granite, and as up to 0.42 wt % S as pyrrhotite in the biotite schist. In order to access the kimberlite ore, the country rock is blasted, hauled and dumped on surface as a waste-rock stockpile which is expected to reach up to 120 Mt and a height of up to 80 m by mine closure (DDMI, 2011). During mining operations, waste rock is tested for sulfur content and segregated into three different types. Type I waste rock is primarily composed of granite and contains < 0.04 wt % S. It is considered non-acid generating and is used for construction throughout the mine site with surplus being dumped in the stockpile (Smith et al. 2012b). Type II waste rock contains 0.04 to 0.08 wt % S, has uncertain acid generating potential, and comprises a small volume within overall waste rock removed. Type III waste rock contains > 0.08 wt % S due to the higher biotite schist content. It is considered potentially acid generating and stockpiled in specific areas of the waste-rock dump.

The Diavik Waste Rock Research Project began in 2005 with the objective of characterizing the responses of stockpiling waste rock subaerially in the continuous

permafrost region. For the study, six 2 m by 2 m lysimeters and three test piles were constructed. The lysimeters are designated Type I and Type III Active Zone Lysimeters (AZLs) and were constructed with Type I and Type III waste rock. The drainage from the AZLs is directed into plexiglass cells for geochemical sampling and flow measurements (Smith et al. 2012a). The three test piles were built on lined pads in order to collect all flow that passes through them. There are two uncovered test piles measuring 50 m by 60 m at the base and 15 m high constructed with the same end-dumping procedures as are used for the operational waste-rock stockpile. The Type I test pile has an average sulfur content of 0.035 wt % S in the <50 mm fraction, at the upper end of the Type I classification. Water is directed through lysimeters at the base of the test pile, and through a basal drain that runs through the centre of the lined test-pile base. The Type III test pile was constructed in a similar manner and has an average sulfur content of 0.053 wt % S in the <50 mm fraction. The base of the test pile is graded to direct water flow to basal drains that run along the north and south edges of the test pile. All of the lysimeter and basal drain flow is collected in dedicated flow-through cells. The third test pile was constructed based on an approved closure concept with a Type III waste rock core, a 1.5 m lower permeability glacial till layer, and a 3 m Type I waste rock cover (DDMI, 2011). The footprint of this test pile is 80 m by 125 m. Flow cells that are open to atmospheric conditions, which are appropriate for use in this system because both the AZLs and test piles have been measured to be fully saturated with atmospheric gases. Changes in oxygen concentration *in situ* therefore do not control

sulfide oxidation rates within the waste rock. A detailed description of the construction and instrumentation of the AZLs and test piles is provided by Smith et al. (2012a).

In 2010, the Diavik Waste Rock Research Project expanded its scope to include studies of the operational waste-rock stockpile. Instrumentation including thermistors, gas sampling ports, permeability measurement devices and unsaturated zone water samplers was installed in three boreholes located on the Upper Type III section of the stockpile in May 2010. Additional boreholes were drilled and instrumented in the summer of 2011 in separate locations of the waste-rock stockpile to gain information about the interior and the batter sections. The ongoing monitoring and expansion of the multi-scale research project will continue to enhance the characterization of waste rock stored subaerially in a permafrost environment (Amos et al. 2009; Bailey et al. 2012; Chi et al. 2012a; Chi et al. 2012b; Fretz et al. 2011; Neuner et al. 2012; Pham et al. 2012; Smith et al. 2012a; Smith et al. 2012b; Smith et al. 2012c).

1.2 Thesis organization and scope

This thesis consists of four chapters. Chapter 2 describes the geochemical trends observed in the test piles and AZLs throughout 2010 and 2011. Chapter 3 discusses the mineralogical and geochemical observations and correlations between waste rock samples from the waste rock dump and the geochemistry of the Type III test pile. Chapter 1 provides an overall introduction, and Chapter 4 summarizes and concludes the contents of this thesis.

1.3 Figures

Figure 1-1: Location of the Diavik Diamond Mine site in the Northwest Territories Canada

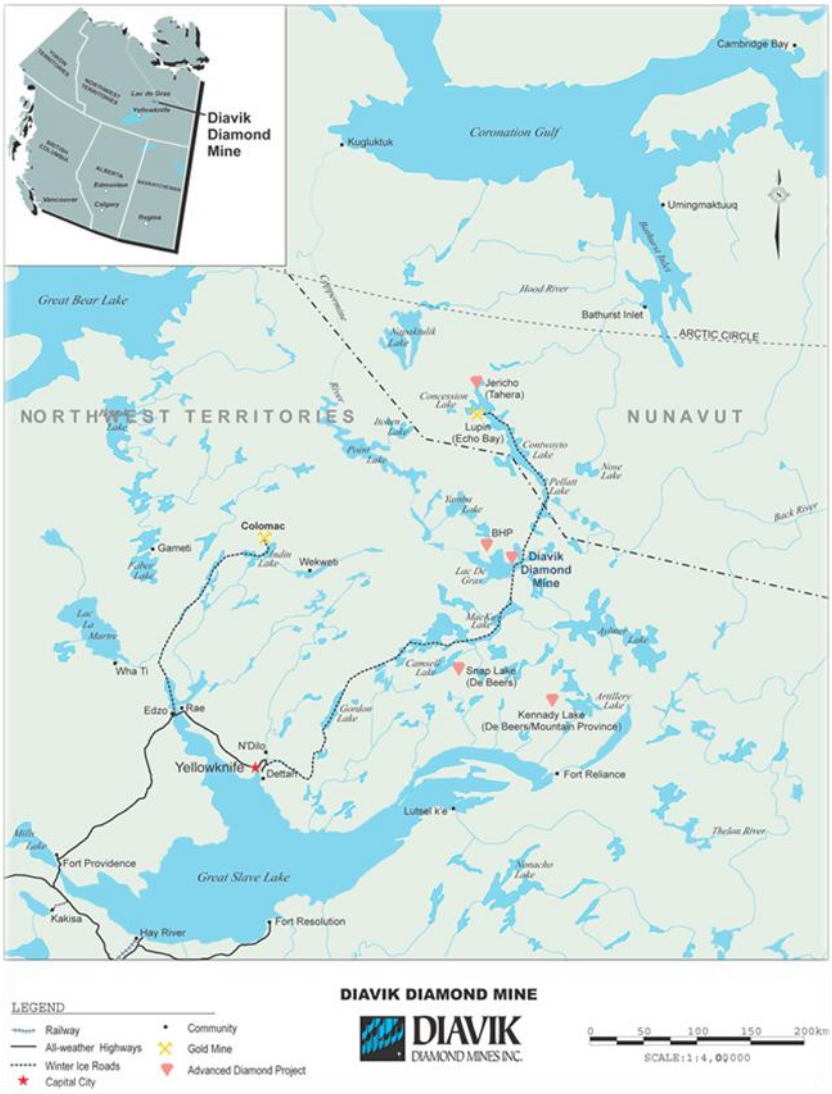

Chapter 2

2010-2011 Geochemical trends in experimental waste rock test piles at the Diavik Diamond Mine

2.1 Introduction

The oxidation of sulfide minerals within mine waste rock has the potential to generate acidic drainage water with elevated concentrations of dissolved metals. If not managed properly, there can be detrimental effects on the surrounding environment. Several studies have examined the impacts of sulfide-mineral weathering from mine wastes in temperate climates (Blowes & Jambor 1990; Hudson-Edwards, Schell & Macklin 1999; Nordstrom & Alpers 1999; Johnson et al. 2000; Espana et al. 2005; Moncur et al. 2005; Gunsinger et al. 2006); however, fewer have been conducted regarding mine sites in continuous permafrost regions. As mining activities in the North continue to expand, it is important to understand the implications of subaerial waste rock storage to develop effective closure plans and remediation strategies.

The waste rock at the Diavik Diamond Mine (Diavik) contains a low concentration of sulfide minerals; however, this rock also lacks appreciable concentrations of carbonate minerals. As a consequence, the acid generating potential (AP) and the acid neutralization

potential (NP) of the Diavik waste rock are similar. When this rock is exposed to oxygen and water, there is potential for some of the Diavik waste rock to generate sufficient acidity to exhaust buffering capacity, resulting in the release of lower pH effluent with high dissolved metal concentrations.

Also of interest in this study is the behaviour of chemicals related to blasting of the waste rock. Previous studies conducted at Diavik focused on the construction of three test piles (Smith et al. 2012a), particle size and sulfur characterization (Smith et al. 2012b; Chi et al. 2012), geochemistry (Smith et al. 2012c; Bailey et al. 2012; Bailey 2012), thermal characteristics of the test piles (Pham et al. 2012); wind-induced gas transport (Amos et al. 2009; Chi et al. 2012), test pile hydrology (Neuner et al. 2012), and microbiology (Bailey 2012). Smith et al. (2012c) described the initial geochemistry of the test piles in 2007, and Bailey et al. (2012) and Bailey (2012) described the geochemical evolution of the test piles through 2010. This chapter describes the continuation of geochemical studies into 2010 and 2011 to further examine the influence of sulfide oxidation and the presence of blasting agents on the test pile effluent.

2.1.1 Site description and history

Diavik is located 300 km northeast of Yellowknife, Northwest Territories, Canada, in the continuous permafrost region (Figure 2-1). The mine infrastructure, which was constructed on a 20 km^2 island in the oligotrophic lake Lac de Gras, consists of two open pits and underground workings to mine three kimberlite pipes. Before ore was mined from the open

pits, the surrounding country rock was removed. The kimberlite ore deposits are hosted in Archean country rock primarily composed of granite and granite pegmatite, which include xenoliths of biotite schist and minor amounts of diabase, present as dykes that crosscut the area. The excavated country rock is stockpiled on surface in a waste-rock pile which is expected to reach up to 120 Mt at mine closure.The majority of the sulfide minerals are hosted in the biotite schist xenoliths which occur within the granite (Jambor 1997; Smith 2009). Because the biotite schist is intimately mixed with the granite, waste rock at Diavik is separated into three categories based on total sulfur content. Type I waste rock is primarily composed of granite and granite pegmatite and has a nominal sulfur content of < 0.04 wt % S. Type I waste rock is considered non-acid generating and contains minimal sulfide minerals generally as small grains of pyrite (Jambor 1997; Smith et al. 2012b). Type II waste rock comprises a smaller portion of the total waste rock on site (< 5%) and has a target sulfur content of 0.04-0.08 wt % S. The sulfide content is due to the presence of small amounts of biotite schist and the waste rock has low acid generating potential (Smith et al. 2012a). Type III waste rock contains a greater proportion of biotite schist, has a target sulfur content of > 0.08 wt % S, and is considered potentially acid generating. As the carbonate content of all types of waste rock is very low, the higher S content Type III waste rock requires additional precautions and monitoring when stockpiled on surface (DDMI 2011; Smith et al. 2012b).

A large-scale field-based study is being conducted at Diavik, with complementary laboratory testing conducted at the University of Waterloo, to study the effects of stockpiling waste rock on the Earth's surface under continuous permafrost conditions and for a changing climate. Three test piles have been constructed on site and fully instrumented for physical and geochemical characterization (Smith et al. 2012a) (Figure 2.2) . The Type I and Type III test piles measure 50 m by 60 m at the base and are 15 m high with a slope at the angle of repose of the waste rock (38°) when placed using the same methods used on the full-scale waste-rock stockpile (Smith et al. 2012a). The Type I test pile has an average S content of 0.35 wt % S in the <50 mm fraction, within the target S content. The Type III test pile has an average sulfur content of 0.053 wt % S in the <50 mm fraction, which is less than the operational target of > 0.08 wt % S. A third test pile was constructed based on the closure concept for Type III waste rock and has a Type III core (average 0.082 wt % S in the <50 mm fraction) with slopes contoured to 18°, a 1.5 m till layer and a 3 m layer of Type I waste rock (DDMI 2011) (Figure 2-2). Most of the water flowing through the test piles reports to basal drains which collect water from the lined base of each test pile. Lysimeters were also installed within each test pile to collect water reporting through discrete areas, as opposed to bulk pile flow (Smith et al. 2012a). In addition to the test piles, six 2 m by 2 m Active Zone Lysimeters (AZL) were constructed to focus on examination of the active zone of the waste rock stockpiles. Two were filled with Type I waste rock, two with Type III waste rock on site (Figure 2-2) and two were filled with Type I waste rock and capped with 1.5 m of till and 3 m of Type I waste rock. These covered AZLs have not reported water.

This chapter examines the geochemistry of the effluent from the four AZLs and from the basal drains of the three test piles over the course of 2010 and 2011, four and five years after construction. The AZLs are designated 'Type I East,' 'Type I West,' Type III East,' and 'Type III West' which indicate the waste rock type and location of each lysimeter. The Type I and Covered test pile geochemistry was interpreted from their respective basal drains. The Type III test pile has two basal drains that run along the north and south edges designated the Type III North and South basal drains. Previous geochemical studies span the years from the first flow post-construction in 2007 to 2010 (Smith et al. 2012c; Bailey et al. 2012; Bailey 2012).

2.2 Methods

2.2.1 Geochemical sampling and analysis

Samples for geochemical analysis were collected from dedicated sampling cells at each location. Samples from basal lysimeter locations and the Type III North basal drain were collected from approximately 500 mL plexiglass flow-through cells. Samples from the Type I, Type III South and Covered test pile basal drains, and the AZLs were collected from high-flow plexiglass cells that were in contact with the atmosphere. These larger cells were installed between June 2010 and May 2011 to improve the quality of the flow data by preventing air locks and water leaks.

Water samples were collected from dedicated 6.35 mm PVC tubing using a clean 60 mL syringe triple rinsed with sample water and dispensed into triple-rinsed 60 mL HDPE wide-mouth bottles. Off-site analysis of total cations, environmental isotopes and microbiology was conducted on unfiltered samples. Samples for measurement of the concentrations of dissolved cations, anions, nutrients and nitrogen isotopes were immediately filtered through 0.45 µm cellulose syringe filters and dispensed into sample bottles. Samples for cation measurements were preserved with analytical grade HNO_3 and nutrients samples with analytical grade H_2SO_4 to a pH less than two. All samples were refrigerated at 4°C until analysis, with the exception of nitrogen isotopes, which were kept frozen.

Immediately after sampling, pH, Eh, electrical conductivity and temperature were measured on unfiltered, unpreserved samples. The pH was measured with a combination electrode (Orion ROSS Ultra ® 8156, Thermo Scientific, USA) which was calibrated using three standard buffer solutions encompassing the anticipated pH range of the sample (pH 1.68, 4.0, 7.0,10). The Eh was measured with the Thermo Orion platinum redox electrode (Orion 96-78; Thermo Scientific, USA). Before each use, the Eh of standard Zobell (Nordstrom 1977) and Light's (Light 1972) solutions was measured, and sample measurements were corrected based on these values within their respective calibration curves. Conductivity and temperature measurements were taken with an Orion 3-Star Plus Conductivity Meter calibrated with standard conductivity solutions spanning the sample range. Field alkalinity was determined on samples filtered through 0.45 µm cellulose syringe

filters using a Hach Digital Titrator with standardized 0.16 N H_2SO_4 and bromcresol green/methyl red indicator. Determination of NH_3-N (Hach method 10031), H_2S (Hach method 8131), Fe^{2+} (Hach method 8146) and PO_4^{3-} (Hach method 8048) was measured on filtered samples filled full and sealed in bottles using a Hach DR/8400 Spectrophotometer at a laboratory on site shortly after sampling.

Samples collected for determination of dissolved cations and anions were analyzed at the University of Waterloo, Waterloo, Ontario. Dissolved concentrations of Ca, K, Mg, Na and Si were determined using a Thermo Scientific ICP-OES (iCAP 6000, Thermo Scientific, USA) and Al, As, Ba, Be, Cd, Co, Cr, Cu, Fe, Mn, Mo, Ni, Pb, Sb, Se, Sr, Ti, U, and Zn with a Thermo Instruments X-Series ICP-MS (X-Series 2, Thermo Scientific, USA). Concentrations of the anions Br^-, Cl^-, NO_2^-, NO_3^-, and SO_4^{2-} were determined with ion chromatography (IC DX600; Dionex, USA). Quality control and accuracy were checked throughout the sampling and analysis protocol with field and instrument blanks and duplicates, and analysis of standards over the course of instrument operation.

2.2.2 Geochemical modeling

Geochemical equilibrium modeling was performed to determine saturation indices of discrete mineral phases based on water samples from the test pile basal drains and AZLs. The equilibrium/mass-transfer software PHREEQCI was used with a database modified from WATEQ4F (Ball & Nordstrom 1991), which included addition of solubility data for

lepidocrocite sourced from the MINTEQ.V4 database. Alkalinity was input in units of mg L^{-1} $CaCO_3$, where applicable and measured Eh values were converted to pe.

2.3 Results and discussion

2.3.1 Active zone lysimeter geochemistry

2.3.1.1 Flush of blasting agents

Blasting at Diavik is conducted using a combination of emulsion (70-80%), ammonium nitrate and fuel oil (ANFO; 20-30%), and accelerators containing perchlorate. Use of these explosives releases nitrogen to the environment through drainage water in the form of NH_4^+ and NO_3^- (Pommen 1983). Ammonia is present as NH_3 or NH_4^+ depending on the pH, with higher pH favouring the formation of NH_3. Under aerobic conditions, NH_3 can be bacterially oxidized to NO_2^- and subsequently NO_3^- by the Nitrosomonas and Nitrobacter groups of bacteria. NO_2^- is a relatively short-lived unstable intermediate, and in contrast, NO_3^- is stable and soluble under aerobic conditions (Sawyer & McCarty 1967). Additional dissolved constituents derived from the blasting residuals include perchlorate and Cl^- released from oxidation and dissolution of accelerators.

The behaviour of blasting residuals in the AZLs at Diavik from first flush to near depletion (2007-2009) has been described by Bailey et al. (2012). Nitrogen species released due to blasting with the explosives used at Diavik include NH_3, NO_3^-, and NO_2^-. Concentrations of NH_3 and NO_2^- in the Type I AZLs remained close to or below detection for

the majority of 2010 and 2011. Concentrations of NO_2^- in the Type I East AZL briefly reached levels between 0.39-0.82 mg L^{-1} NO_2^--N in July and October 2010. In the Type I West, NO_2^- reached concentrations 0.32-0.56 mg L^{-1} NO_2^--N in July and October 2010, then again in July and August 2011. Concentrations of NO_3^- in the Type I AZLs were higher than the other nitrogen species, but considerably lower than observed in previous years as the blasting residuals were initially flushed from the AZLs (Bailey et al. 2012). Concentrations of NO_3^- in the Type I East AZL remained between 32-48 mg L^{-1} NO_3^--N early in 2010 with a rapid increase to 220 mg L^{-1} NO_3^--N at the end of July as flow rates declined. Concentrations of NO_3^- remained < 38 mg L^{-1} NO_3^--N during the second flow event in 2010 and < 18 mg L^{-1} NO_3^--N throughout 2011. In the Type I West AZL, NO_3^- concentrations peaked in July of 2010 at 120 mg L^{-1} NO_3^--N before decreasing to below 30 mg L^{-1} NO_3^--N for the remainder of 2010. In 2011, NO_3^- peaked only briefly at 47 mg L^{-1} NO_3^--N and otherwise remained below 28 mg L^{-1} NO_3^--N (Figure 2-3).

The Type III AZLs showed slightly higher concentrations of NH_3 throughout 2010 and 2011than the Type I AZLs, generally confined to the first flow event from mid-June to August 2010. Both Type III AZLs began with higher concentrations (East 1.3 mg L^{-1} NH_3-N; West 1.8 mg L^{-1} NH_3-N) before decreasing gradually then reaching their highest concentrations as flow slowed in August (East 2.3 mg L^{-1} NH_3-N, West 4.3 mg L^{-1} NH_3-N). For the remainder of 2010 and 2011, NH_3 concentrations of both Type III AZLs generally remained below 0.6 mg L^{-1} NH_3-N with single measurements reaching concentrations up to

1.4 mg L^{-1} NH_3-N. Significant concentrations of NO_3^- were detected in the Type III AZLs throughout 2010 reaching peak concentrations in the East lysimeter of 97 mg L^{-1} NO_3^--N at the end of July, and the West reaching 115-120 mg L^{-1} NO_3^--N in June and August 2010. Concentrations of both Type III AZLs remained < 35 mg L^{-1} NO_3^--N for the remainder of 2010, and < 22 mg L^{-1} NO_3^--N in 2011. NO_2^- was only detected briefly in the Type III East AZL when concentrations reached 2.2 mg L^{-1} NO_2^--N at the end of September 2010 (Figure 2-3).

Chloride is released upon blasting of the waste rock from oxidation of the blasting caps used as accelerators for the explosives. Rapid oxidation releases perchlorate which then breaks down into Cl^-. The concentrations of Cl^- can be used as a tracer to determine when the first flush of blasting residuals has passed through the AZLs (Bailey et al. 2012). Between 2007 and 2009, Bailey et al. (2012) observed Cl^- concentrations derived from blasting residuals in the AZL effluent of up to 370 mg L^{-1}. By 2010, almost all traces of Cl^- had been flushed from the Type I AZLs. Concentrations in 2010 were consistently < 25 mg L^{-1} with point measurements reaching 40 mg L^{-1}, and remained < 15 mg L^{-1} in 2011. Concentrations of Cl^- in the Type III AZLs were higher in 2010; the Cl^- concentration in the East AZL reached 310 mg L^{-1} at the end of flow in July 2010 and Cl^- in the West AZL reached maxima of 350-360 mg L^{-1} in June and August 2010. The Cl^- concentration in Type III East AZL effluent remained below 40 mg L^{-1} for the remainder of 2010 and 2011. The Cl^- concentration in the effluent from the Type III West AZL was generally below 80 mg L^{-1} and

decreased to 8.5 mg L^{-1} by the end of flow in October 2011 (Figure 2-3). These results suggest that the remaining traces of blasting residuals have been almost entirely flushed from the system, with the possible exception of future contributions from flowpaths in the AZLs which remain unexposed to water.

2.3.1.2 pH and alkalinity

The waste rock deposited into the two Type I AZLs is considered non-acid generating with an average sulfur content of 0.014 wt. % S in the <50 mm fraction (Bailey 2012). The pH and alkalinity measurements throughout 2010 and 2011 reflect this characteristic. Alkalinity consistently remains measureable for both lysimeters, with the Type I East generally showing values < 20 mg L^{-1} $CaCO_3$, and the Type I West varying between 30-80 mg L^{-1} $CaCO_3$. Trends in alkalinity in the Type I AZLs are generally consistent with measured pH. The higher-alkalinity Type I West AZL exhibits pH values between 7.5 and 8.5, with highest pH values generally occurring at the start of flow events then decreasing steadily as flow slows and water has experienced longer residence time in contact with oxidizing sulfide minerals. The Type I East lysimeter follows similar trends, but at a lower pH with values decreasing within the range of pH 7.3 to 5.8 (Figure 2-4).

The Type III AZLs contain rock with a target sulfur content of > 0.08 wt. % S which is considered potentially acid generating, however measurements of the sulfur content of the rock placed in the Type III AZLs indicate a content of 0.035 wt % S in the <50 mm fraction and are considered potentially acid generating (Smith et al. 2012b). Alkalinity is rarely

measureable throughout 2010 and 2011 consistent with the lower pH of both lysimeters which remained at levels between pH 2.8-3.7 (Figure 2-4). The pH and alkalinity behaviour of the Type III AZLs show that the weathering of sulfide minerals, principally pyrrhotite, in the biotite schist component of the Type III waste rock has the potential to generate lower pH drainage. Although the sulfur content of the rock is low overall, the lack of significant carbonate minerals limits the capacity to buffer the effluent pH at the circum-neutral levels seen in the Type I AZLs.

2.3.1.3 Sulfide oxidation and dissolved metals

The mass of dissolved SO_4^{2-} contained in the effluent of the Type I AZLs was lower than that of the Type III AZLs over the course of both the 2010 and 2011 field seasons. The effluent SO_4^{2-} concentration from each lysimeter rarely exceeded 600 mg L^{-1} SO_4^{2-} and generally remained in the range of 100-300 mg L^{-1} SO_4^{2-} throughout 2010 and 2011. Iron concentrations remain < 0.068 mg L^{-1} increasing to maximum levels as flow terminates at the end of each field season. Metals commonly associated with sulfide mineral oxidation also remain at low concentrations throughout the 2010 and 2011 field seasons, including Cu (max. 0.034 mg L^{-1}), Ni (max 0.38 mg L^{-1}), Co (max 0.071 mg L^{-1}), Zn (max 0.084 mg L^{-1}), and Cd (max 1.8 µg L^{-1}). These trends are consistent with the low sulfide content of the Type I rock, and the net acid consuming nature of this rock.

Concentrations of major cations (Ca, Mg, Na, K) follow very similar trends throughout 2010 and 2011; generally higher at lower pH and varying minimally within a

small concentration range. In 2010-2011, concentrations of the major ions are greatest early in the year and decrease progressively, with the lowest concentrations observed at the end of flow in November. A notable spike in concentration occurred in July/August 2010 at the end of the first flow event as flow rates decreased substantially. In the Type I East AZL, concentrations of the major ions show an overall decreasing trend over the course of each field season. The highest concentrations of Ca remain just below 100 mg L^{-1} and decrease to a minimum of 16 mg L^{-1} in November 2011. The concentrations of both Na and Mg decrease from approximately 50 mg L^{-1} to 10 mg L^{-1} from the start of flow in 2010 to November 2011. Both Na and Mg increased sharply to approximately 300 mg L^{-1} near the end of July 2010 as flow rates slow significantly. Concentrations of K are the lowest in the group of major cations, generally remaining within the range of 15-30 mg L^{-1} and following similar trends to Na and Mg, with a maximum concentration of 180 mg L^{-1} at the end of July 2010. Major cation concentrations in the Type I West AZL remain at similar levels and follow nearly the same trends as the East AZL. A deviation occurs in June of 2010 where concentrations increase steadily to maxima for Ca (220 mg L^{-1}), Mg (110 mg L^{-1}), Na (80 mg L^{-1}) and K (80 mg L^{-1}) at the end of June before decreasing and returning to follow the trend of the Type I East AZL (Figure 2-4).

The Type III AZLs have consistently higher concentrations of dissolved metals than the Type I AZLs. This difference is due to the higher sulfur content in the Type III waste rock, with a neutralization potential that is similar to the Type I rock, which results in a lower

effluent pH, which promotes dissolution of many metals. The SO_4^{2-} concentrations are higher than in the Type I AZLs, generally increasing with decreasing pH, with the exception of increases in SO_4^{2-} concentrations that occur at the end of the first 2010 flow event in August. Furthermore, the SO_4^{2-} concentrations are consistently higher in the Type III West AZL than in the Type III East AZL. The West AZL also has the lowest pH of the two Type III AZLs. The SO_4^{2-} concentrations in the Type III West AZL remain in the range of 2000-4000 mg L^{-1} throughout 2010, with the exception of a maximum of 7000 mg L^{-1} in late August 2010. In 2011, concentrations followed a decreasing trend within the range of 4800-1200 mg L^{-1}. In the Type III East AZL, SO_4^{2-} concentrations decrease throughout 2010 from 2400 to 630 mg L^{-1} with a maximum of 8600 mg L^{-1} at the end of the first flow event in August 2010. In 2011, SO_4^{2-} concentrations decreased relatively steadily from 3500 mg L^{-1} to 560 mg L^{-1} (Figure 2-4).

Concentrations of sulfide oxidation products in the effluent of the Type III AZLs follow the trends that are similar to the SO_4^{2-} concentrations. In general, concentrations of Fe, Cu, Ni, Co, Zn and Cd are higher in the Type III West AZL. In the Type III East AZL, concentrations of Fe were 3.1 mg L^{-1} in June of 2010 before decreasing steadily to 0.077 mg L^{-1} at the beginning of August, then increasing to 1.2 mg L^{-1} Fe as flow rates decreased. The Fe concentrations during the second flow event in 2010 and throughout all of 2011 remained between 0.052-0.81 mg L^{-1}. In the Type III West AZL effluent, the Fe concentration at the start of flow in 2010 was 0.73 mg L^{-1}, and increased in July 2010 to

11 mg L^{-1}, followed by a decrease to 0.13-0.62 mg L^{-1} for the remainder of 2010. In 2011, Fe concentrations remained between 0.12-1.0 mg L^{-1}, with the exception of a brief period in August where a maximum of 2.6 mg L^{-1} Fe was reached.

PHREEQCI equilibrium calculations indicate that the effluent of the Type III East AZL was supersaturated with respect to jarosite early in 2010. Later in 2010 the saturation index values indicate a steady decrease to undersaturation beginning at the end of June, and for the remainder of 2010. In 2011, the effluent was undersaturated with respect to jarosite for the majority of the flow season, with the exception of a brief period at the start of flow in June 2011 when saturation with respect to jarosite was attained. The Type III West AZL followed similar trends, however calculations indicate that saturation with respect to jarosite also was attained at the end of the first flow event in August 2010 when the pH and SO_4^{2-} concentrations both increased. Saturation with respect to jarosite was rarely observed during 2011. Both Type III AZLs remained undersaturated with respect to ferrihydrite and supersaturated with respect to goethite throughout all of 2010 and 2011 (Figure 2-6). These trends in saturation indices suggest that precipitation and dissolution of secondary Fe phases affect dissolved concentrations of Fe.

Concentrations of Cu, Ni, Co, Zn and Cd in both Type III AZLs followed trends that were consistent with the SO_4^{2-} concentrations. Dissolved Cu in the drainage is derived from traces of chalcopyrite in the biotite schist. In the Type III East AZL, peaks in Cu concentrations occurred at the end of June 2010 (2.6 mg L^{-1}) and at the end of July 2010

(7.9 mg L^{-1}). Dissolved Cu concentrations decreased from 2.0 to 0.89 mg L^{-1} throughout October 2010. In 2011, Cu concentrations ranged from 0.90 to 4.4 mg L^{-1} with the maximum concentrations observed in August. Dissolved Cu concentrations were higher in the Type III West AZL, with a maximum concentration of 9.5 mg L^{-1} observed in August 2010 which then decreased from 3.3 mg L^{-1} to 1.8 mg L^{-1} in October. In 2011, Cu concentrations followed the same trend with maximum concentrations observed in August in the range of 1.4 to 4.3 mg L^{-1} (Figure 2-4). Both Type III AZLs remained undersaturated with respect to the secondary Cu phases $Cu(OH)_2$, $CuCO_3$, azurite, brochantite and malachite throughout 2010 and 2011, suggesting that precipitation of these secondary mineral does not control Cu concentrations.

Concentrations of Ni and Co were strongly correlated in both Type III AZLs, with an average Ni:Co ratio of 4.7:1 (σ=0.66, n=117). Both Ni and Co are present in the pyrrhotite at Diavik at an approximate 4:1 ratio, as determined by microprobe analyses during baseline mineralogical investigations (Jambor 1997). Dissolved Ni concentrations in the Type III East AZL reached maxima of 29 mg L^{-1} at the end of June, and 86 mg L^{-1} at the end of July 2010, and then decreased in October from 12 mg L^{-1} to 8.4 mg L^{-1}. In 2011, the dissolved Ni concentration gradually increased to a maximum concentration of 41 mg L^{-1} in August, then decreased to 5.6 mg L^{-1}. Dissolved Co concentrations reached 6.5 mg L^{-1} at the end of June 2010 and 19 mg L^{-1} at the end of July, and then decreased from 3.3 mg L^{-1} to 1.1 mg L^{-1} in October. In 2011, Co increased gradually to 8.4 mg L^{-1} in June before decreasing to

1.2 mg L^{-1} in October. Dissolved Ni in the Type III West AZL effluent at the beginning of the 2010 season was 58 mg L^{-1}, and decreased to 17 mg L^{-1} at the end of June, before increasing at the end of July to 68 mg L^{-1}. In October 2010, concentrations decreased steadily from 26 mg L^{-1} to 10 mg L^{-1}. In 2011, trends were similar to the Type III East AZL, peaking at 38 mg L^{-1} at the end of July and decreasing steadily to 8.1 mg L^{-1} at the end of October. In the Type III West AZL, Co concentrations reached a maximum of 15 mg L^{-1} in June, before decreasing rapidly to 3.6 mg L^{-1} then increasing to 15 mg L^{-1} again at the end of July 2010. In October, concentrations gradually dropped from 5.4 mg L^{-1} to 2.0 mg L^{-1}. In 2011, concentrations peaked in June at 6.9 mg L^{-1} before decreasing gradually to 1.8 mg L^{-1} at the end of October (Figure 2-4). PHREEQCI equilibrium modeling does not show secondary mineral controls on Ni and Co in the Type III AZLs.

Traces of sphalerite have been observed in previous mineralogical studies of the biotite schist . Oxidation and dissolution of sphalerite contributes dissolved concentrations of Zn and Cd in the Type III AZL effluent. Trace amounts of Cd exist in the sphalerite lattice. Dissolved Zn and Cd concentrations in the Type III AZL effluent had an average correlation ratio of 234:1 (σ=40, n=117), Zn:Cd. Concentrations of Zn in the Type III East AZL drainage increased at the end of June (20 mg L^{-1}) and end of July 2010 (50 mg L^{-1}), then decreased gradually from 8.7 mg L^{-1} to 3.7 mg L^{-1} in October. In 2011, concentrations peaked at 22 mg L^{-1} in June before gradually falling to 4.0 mg L^{-1} in October. Dissolved Zn concentrations in the Type III West AZL reached 42 mg L^{-1} in June and 43 mg L^{-1} in August

2010, and then decreased from 17 mg L^{-1} to 6.7 mg L^{-1} in October. In 2011, Zn concentrations peaked at the end of July at 23 mg L^{-1} before decreasing gradually to 5.0 mg L^{-1} at the end of October. The dissolved Cd concentrations in both Type III AZLs are on the order of µg L^{-1}, with the Type III East concentrations peaking at the end of June (72 µg L^{-1}) and July 2010 (255 µg L^{-1}) then decreasing in October from 50 µg L^{-1} to 19 µg L^{-1}. In 2011, concentrations gradually increased to a maximum of 84 µg L^{-1} before decreasing to 18 µg L^{-1} at the end of October. Dissolved Cd from the Type III West AZL reach maxima of 167 µg L^{-1} in June and 184 µg L^{-1} at the end of July 2010 then decreased from 70 µg L^{-1} to 30 µg L^{-1} in October. In 2011, dissolved Cd concentration increased to 93 µg L^{-1} at the end of July and gradually decreased to 20 µg L^{-1} in October (Figure 2-4). PHREEQCI calculations indicate the effluent of the Type III AZLs is undersaturated with respect to the secondary minerals included in the WATEQ4F database, suggesting that precipitation of these phases does not limit Zn and Cd concentrations.

Concentrations of the major cations (Ca, Mg, Na, K) in the Type III AZLs again showed common trends. In the Type III East AZL, Ca concentrations are highest at the beginning of the each flow season, reaching 360 mg L^{-1} in 2010 and 570 mg L^{-1} in 2011 and lowest as the season ends in October falling to approximately 55 mg L^{-1} both years. Dissolved Ca concentrations in the Type III West AZL peaked at the start of the flow season in June 2010 (505 mg L^{-1}) and later in the 2011 season at the end of July (580 mg L^{-1}). Minimum concentrations of Ca ranged between 130 and 150 mg L^{-1} in 2010 and 2011.

Dissolved Mg, Na and K concentrations did not follow the same trend seen in Ca concentrations. Maximum concentrations of Mg, Na and K generally occurred at the end of the first flow event in August 2010 and in the middle of the flow season in August 2011. In 2010, the Type III East AZL effluent showed maximum concentrations of Mg (1040 mg L^{-1}), Na (400 mg L^{-1}) and K (984 mg L^{-1}) at the end of July. In 2011, mid-season maxima occurred in August for Mg (332 mg L^{-1}), Na (85 mg L^{-1}) and K (222 mg L^{-1}). Minimum concentrations in 2010 and 2011 remained in the range of 45 to 70 mg L^{-1} for Mg, 15 to 20 mg L^{-1} for Na and 50 to70 mg L^{-1} for K. In the Type III West AZL drainage, maximum concentrations in 2010 for Mg (903 mg L^{-1}), Na (305 mg L^{-1}) and K (896 mg L^{-1}) occurred at the end of July/early August. In 2011, maxima occurred near the end of July for Mg (547 mg L^{-1}), Na (135 mg L^{-1}) and K (362 mg L^{-1}) before concentrations gradually decreased until the end of the flow season. Minimum concentrations for 2010 and 2011 remained between 90 to 135 mg L^{-1} for Mg, 20 to 35 mg L^{-1} for Na, and 85 to 115 mg L^{-1} for K (Figure 2-5).

2.3.1.4 Neutralization sequence

Oxidation of the sulfide minerals in waste rock has the potential to generate acidic pore water, which can be neutralized by reaction with gangue minerals that are capable of contributing acid neutralization capacity (Gunsinger et al. 2006, and references therein). Common minerals observed to contribute to acid neutralization in mine wastes are carbonates, Al- and Fe-hydroxides and aluminosilicates (Blowes & Ptacek 1994; Blowes et

al. 2003). Based on PHREEQCI geochemical equilibrium calculations, both Type III and the Type I East AZLs remained undersaturated with respect to calcite, siderite and other carbonate species throughout 2010 and 2011 (Figure 2-6). The Type I West AZL consistently had the highest pH and remained at or slightly below saturation with respect to calcite, suggesting that acid neutralization capacity from carbonate minerals remained in this lysimeter. In general, the saturation indices for calcite decreased steadily from the beginning to the end of each season as sulfide mineral oxidation progressed.

PHREEQCI calculations indicate that the effluent from both the Type I and III AZLs remained undersaturated with respect to amorphous $Al(OH)_3$ throughout all of 2010 and 2011. The Type I AZL effluent approached saturation with respect to the crystalline Al hydroxide mineral gibbsite for the majority of both field seasons, with undersaturation observed when pH decreases occurred. The Type III AZLs consistently remained undersaturated with respect to gibbsite. Saturation with respect to ferrihydrite was observed in both the Type I AZLs for the majority of 2010 and 2011, with the exception of periods of 2011 when the Type I East AZL decreased slightly below saturation. Given the circum-neutral pH range and low sulfide content seen in the Type I AZLs, it is expected that ferrihydrite dissolution would contribute little to buffering the effluent pH (Jurjovec et al. 2002). The Type III AZLs consistently remained undersaturated with respect to ferrihydrite. The pH range of these Type III lysimeters generally fell between 2.5 and 4, a region in which Al- and Fe-(oxy)hydroxides are expected to contribute to the buffering capacity of the

effluent . Both Type I and III AZLs remained supersaturated with respect to goethite (Figure 2-6).

2.3.2 Type I and Type III test pile geochemistry

The average rainfall measured on the crest of the test piles between 2007 and 2010 was 103 mm per year (Fretz et al. 2012). This amount represents approximately 37 % of the total average precipitation of 280 mm per year reported by Environment Canada for the period of 1998-2007 (Environment Canada, 2012), which is consistent with reports that approximately 40 % of precipitation fell as rain during this period. Artificial rainfall events were applied to the crest of the Type III test pile in 2006 and 2007 to investigate flow response to heavy rainfall and to initiate tracer tests (Neuner et al. 2012). These tests artificially elevated the annual rainfall on the crest of the Type III test pile to 233 mm in 2006 and 153 mm in 2007 (Neuner et al. 2012; Fretz et al. 2012), which contributed to the substantially higher flow that reported to the Type III test pile basal drains than the Type I test pile (Fretz et al. 2011). The Type I and Type III test piles both freeze completely each winter (Pham et al. 2009). Every spring, the test piles thaw from the batters inward, with initial flow reporting to the basal drains likely originating from the batters (Fretz et al. 2011). As the test piles continue to thaw completely, flow reports from increasingly longer and more central flowpaths. Flow rates generally decrease substantially in September and October as the temperature of the test piles decreases below freezing.

2.3.2.1 Persistence of blasting agents

Concentrations of dissolved constituents derived from the use of explosives, including nitrogen species, Cl^- and SO_4^{2-} increased throughout each field season as ambient temperature increased. The increase in the concentrations of these species was accompanied by a decrease in the pH. As with the AZLs, the release of blasting residuals from the Type I and Type III test piles can be used to monitor the progress of the "first flush" through the test piles. In 2010-2011, higher concentrations of nitrogen species and Cl^- were present in the effluent from the basal drain of the Type I test pile, than the effluent from the Type III North and South basal drains, indicating that substantial quantities of blasting residuals remained in the Type I test pile. High SO_4^{2-} concentrations in the Type III test pile coupled with the lower concentrations of blasting residuals indicate that *in situ* sulfide oxidation is the principal contributor to the higher levels of SO_4^{2-}. In general, nitrogen species in the Type I test pile gradually increased to a peak in 2010 before decreasing in 2011. Maximum concentrations were observed during the final days of flow in each field season with the exception of NO_2^-. Concentrations of NH_3 in the Type I basal drain showed a significant decrease from 2010 to 2011 reaching a maximum of 400 mg L^{-1} NH_3-N at the end of flow in November 2010, and 160 mg L^{-1} NH_3-N at the end of flow in 2011 (Figure 2.7). The NO_3^- concentration also decreased between 2010 and 2011, from a maximum of 2050 mg L^{-1} NO_3^--N in 2010 to 1470 mg L^{-1} NO_3^--N in 2011 (Figure 2.7). Peaks in NO_2^- concentrations occurred shortly before the end of each flow season in October reaching a maximum of 7.4 mg L^{-1} NO_2^--N in 2010

and 5.7 mg L^{-1} NO_2^--N in 2011 (Figure 2.7). Nitrite is not a component of the explosives used at Diavik, but is an intermediate oxidation product generated during oxidation of NH_3 to NO_3^- (Bailey et al. 2012). Nitrite can persist instead of NO_2^- when the conditions are unfavourable for NO_2^- oxidation, when the number or activity of nitrifying bacteria (e.g., Nitrosomonas) are limited, or if high concentrations of unionized ammonia (NH_3) are present (Anthonisen et al. 1976). The cold temperatures prevalent at Diavik may be a factor contributing to incomplete oxidation of NO_2^- within the waste rock. The high concentrations of Cl^- present in the Type I basal drain effluent are likely derived from the reduction of perchlorate included in the blasting accelerants. The concentration of Cl^- reached maxima of 2850 mg L^{-1} in the final days of flow in 2010, and 1890 mg L^{-1} in 2011 (Figure 2-7). The decrease in concentrations of blasting residuals in the Type I test pile from 2010 to 2011 suggests that the first flush of water has begun to proceed through to the basal drains. Further observation through 2012 and 2013 is necessary to confirm this trend.

In 2010 and 2011, concentrations of blasting residuals observed in the Type III test pile basal drains were considerably lower than in the Type I test pile, however Bailey, et al. (2012) observed much higher concentrations of blasting residuals in the Type III basal drains in the period between 2007 and 2010. The concentrations of blasting residuals in the Type III South basal drain were higher than the North. Significantly higher volumes of water report to the South basal drain which, combined with the higher concentrations, would indicate that a larger proportion of the flow passing through the Type III test pile reports to the South Basal

drain. The high concentrations of blasting residuals present in the Type III basal drain effluent suggests that the total mass of residuals initially present in the Type III test pile have yet to be depleted, and that the entire initial flush of water has yet to pass through this test pile (Bailey et al. 2012; Fretz 2012).

In 2010, concentrations of blasting residuals in the Type III South basal drain reached maxima in October, shortly before the end of the flow season. In 2011, the geochemistry deviated from trends seen in the previous 4 years (Bailey 2012) with higher concentrations of many parameters observed at the beginning the season, followed by lower concentrations in July and increasing concentrations observed at the end of the flow season. One possible cause of this difference may be a malfunction of the basal-drain heat trace, causing a back-up of drainage water that was unable to report to the drain at the end of the 2010 flow season.

Ammonia concentrations in the Type III South basal drain decreased from 2010 to 2011, peaking at 65 mg L^{-1} NH_3-N in October 2010 and reaching only 33 mg L^{-1} NH_3-N at the end of flow in 2011 (Figure 2-7). The concentrations of the intermediate species NO_2^- were also higher in 2010 reaching 0.33 mg L^{-1} NO_2^--N in October. In 2011, NO_2^- concentrations remained below detection for the majority of the season with a brief maximum reaching 0.088 mg L^{-1} NO_2^--N in September. In contrast, the NO_3^- concentrations increased from 2010 to 2011 (Figure 2.7), suggesting increased contributions from portions of the Type III test pile that had not been fully flushed previously. In 2010, the maximum NO_3^- concentration of 665 mg L^{-1} NO_3^--N was observed in October. The NO_3^- concentration

was greater in 2011, when 740 mg L^{-1} NO_3^--N was observed near the end of flow in 2011. Cl^- concentrations also increased from 207 mg L^{-1} in October 2010 to 266 mg L^{-1} in November 2011 (Figure 2-7).

In the Type III North basal drain, concentrations of blasting residuals peaked in September 2010 before flow stopped, and at the end of flow in October 2011. Maximum concentrations of NH_3 were 7.2 mg L^{-1} NH_3-N in 2010 and 5.6 mg L^{-1} NH_3-N at the end of 2011. The NO_2^- concentrations remained below detection for the majority of 2010 and 2011 with an increase in September 2010 to 0.10 mg L^{-1} NO_2^--N, and a maximum concentration of 0.071 mg L^{-1} NO_2^--N observed in 2011. A maximum of 292 mg L^{-1} NO_3^--N was observed in 2010 shortly after maximum NH_3 concentrations were observed, but concentrations otherwise remained below 72 mg L^{-1} NO_3^--N in 2010. In 2011, NO_3^- concentrations increased steadily to a maximum of 100 mg L^{-1} NO_3^--N at the end of flow in October. The Cl^- concentrations also exhibited a brief (3 to 5 days) dramatic spike in September 2010, reaching 77 mg L^{-1} concurrent with the NO_3^- levels but remained below 21 mg L^{-1} for the majority of the season. The dissolved Cl^- concentrations in 2011 increased steadily to 42 mg L^{-1} (Figure 2-7).

2.3.2.2 pH and alkalinity

The average S content in the Type I test pile is 0.035 wt % S in the <50 mm fraction, placing the waste rock at the upper end of the Type I classification (Smith et al. 2012b). Throughout 2010 and 2011, the pH of the Type I test pile remained circum-neutral, decreasing from a

maximum of 8.1 to minimum 5.4 from start to end of each flow season. Alkalinity followed a similar trend, decreasing from approximately 40 mg L^{-1} $CaCO_3$ to a minimum of 5 mg L^{-1} $CaCO_3$ by the end of the season. Minor deviations from the pH trend were reflected in the alkalinity measurements, which can be seen from the minor peaks in measureable alkalinity in August and September 2010, and October 2011 that correspond to variations in the pH (Figure 2-8).

The waste rock of Type III test pile is considered potentially acid generating based on NP:AP calculations, and has a low acid neutralization potential (Jambor 1997; Smith et al. 2012c). The acid generating potential is due to the higher sulfide content contributed by the greater proportion of biotite schist in the Type III waste rock, which increases the average S content in the waste rock of the Type III test pile to 0.053 wt % S in the <50 mm fraction. Carbon concentrations measured in the <50 mm fraction of Type III waste rock samples from construction ranged from 0.008-0.32 wt % C, with an average of 0.031 wt % C (Smith et al. 2012c). At the beginning of flow in both 2010 and 2011, the pH of the effluent from both basal drains (North and South) of the Type III test pile was slightly below neutral and decreased throughout the year. The pH of the Type III North basal drain decreased steadily from 6.9 in May to 4.5 in October during the 2010 flow season (Figure 2-8), and from 7.6 in May to 4.1 in October 2011. The Type III South basal drain showed a steady decrease in pH from 7.0 to 5.0 in 2010. In 2011, the pH decreased from 5.9 in May to 4.6 in November, but deviated from the normal trend in August for approximately 38 days reaching a maximum on

August 18 of pH 6.78 before dropping to values consistent with the previous trend near the end of flow (Figure 2-8).

Alkalinity in the Type III basal drains was lower than observed in the effluent of the Type I test pile due to the more rapid depletion of carbonate minerals. Alkalinity concentrations in the Type III South basal drain remained measureable throughout 2010 and most of 2011, only decreasing below detection limits at the end of the flow season in November 2011. Changes in alkalinity concentrations corresponded to variations in pH during the flow season, decreasing from 15 mg L^{-1} $CaCO_3$ to between 1 to 3 mg L^{-1} $CaCO_3$ in 2010 and from 6 mg L^{-1} $CaCO_3$ to below detection in 2011 with a peak to 14 mg L^{-1} $CaCO_3$ in late August corresponding to the pH increase at that time. The Type III North basal drain showed a depletion of measurable alkalinity near the end of both flow seasons, corresponding with the lowest pH values. Peak alkalinity levels at the start of the season were 13 mg L^{-1} $CaCO_3$ and 38 mg L^{-1} $CaCO_3$ for 2010 and 2011, respectively (Figure 2-8). As the pH of the Type III North basal drain is overall lower than the South, the depletion of measureable alkalinity is anticipated.

2.3.2.3 Sulfide oxidation and dissolved metals

Concentrations of sulfide oxidation products in the Type I test pile effluent were lower than observed for the Type III test pile, due to the low sulfide content of the granite. Disseminated pyrite is the principal sulfide mineral identified in the granite, which comprises most of the Type I waste rock (Jambor 1997). Pyrite weathers slowly at circum-neutral pH due to higher

activation energies for oxidation (Williamson & Rimstidt 1994; Rimstidt & Vaughan 2003). Dissolved SO_4^{2-} levels in the Type I test pile effluent remained below 1000 mg L^{-1} during the first three years of observation (Bailey et al. 2012). In 2010 and 2011 however, SO_4^{2-} concentrations increased at the end of each flow season to maxima between 1100 to 1500 mg L^{-1}. In 2010, the start of flow was delayed until July due to malfunctions in the heat trace of the Type I basal drain. After repair of the heat trace, reported outflow volumes in 2010 and 2011 were much greater than in 2009 (Fretz 2012). Dissolved SO_4^{2-} concentrations at the start of 2010 began between 90 to 260 mg L^{-1}, increasing to a maximum of 1400 mg L^{-1} when flow stopped in November 2010. In 2011, flow began in May and early concentrations generally remained between 20 to 100 mg L^{-1} before increasing to 1100 mg L^{-1} in November (Figure 2-8).

Dissolved Fe concentrations in the Type I test pile followed trends similar to those observed for dissolved SO_4^{2-}, but at much lower concentrations, increasing from 0.11 to 0.51 mg L^{-1} in 2010, and from below detection to 0.28 mg L^{-1} in 2011 as effluent water decreased in pH. Geochemical calculations conducted using PHREEQCI, and assuming equilibrium conditions, indicate that the effluent water samples remained saturated with respect to ferrihydrite and goethite throughout the field season, suggesting that dissolution of these phases did not occur and that formation of these secondary minerals may have limited dissolved Fe concentrations.

Concentrations of metals associated with sulfide oxidation remained lower in the Type I test pile effluent than observed in the Type III test pile (Figure 2-8), and followed a trend of increasing in warmer months. At the end of flow, the concentrations peaked for Cu (2010: 0.88 mg L^{-1}, 2011: 0.09 mg L^{-1}), Ni (2010: 1.2 mg L^{-1}, 2011: 0.81 mg L^{-1}), Zn (2010: 0.25 mg L^{-1}, 2011: 0.068 mg L^{-1}), Co (2010: 0.21 mg L^{-1}, 2011: 0.13 mg L^{-1}), and Cd (2010: 16 µg L^{-1}, 2011: 11 µg L^{-1}) (Figure 2-8). PHREEQCI calculations indicate that all of the effluent water samples remained undersatured with respect to all of the Cu, Ni, Co, Zn and Cd-bearing secondary phases included in the WATEQ4F database, suggesting that these minerals did not provide a solubility limit on the aqueous concentrations of these metals.

Concentrations of the major cations (Ca, Mg, Na, K) in the Type I test pile increased steadily and peaked at the end of flow each year, with slight deviations occurring in August 2010 and November 2011 when concentrations briefly declined, before increasing further. The maximum concentrations at the end of 2010 and 2011 respectively were; Ca, 2000 and 1600 mg L^{-1}; Mg, 1100 and 800 mg L^{-1}; Na, 600 and 400 mg L^{-1}; K, 300 and 200 mg L^{-1} (Figure 2-9).

Higher concentrations of sulfide oxidation products were observed in the Type III test pile effluent. This increase was undoubtedly due to the presence of biotite schist which contributes the majority of the sulfide content. The sulfide mineral assemblage is mainly composed of pyrrhotite with traces of pyrite, chalcopyrite and sphalerite (Jambor 1997; Blowes & Logsdon 1998). Pyrrhotite oxidation can occur up to 20-100 times faster than

pyrite under standard atmospheric conditions (Janzen et al. 2000), which likely resulted in higher concentrations of dissolved SO_4^{2-} and metals in the Type III test pile effluent. In 2011, all parameters measured in the Type III South basal drain show a pattern that is distinct from that observed between 2007 and 2010. Concentrations began high early in the season before dropping to a minima and increasing steadily until the end of flow. The deviations are attributed to problems encountered with the heat trace of the Type III South basal drain in the winter of 2011. The failure of the heat trace would have limited flow preventing the release of the final high-concentration effluent of 2010. When flow began in 2011, the initial water would have been derived from the end of the previous field season giving concentrations corresponding to the peak levels in November 2010.

Dissolved SO_4^{2-} concentrations in the Type III test pile were higher than those in the Type I but followed a similar seasonal trend. As seen earlier, blasting residuals were not been flushed completely from the system, as a consequence, SO_4^{2-} concentrations were derived both from blasting residuals and from *in situ* sulfide oxidation. The SO_4^{2-} concentrations in the Type III South basal drain peaked at higher levels at the end of flow in 2010 and 2011 (2400 and 3150 mg L^{-1}) than in the North basal drain (900 and 1300 mg L^{-1}) (Figure 2-8).

Concentrations of Fe in the Type III test pile varied more noticeably around the increasing trend during the field season than in the Type I test pile, with increased concentrations observed during the warmest months of July and August. Increased rates of sulfide oxidation can cause a deviation from the general trend because oxidation rates can

vary throughout the field season depending on temperature. In general, both the Type III North and South basal drains follow a similar trend. The maximum dissolved Fe concentrations in the Type III North basal drain were 0.35 to 0.38 mg L^{-1} in 2010 and increased to 0.60 to 0.74 mg L^{-1} in 2011. The dissolved Fe concentration in the Type III South basal drain increased from 0.46 to 0.58 mg L^{-1} in 2010 to 0.51 to 0.70 mg L^{-1} in 2011. Equilibrium calculations with PHREEQCI show the Type III North basal drain remained close to, or reached saturation with respect to jarosite throughout 2010 and remained at saturation after July 2011. Saturation with respect to ferrihydrite was observed for the first few months of each field season, before the water became undersaturated with respect to ferrihydrite. This trend suggests that ferrihydrite provides a secondary mineral control on Fe concentrations early in the flow season. The effluent in Type III South basal drain followed a slightly different trend. Initially in 2011, the effluent water was near saturation with respect to jarosite, falling below saturation in July and September, corresponding to decreases in dissolved SO_4^{2-} concentrations. Saturation with respect to ferrihydrite was maintained for longer periods of time in the higher-pH Type III South basal drain effluent, with periods of 1 to 32 days when undersaturation (between SI 0 to -1) was observed. Both Type III basal drains remained oversaturated with respect to goethite throughout both years of monitoring (Figure 2-10). Trends in saturation indices in both Type III basal drains and lower concentrations of dissolved Fe indicate that precipitation of Fe-(oxy)hydroxide phases acts as a control on Fe concentrations in the drainage reporting to each basal drain.

Higher concentrations of other sulfide oxidation products were observed in the effluent from the Type III basal drains than the Type I basal drain, which is consistent with the higher sulfide content of Type III waste rock and the greater diversity of sulfide minerals in the biotite schist component of the Type III rock. Concentrations of Cu, Ni, Co, Zn and Cd increased steadily from the beginning to the end of the flow season for both basal drains (Figure 2-8); with the exception of the Type III South basal drain effluent in 2011. As with SO_4^{2-}, measurements of dissolved metals at this location exhibit the initial high values at the beginning of the season before decreasing in July and increasing steadily until November 2011.

Overall dissolved Cu concentrations increased in 2011 from 2010 in the Type III basal drains. The maximum stable Cu concentrations measured for the effluent from the Type III North basal drain were 1.8 mg L^{-1} in 2010 and 1.6 mg L^{-1} in 2011 with single point measurements in 2011 reaching values up to 4.6 mg L^{-1}. Dissolved Cu concentrations in the Type III South basal drain reached end-of-season maxima of 0.51 mg L^{-1} in 2010 and 2.4 mg L^{-1} in 2011, with three measurements in June 2011 reaching 5.0 mg L^{-1} (Figure 2-8). Copper is present in traces of chalcopyrite within the sulfide mineral assemblage of the biotite schist (Jambor 1997). Equilibrium calculations with PHREEQCI show that the effluent from both Type III basal drains remained undersaturated with respect to the secondary Cu phases $Cu(OH)_2$, $CuCO_3$ and azurite throughout 2010 and 2011; however the Type III South basal drain approached saturation with respect to brochantite and malachite in

July 2010. If Cu concentrations continue to increase, brochantite and malachite may precipitate and act as secondary mineral controls to the Cu concentrations in future years.

Both Ni and Co occur in the pyrrhotite present in the Diavik country rock (Jambor 1997) and dissolved concentrations of these elements are highly correlated in the Type III North and South basal drains with ratios of 4.8:1 (σ=0.76, n=188), Ni:Co, similar to the ratios seen in the Type III AZLs and corresponding to previous geochemical observations by Bailey (2012). Concentrations of these elements also increased from 2010 to 2011, indicating that flow is reporting to the Type III basal drains from locations within the test pile that undergo higher rates of pyrrhotite oxidation. Maximum Ni and Co concentrations in the Type III North basal drain occurred at the end of each flow season in October: Ni peaks at 5.3 mg L^{-1} in 2010 and 7.8 mg L^{-1} in 2011, and Co at 1.1 mg L^{-1} and 1.9 mg L^{-1}. The Type III South basal drain concentrations for these elements achieved maxima at the end of each field season, with the exception of Co in 2011. Dissolved Ni concentrations at the end of 2010 reached 7.2 mg L^{-1} and in 2011 reached 19 mg L^{-1}. Cobalt concentrations peaked in November 2010 at 1.7 mg L^{-1}, in June 2011 at 3.9 mg L^{-1} and in November 2011 at 3.5 mg L^{-1} (Figure 2-8). PHREEQCI equilibrium modeling does not suggest that there are secondary mineral controls on Ni and Co in the Type III test pile; however, concentrations may be limited by adsorption or coprecipitation reactions.

Zinc and Cd in the Type III basal drain effluent occur as a result of sphalerite weathering. Traces of sphalerite have been documented in previous mineralogical reports on

the biotite schist present at Diavik (Jambor 1997). Concentrations of dissolved Zn and Cd in both Type III basal drains are highly correlated, generally corresponding to a ratio of 228:1, Zn:Cd (σ=48, n=91) in the North basal drain effluent, and 140:1, Zn:Cd (σ=45, n=96) in the South basal drain, which are consistent with previous observations of Bailey (2012). Dissolved Zn concentrations in the Type III North basal drain reached a maximum of 2.9 mg L^{-1} in October 2010 and 2.7 mg L^{-1} in October 2011. Dissolved Cd maxima occurred at the same time, with maximum concentrations reaching 12.9 µg L^{-1} in both 2010 and 2011. The Type III South basal drain Zn concentrations reached maximum values of 1.8 mg L^{-1} in November 2010, 6.5 mg L^{-1} in June 2011 and 4.7 mg L^{-1} in November 2011. Dissolved Cd concentrations during the same time periods reached 19 µg L^{-1}, 35 µg L^{-1} and 39 µg L^{-1}, respectively (Figure 2-8). Again, there are no indications from equilibrium calculations that there are secondary mineralogical controls on Zn or Cd concentrations in the Type III test pile.

Concentrations of the major cations (Ca, Mg, Na, K) all follow a general increasing trend from the beginning to end of each flow season. Similar to other species in 2011, concentrations of these cations were initially higher in the Type III South basal drain than in previous years, before decreasing and finally following an increasing trend that is consistent with the trend observed from 2007 to 2010. At the end of both 2010 and 2011, dissolved Ca concentrations in the Type III test pile effluent are considerably lower than in the Type I test pile effluent. The Ca concentrations in the Type III North basal drain attained maxima of

120 mg L^{-1} in 2010 and 160 mg L^{-1} in 2011, and in the Type III South basal drain maximum concentrations were 380 mg L^{-1} in 2010 and 570 mg L^{-1} in 2011 (Figure 2-9). Dissolved Mg concentrations were generally higher in the Type III South basal drain than the North, reaching 530 mg L^{-1} in November 2010, 610 mg L^{-1} in May 2011 and 940 mg L^{-1} in November 2011. The Mg concentrations in the Type III North basal drain reached 110 mg L^{-1} in October 2010 and 230 mg L^{-1} in October 2011. Dissolved Na concentrations in the Type III North basal drain reached maxima of 77 mg L^{-1} in late September 2010 and 63 mg L^{-1} in October 2011, and dissolved K concentrations reached 65 mg L^{-1} and 85 mg L^{-1} during the same time periods. In the Type III South basal drain, Na concentrations peaked in October 2010 at 280 mg L^{-1}, in May 2011 at 180 mg L^{-1} and in November 2011 at 350 mg L mg L^{-1}. Dissolved K concentrations were lower overall, reaching 140 mg L^{-1} in October 2010, 90 mg L^{-1} in May 2011 and 170 mg L^{-1} in November 2011 (Figure 2-9).

2.3.2.4 Neutralization sequence

PHREEQCI calculations show that both Type I and Type III basal drains remained undersaturated with respect to calcite throughout 2010 and 2011, with the exception of a short period in July 2011 when the Type I basal drain effluent attained equilibrium with respect to calcite. Saturation with respect to calcite occurred when the Type I test pile effluent reached an approximate pH of 8. Saturation indices for amorphous $Al(OH)_3$ and ferrihydrite followed pH trends, generally decreasing over the course of each field season with concurrent increases in Al and Fe concentrations. Saturation indices of these minerals in

the Type III basal drains were generally lower than those calculated for the Type I basal drain. The effluent water from all of the drains approached saturation with respect to gibbsite for the majority of both field seasons with minor deviations just below saturation occurring at various short periods. This water also remained supersaturated with respect to goethite throughout all of 2010 and 2011 (Figure 2-10). PHREEQCI calculations indicate that the pH of the Type III test piles basal drains was primarily buffered by the dissolution of Al- and Fe-(oxy)hydroxides when pH decreases, which is supported by concurrent elevations in Al concentrations.

2.3.3 Covered test pile geochemistry

The Covered test pile consists of a Type III waste rock core with an average S content of 0.082 wt % S in the <50 mm fraction, which is at the lower end of the operational target S content for Type III waste rock of > 0.08 wt % S (Smith et al. 2012b). The S content within the core samples exhibited the highest variability of the three test piles (Smith et al. 2012b). The Type III core was instrumented with the same variety of instruments as the uncovered test piles, including thermistor strings, thermal conductivity access ports, gas content and pressure measurement points, gas-permeability measurement devices, soil-water solution samplers, and microbiology sampling ports (Smith et al. 2012a). The Type III waste rock was re-sloped to a 3H:1V (18.4°) grade and covered with 1.5 m of glacial till and 3 m of Type I waste rock. Additional instrumentation was installed in the till and Type I cover layers to closely monitor cover performance. Although the till layer is lower permeability, the oxygen

content measured throughout the entire test pile has remained at atmospheric levels since construction (Smith et al. 2012a). Similar to the Type I and Type III test piles, basal lysimeters were installed below the centre and batters of the Covered test pile to monitor flow from discrete areas within the test pile (Smith et al. 2012a). To prevent freezing of drain lines, the lysimeters are fully heat-traced. From completion of construction until June 2011, the basal lysimeter heat trace within the Covered test pile was set at > 20°C, which, combined with the thermal insulation provided by the cover, caused artificial heating within the pile. This caused the till layer above the basal lysimters to remain unfrozen, which allowed flow to report to the basal drain on a nearly continuous basis. Temperatures observed at the innermost first tip-face of the Covered test pile remained above freezing throughout each year, following an opposing trend to the seasonality of the uncovered test piles. Temperatures at the first tip-face are higher throughout the winter than in the summer, exhibiting significant lag-time for heat transfer (Pham et al. 2009). In contrast, temperatures measured in the centre region at the outermost fourth tip-face decreased through the fall due to cooling of the test pile surfaces (Pham et al. 2009). The opposing temperature trends promoted a shift in the flow and geochemical trends observed in the Covered test pile basal drain relative to the trends observed in the uncovered piles. Maximum flow rates occurred in the fall of each year and minima occurred mid-summer. In addition, the maximum solute concentrations generally occurred as flow rates decreased in June. Minima occurred in the fall and concentrations increased throughout the winter months as temperatures within the core of the Covered test pile increased.

2.3.3.1 Persistence of blasting agents

Concentrations of dissolved constituents associated with blasting residuals, N species, Cl^-, and ClO_4^-, closely followed the trends seen in the SO_4^{2-} concentrations in the effluent throughout 2010 and 2011. In 2010, concentrations of dissolved constituents attributed to blasting residuals reached a maximum between June and July, which corresponds to periods of decreased flow from the basal drain observed in previous years. On June 28, 2011 the heat trace which had been installed to prevent the core of the covered pile from freezing was turned off in order to monitor the cooling of the test pile. In response to this change, flow rates to the basal drains decreased. In July 2011, concentrations of all blasting residuals, except for NO_2^-, decreased abruptly. This decrease was concurrent with a rapid dramatic increase in flow the flow rate to the basal drain, which could have diluted the effluent reporting to the drain.

Ammonium concentrations reached a maximum of 7.1 mg L^{-1} NH_3-N in June 2010 before decreasing to 1.1 mg L^{-1} NH_3-N abruptly in July and then increasing relatively steadily throughout the winter to a maximum of 9.1 mg L^{-1} NH_3-N in June 2011. During the higher flow volume in July 2011, concentrations decreased to 1.4 mg L^{-1} NH_3-N, then varied erratically between 1.2 and 7.5 mg L^{-1} NH_3-N before stabilizing between 5 and 6 mg L^{-1} NH_3-N at the end of September. Concentrations of NO_2^- remained below detection limits throughout the majority of 2010 and 2011 until shortly before the July 2011 peak flow period, when the concentration increased to 0.072 mg L^{-1} NO_2^--N (Figure 2-11). Detectable

NO_2^- was observed shortly after concentrations of un-ionized ammonia (NH_3) reached their highest. High concentrations of NH_3 have been documented to prevent full nitrification of NO_2^- to NO_3^- (Anthonisen et al. 1976). Concentrations of NO_3^- peaked concurrently with NH_3 in June 2010 at 353 mg L^{-1} NO_3^--N before decreasing to 160 mg L^{-1} NO_3^--N in August 2010 then increasing steadily to a maximum of 367 mg L^{-1} NO_3^--N in June 2011. The July 2011 flow event triggered a decrease to 158 mg L^{-1} NO_3^--N before returning to previous concentrations. Concentrations of Cl^- followed similar trends, with maxima of 100 mg L^{-1} in June 2010, and 97 mg L^{-1} at the end of May 2011. The Cl^- concentration decreased dramatically to 30 mg L^{-1} in July before concentrations increased to over 80 mg L^{-1} (Figure 2-11).

2.3.3.2 pH and alkalinity

Drainage from the Covered test pile exhibited characteristics similar to the Type III test pile indicating that water passing through the Type III core significantly affected the water quality of the effluent. This observation suggests that sulfide-oxidation reactions are not inhibited by the cover. Because of the construction technique, the cover is restricted to the top of the pile at the interface between the test pile and the construction platform, providing an avenue to gas transport into the Type III core of the pile. Furthermore, the sulfide content of the Type III core of the covered pile is very low.

In 2010 and 2011, pH levels remained within a narrower range than observed in the Type I and Type III uncovered test piles. The lowest pH effluent-water generally occurred between

May-August, and maximum pH values were observed in September-November. A decrease in both the minimum and maximum pH values from 2010 to 2011 was observed. In 2010, the pH reached its lowest value at the end of April (pH 4.1), before increasing throughout August and September, to a maximum of approximately pH 4.6. From mid-May to mid-August 2011, the pH maintained around pH 4.1 with measured values of 3.96 occurring in August and September. The highest pH values in 2011 occurred in November, remaining just below 4.4 (Figure 2-12). The trends observed in the Covered test pile contrast with the decrease in pH trends observed in the Type I and Type III test piles over the duration of each year. This difference is due in part to the core of the Covered test pile remaining above freezing temperatures as a result of influence from the cover and from the heat trace installed in the lysimeters and drains at the base of the test pile. Geochemistry in the Covered test pile effluent was thus not subject, in the same way, to the freeze/thaw cycles that occurred in the uncovered test piles (Bailey 2012). The heat trace in the basal lysimeters, but not the basal drain, was disconnected in June 2011.

The low concentrations of alkalinity in the Covered test pile likely were influenced by the presence the Type III core. Oxidation of the sulfide content within the waste rock produced effluent that quickly exhausted the rate of dissolution of the limited carbonate content of the waste rock. Alkalinity in the Covered test pile remained above detection (>1 mg L^{-1}) for the majority of 2010 before decreasing to below detection as the pH dropped in September. As the pH continued to decline into the summer of 2011, the alkalinity

remained near or below the detection limit, until November 2011 when the pH increased to approximately 4.4. The decrease in alkalinity levels is an indicator of buffering capacity depletion increasing from year to year in the Covered test pile as increased sulfide mineral oxidation overwhelmed the limited neutralization potential of the waste rock.

2.3.3.3 Sulfide oxidation and dissolved metals

Concentrations of SO_4^{2-} in the Covered test pile were the highest of the three test piles. This difference is consistent with the higher sulfur content of the Type III core of the Covered test pile, and the enhanced rate of sulfide minerals at temperatures above freezing. In 2010 and 2011, SO_4^{2-} reached the highest concentrations immediately following low pH values. In 2010, the peak concentration occurred at the beginning of June, reaching 3500 mg L^{-1} before decreasing to 2250 mg L^{-1} in mid-August. In 2011, a maximum SO_4^{2-} concentration of 4400 mg L^{-1} was observed at the end of June, corresponding to a period of very low flow reporting to the basal drain. This water would have had a longer residence time in the Type III core of the pile, resulting in the high concentrations of SO_4^{2-}. A sharp drop in SO_4^{2-} concentrations to 1400 mg L^{-1} occurred at the end of July concurrent with a brief increase in the flow rate. Flow rates decreased shortly after, with a coincident increase in the SO_4^{2-} concentration to 3700 mg L^{-1} at the beginning of September. The flow rate subsequently increased and the SO_4^{2-} concentrations decreased to 3100 mg L^{-1}, which is higher than the concentrations in the fall of 2010 (approximately 2500 mg L^{-1}) (Figure 2-12) (Bailey 2012).

Dissolved Fe concentrations followed similar trends to SO_4^{2-} in 2010 and 2011, however there was an overall increase in Fe between 2010 and 2011. This increase was also observed for other metals derived from sulfide-mineral oxidation, including Cu, Ni, Co, Zn and Cd. Copper and Fe concentrations showed the most pronounced increase, possibly indicating that chalcopyrite oxidation is more prevalent in the Type III waste rock core of the Covered test pile. The concentration of Fe remained fairly stable within the range of 0.02 to 0.07 mg L^{-1} from January to September 2010. As pH decreased throughout the fall of 2010, Fe concentrations increased to a maximum of 0.18 mg L^{-1} at the beginning of November. In 2011, the maximum concentrations of Fe occurred in April at 0.17 mg L^{-1} and in December, at 0.21 mg L^{-1} for the final sample collection of the year on December 12, 2011. Trends in Cu concentrations were very similar to those of Fe. Concentrations remained between 0.8-1.5 mg L^{-1} from January to September 2010, and then increased to a maximum of 2.6 mg L^{-1} at the beginning of November. Concentrations were high in April and May 2011 (3.2 to 3.4 mg L^{-1}) then decreased to 0.7 mg L^{-1} at the end of July. The Cu concentration then increased until mid-September 2011 after which it remained stable between 3.4 to 4.0 mg L^{-1} until December (Figure 2-12).

As seen previously in the Type III AZLs and test piles, Ni and Co concentrations in the Covered test pile effluent are highly correlated, with average Ni:Co ratios of 4.7:1 (σ=0.79, n=121) (Bailey 2012). In 2010, the Ni concentrations reached a maximum of 15 mg L^{-1} in June before rapidly dropping below 6.4 mg L^{-1} in September then steadily

increasing to a maximum of 19 mg L^{-1} in May of 2011. The Co concentration peaked in June 2010 at 3.0 mg L^{-1} before decreasing to 1.1 mg L^{-1} in September, followed by a steady increase to a maximum of 3.8 mg L^{-1} in May 2011 (Figure 2-12). PHREEQCI equilibrium calculations do not indicate that there were secondary mineral controls on Ni and Co concentrations.

The dissolved Zn and Cd concentrations follow trends similar to Ni and Co with an average Zn:Cd ratio of 189:1 (σ=25, n=121), similar to the Zn:Cd ratio observed previous years (Bailey 2012d). Maxima in 2010 were reached at the beginning of June (Zn 11 mg L^{-1}; Cd 50 µg L^{-1}) before quickly decreasing to minimum values for the year at the end of July (Zn 4.7 mg L^{-1}; Cd 27 µg L^{-1}). The Zn and Cd concentrations then increased steadily until May 2011, reaching maxima of 14 mg L^{-1} for Zn and 66 µg L^{-1} for Cd. Low concentrations were observed again in July, bringing Zn to 3.9 mg L^{-1} and Cd to 19 µg L^{-1}, before concentrations returned to levels seen in May and decreased to 7.3 mg L^{-1} (Zn) and 37 µg L^{-1} (Cd) in December 2011 (Figure 2-12). Similar to other sulfide oxidation products, PHREEQCI equilibrium calculations do not show secondary mineral controls on Zn and Cd.

Concentrations of the major cations (Ca, Mg, Na, K) follow similar trends throughout 2010 and 2011. In 2010, maximum concentrations were observed in June (Ca 450 mg L^{-1}; Mg 720 mg L^{-1}; Na 230 mg L^{-1}; K 210 mg L^{-1}) shortly after pH reached a minimum. Concentrations gradually decreased to minima in August 2010 (Ca 330 mg L^{-1}; Mg 370 mg L^{-1}; Na 110 mg L^{-1}; K 110 mg L^{-1}) then increased over the course of the winter to

reach maxima at the end of May 2011 (Ca 490 mg L^{-1}; Mg 850 mg L^{-1}; Na 230 mg L^{-1}; K 200 mg L^{-1}). All of the major cation concentrations fluctuated as a result of the flow event in July 2011, which was accompanied by minimum concentrations of the major ions (Ca 230 mg L^{-1}; Mg 250 mg L^{-1}; Na 83 mg L^{-1}; K 77 mg L^{-1}) before levels returned to summer concentration ranges (Figure 2-13).

2.3.3.4 Neutralization sequence

Effluent from the Covered test pile generally exhibited a lower pH than the uncovered test piles, and alkalinity concentrations decreased to below the detection limit by the fall of each year. PHREEQCI equilibrium calculations show that the Covered test pile effluent remained undersaturated with respect to calcite and siderite throughout all of 2010 and 2011 when measurable alkalinity was observed. The effluent also remained undersaturated with respect to amorphous $Al(OH)_3$ and ferrihydrite for the majority of 2010 and 2011, with saturation with respect to ferrihydrite approached at the end of October 2010 and 2011. Unlike the Type III test pile, the Covered test pile remained undersaturated with respect to crystalline gibbsite for the majority of the observation period, only reaching saturation during the higher pH period of July-October 2010 and briefly in July and November 2011. The effluent remained supersaturated throughout 2011 and 2012 (Figure 2-14). These observations suggest that the pH of the Covered test pile effluent is neutralized primarily by dissolution of Al-(oxy)hydroxides with contributions from the dissolution of Fe-(oxy)hydroxides, which promotes fairly stable pH values between 4.0-4.5 (Blowes & Jambor 1990; Johnson et al.

2000; Moore 2009). This observation is supported by an increase in dissolved Al and Fe concentrations from 2010 to 2011.

2.4 Summary and conclusions

The Type I waste rock used in construction of the Type I AZLs and test pile produced drainage with circum-neutral pH and low concentrations of dissolved metals due to the low overall sulfide mineral content of the waste rock. The Type I test pile drainage had a lower average pH than the Type I AZLs throughout 2010 and 2011 demonstrating the greater heterogeneity in waste rock dumping inherent upon increasing size from AZL to test pile scale. Alkalinity remained measurable in both Type I systems indicating that oxidation of the trace sulfide minerals present had not exhausted the buffering capacity of the waste rock. Traces of blasting residuals had been almost completely depleted from the Type I AZLs but persisted in the Type I test pile. Trends in measured parameters over the course of each field season demonstrated the effects of temperature on the waste rock. The pH consistently decreased and dissolved metal concentrations increased as ambient temperature increased and a greater proportion of the test pile contributed to the flow system. Sulfide oxidation also increased as ambient temperature increased during each summer, contributing to the decrease in pH.

Type III waste rock in the Type III AZLs and test pile has a higher sulfide mineral content than the Type I waste rock, due to the presence of more biotite schist in this rock. The Type III AZLs and test pile thus produced drainage with lower pH and higher

concentrations of dissolved metals than the Type I installations. The Type III AZLs had lower pH than the Type III test pile and no measureable alkalinity was detected throughout 2010 and 2011 indicating that oxidation of sulfide minerals had produced sufficient acidity to exhaust the buffering capacity of the waste rock. Equilibrium calculations indicate that the pH of the Type III AZL drainage was neutralized by dissolution of Fe- and Al-(oxy)hydroxides. Both basal drains of the Type III test pile showed pH trending below circum-neutral levels over the course of each field season as temperature, and consequently the rate of sulfide oxidation, increased. Decreases in pH were accompanied by concurrent increases in concentrations of dissolved metals. As carbonate alkalinity decreased throughout each field season, Fe- and Al-(oxy)hydroxides contributed to buffering the pH of the Type III basal drains. Similar to the Type I system, blasting residuals were measured in higher concentrations in the Type III test pile, but had been depleted from the Type III AZLs.

The Covered test pile consistently produced drainage with the lowest pH and the highest dissolved metal concentrations. These observations indicate that the Type III core of the test pile, which has higher sulfur content than the Type III uncovered test pile, had a significant influence on drainage. The Covered test pile does not exhibit the same temperature dependent trends as seen in the Type I and Type III uncovered test piles, due to heating from the basal heat trace, which maintained core temperatures above freezing and a thawed zone in the till layer throughout much of the year. Sulfide oxidation proceeds throughout the year and resulted in a more stable pH than was observed in the uncovered test

iles. Equilibrium calculations indicate that the pH was increasingly buffered by Fe- and Al-(oxy)hydroxides supported by an increase in dissolved Fe and Al concentrations from 2010 to 2011.

2.5 Figures

Figure 2-1 Diavik Diamond Mine, located 300 km northeast of Yellowknife, Northwest Territories, Canada. Location of test piles research site circled. Diavik Satellite image, 2009.

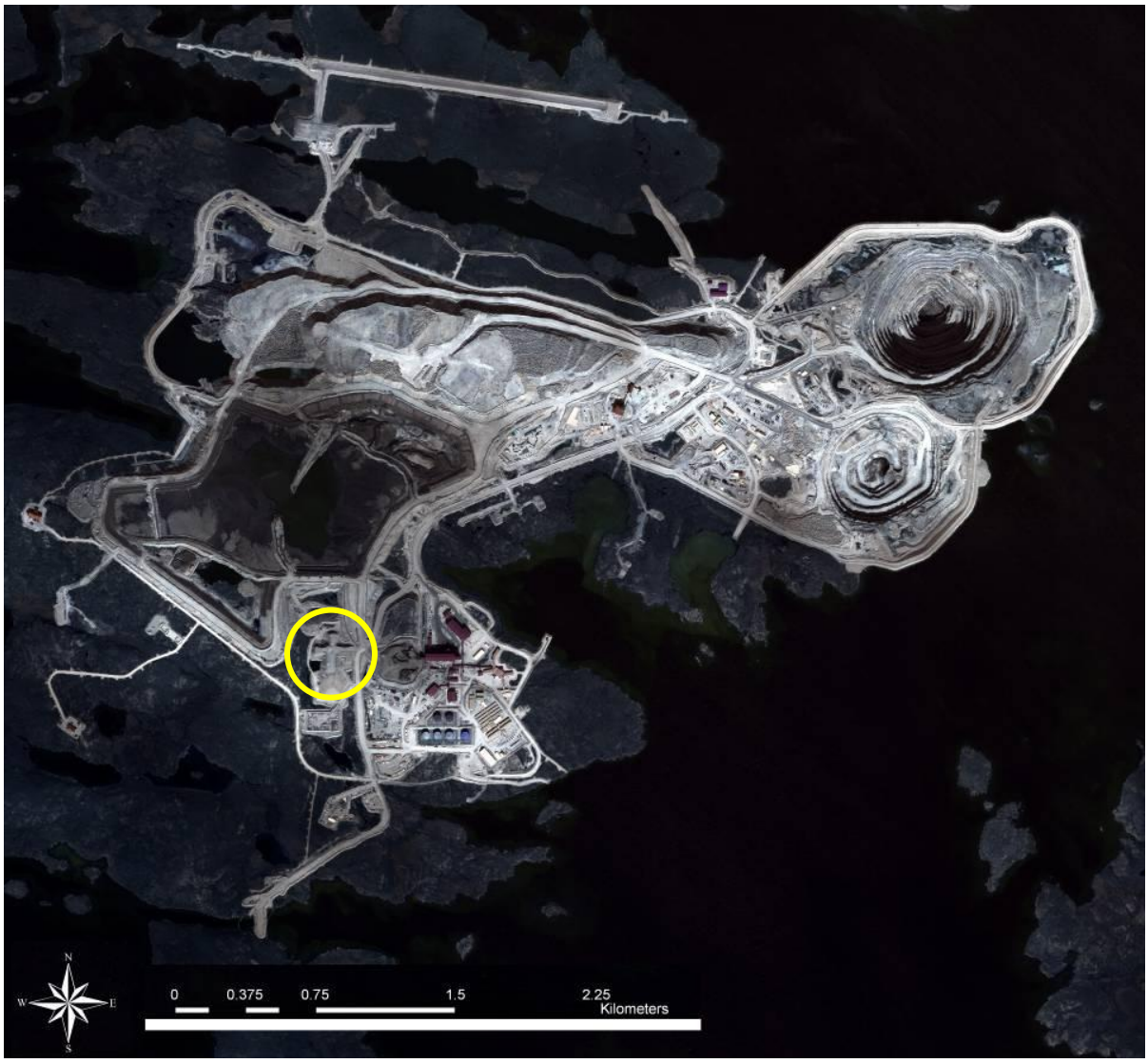

Figure 2-2: Test piles Waste Rock Research Site located at Diavik Diamond Mine.

Figure 2-3: Time-series of blasting agents in all AZL locations.

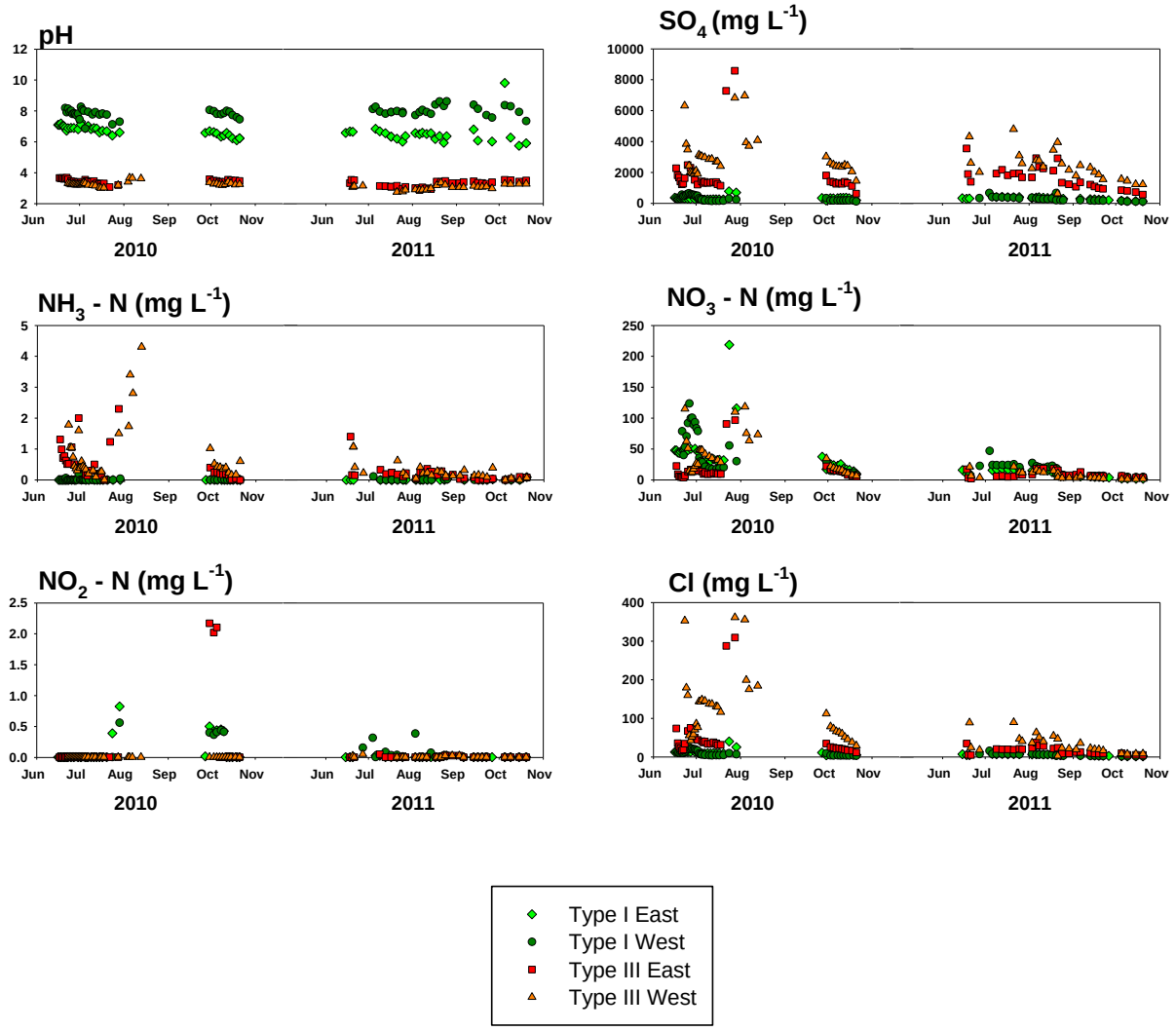

Figure 2-4: Time-series of SO42- and sulfide oxidation products in all AZLs.

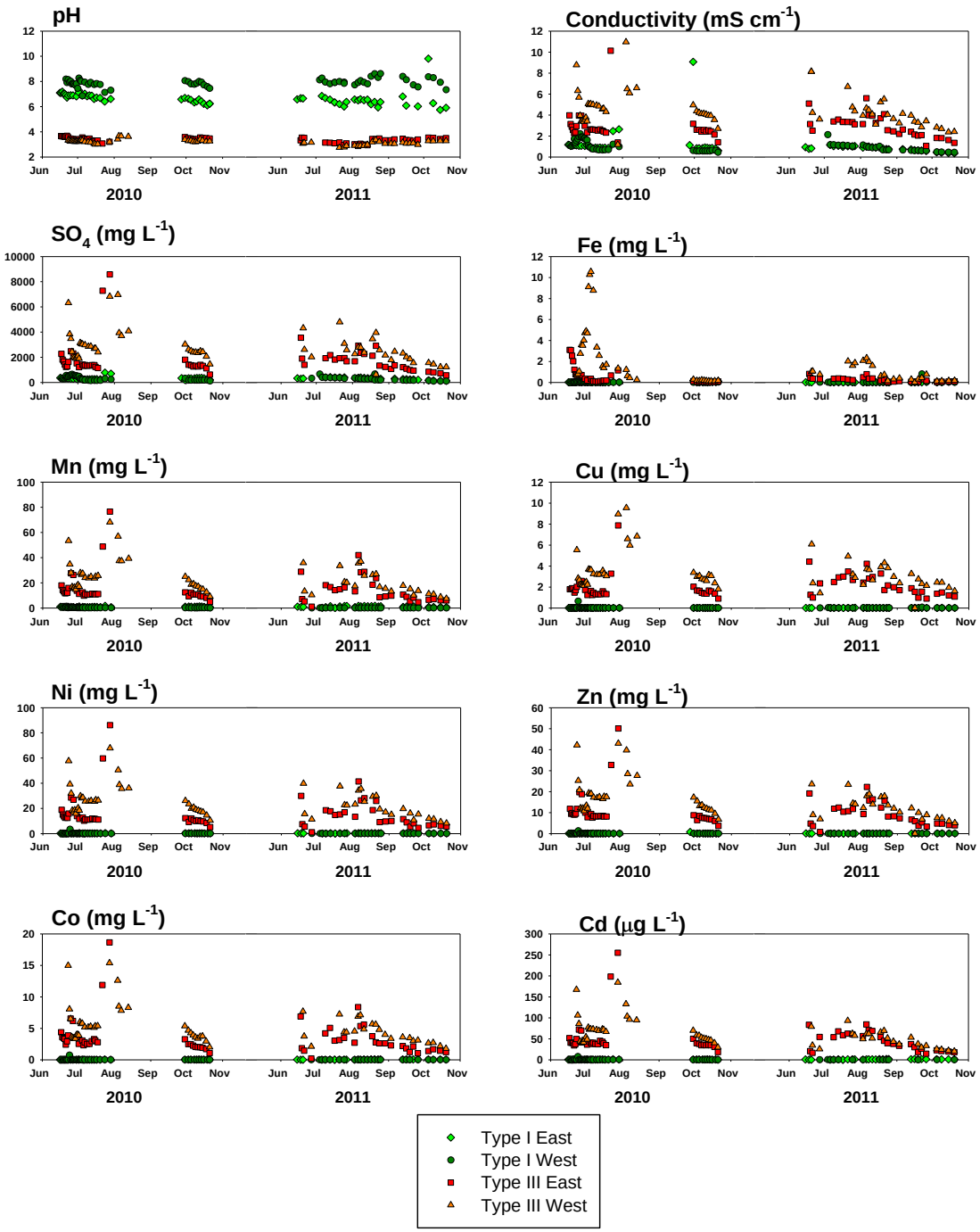

Figure 2-5: Time-series of major cations in all AZLs.

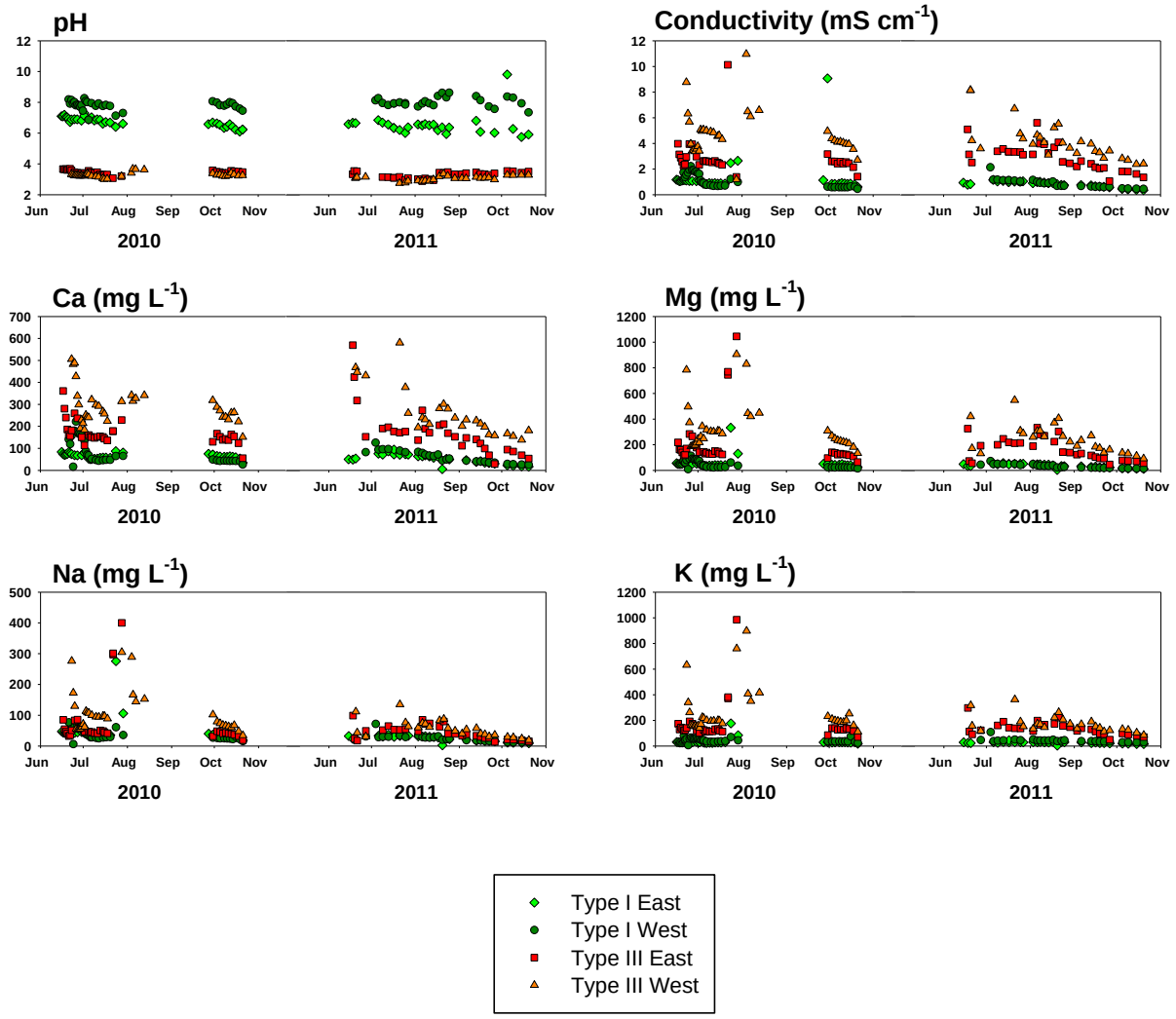

Figure 2-6: Time-series of pH buffering reactions with modeled saturation indices in all AZLs.

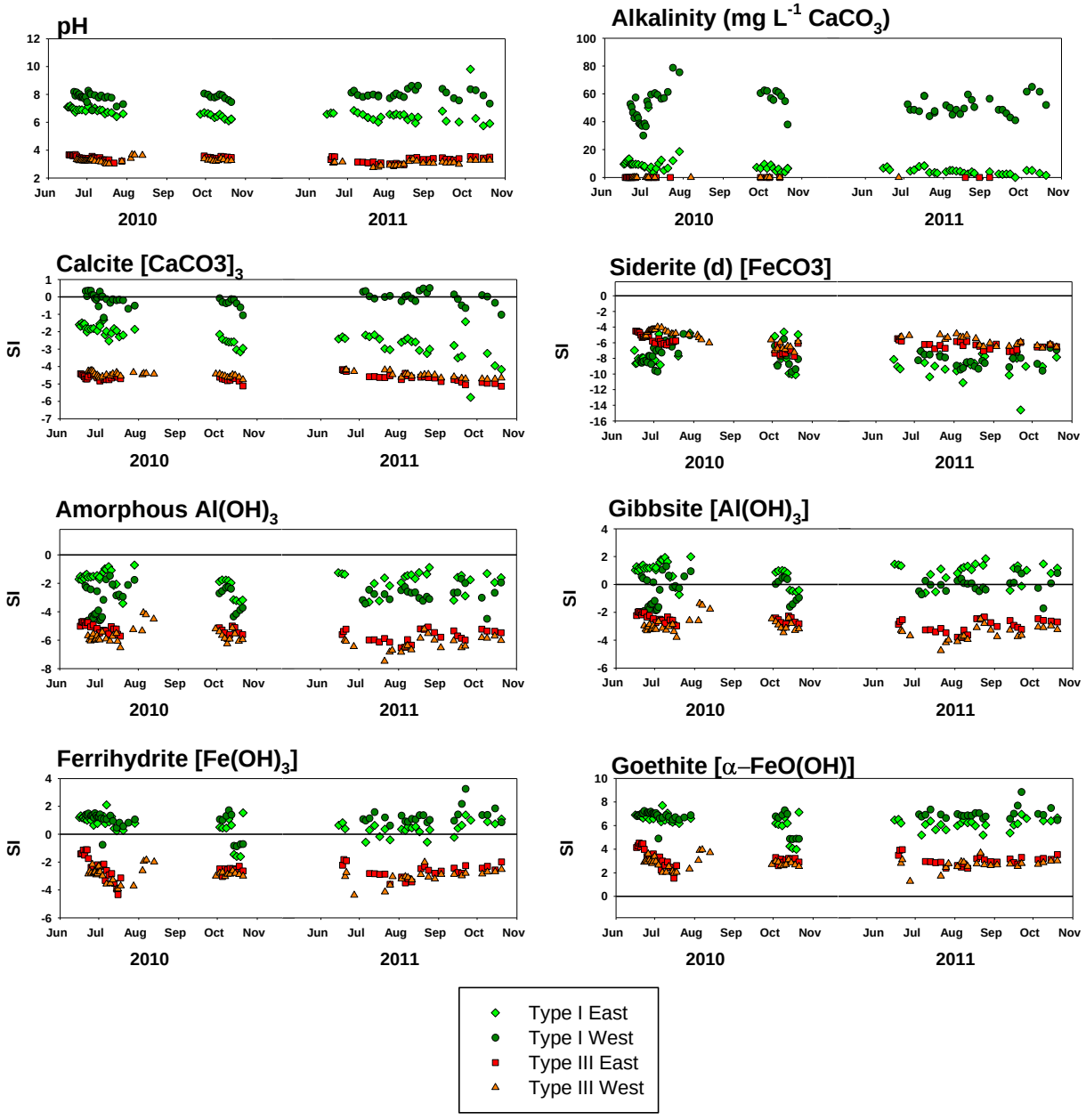

Figure 2-7: Time-series of blasting agents in Type I and III test pile basal drains.

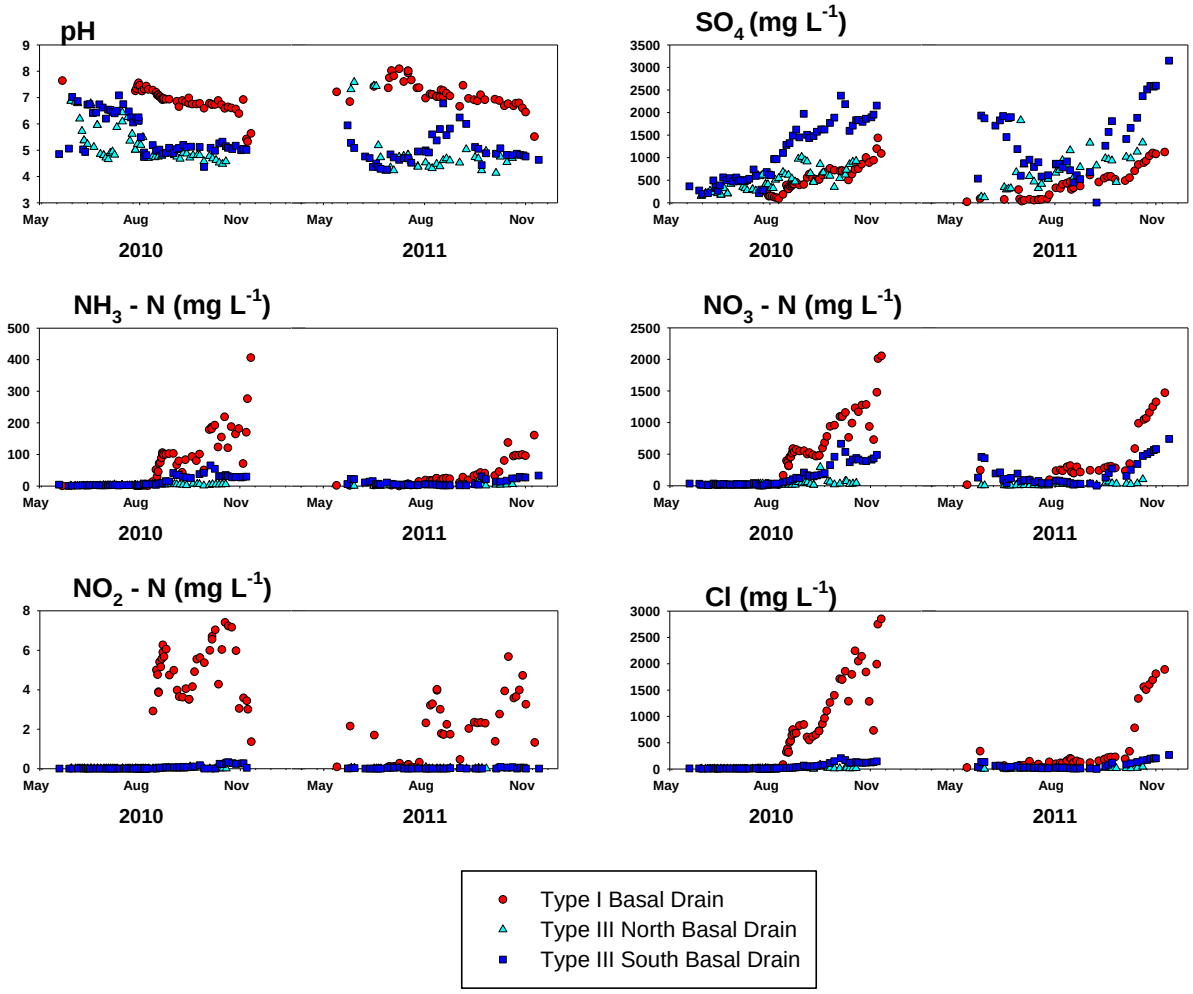

Figure 2-8: Time-series of SO_4^{2-} and sulfide oxidation products in Type I and III test pile basal drains.

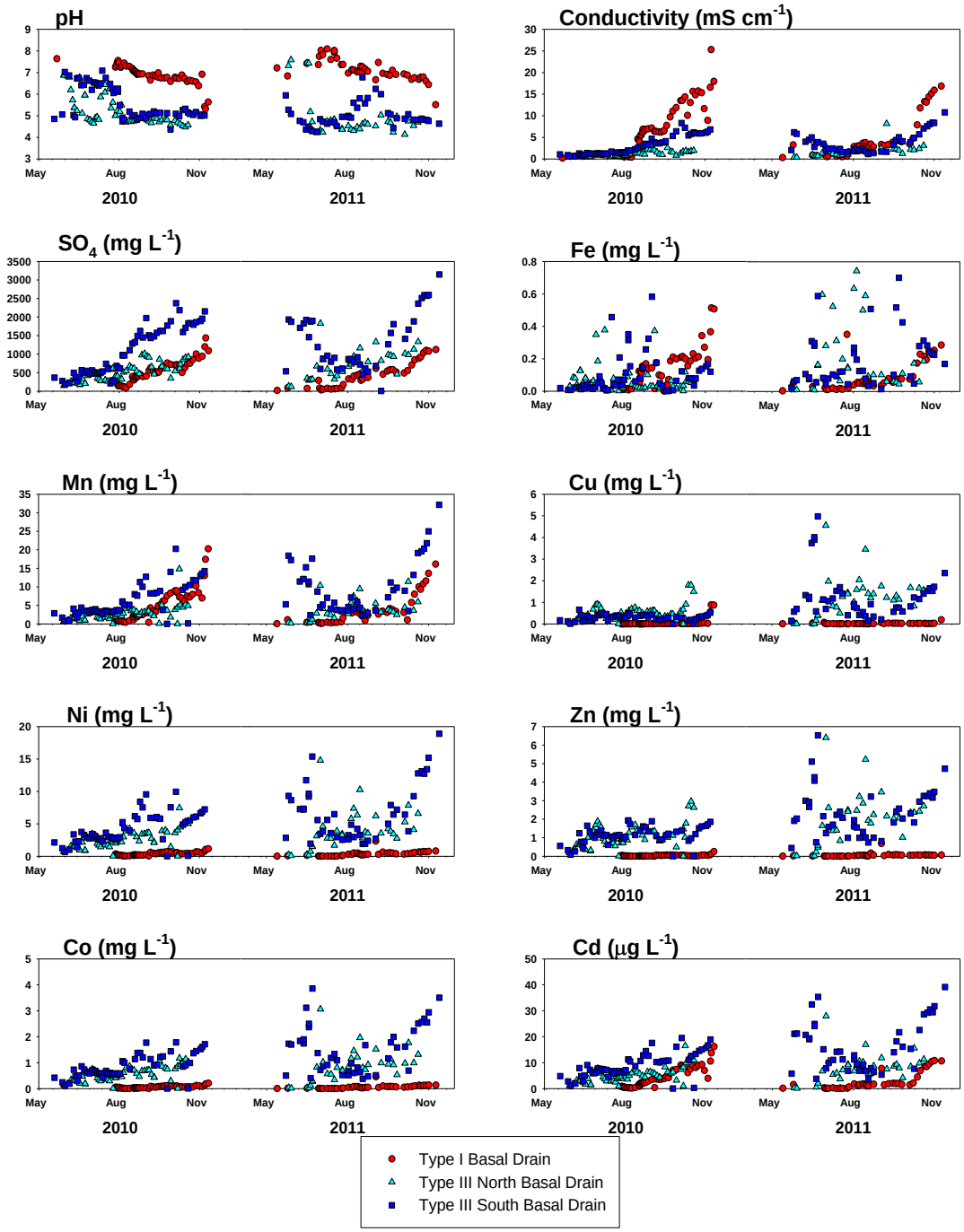

Figure 2-9: Time-series of major cations in Type I and III test pile basal drains.

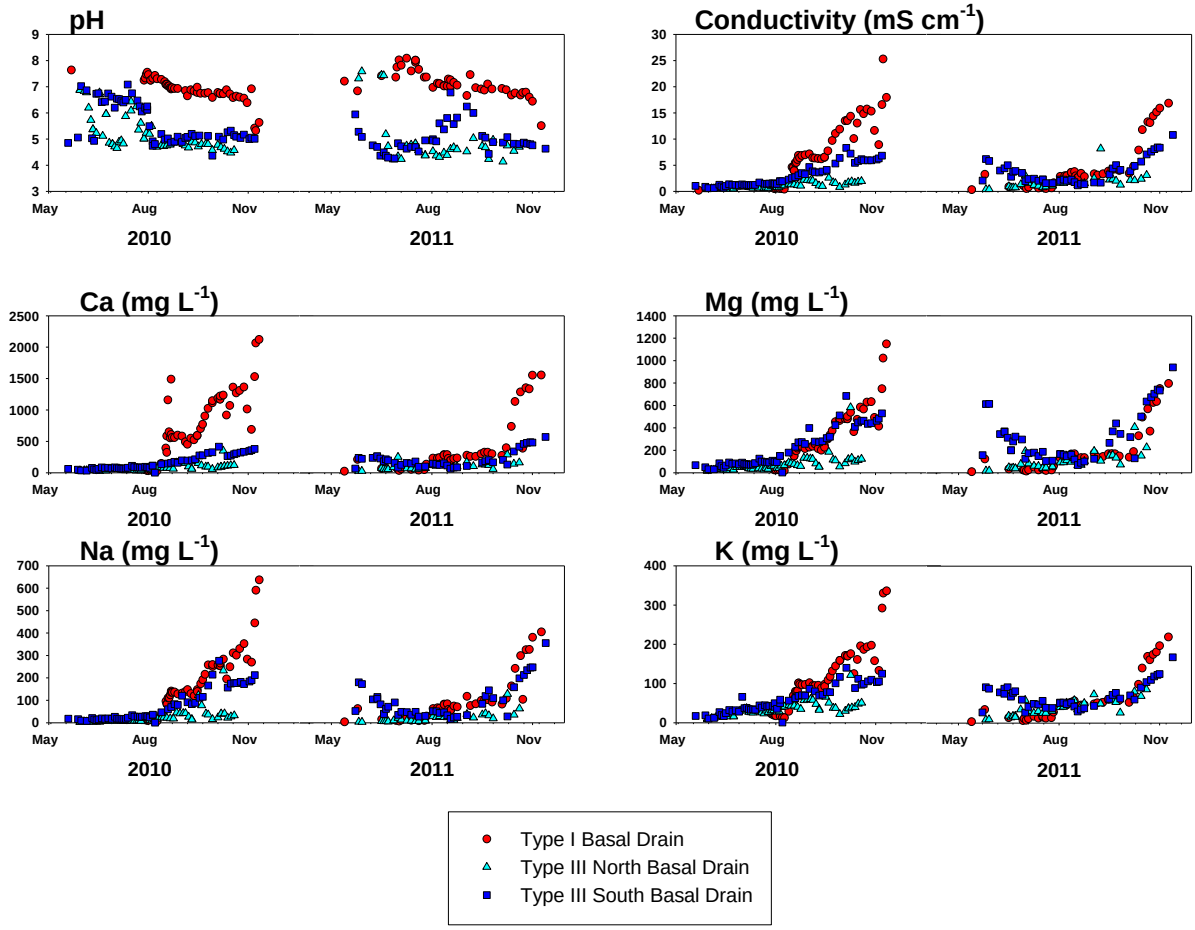

Figure 2-10: Time-series of pH buffering reactions with modeled saturation indices in Type I and III test pile basal drains.

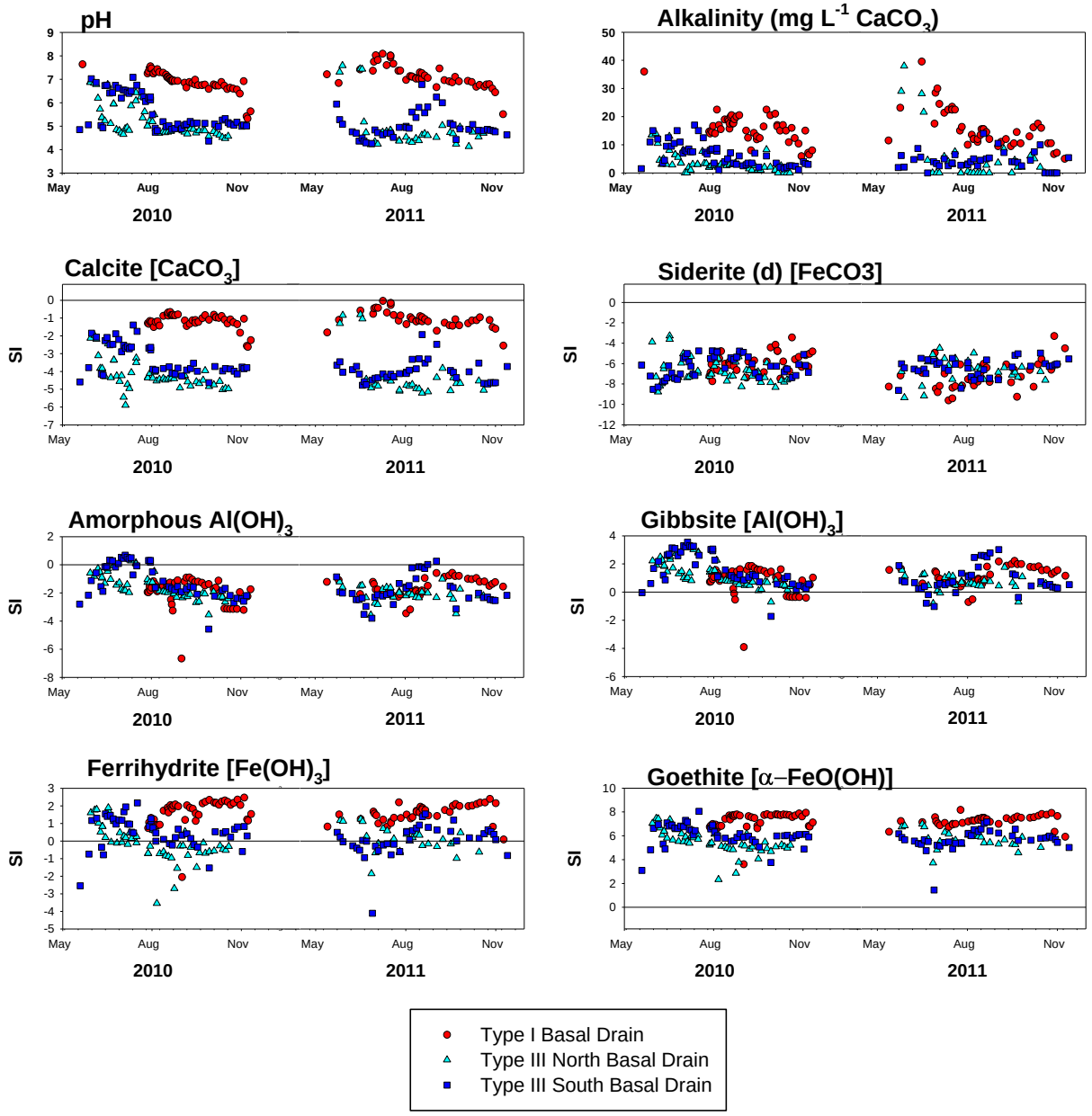

Figure 2-11: Time-series of blasting agents in the Covered test pile.

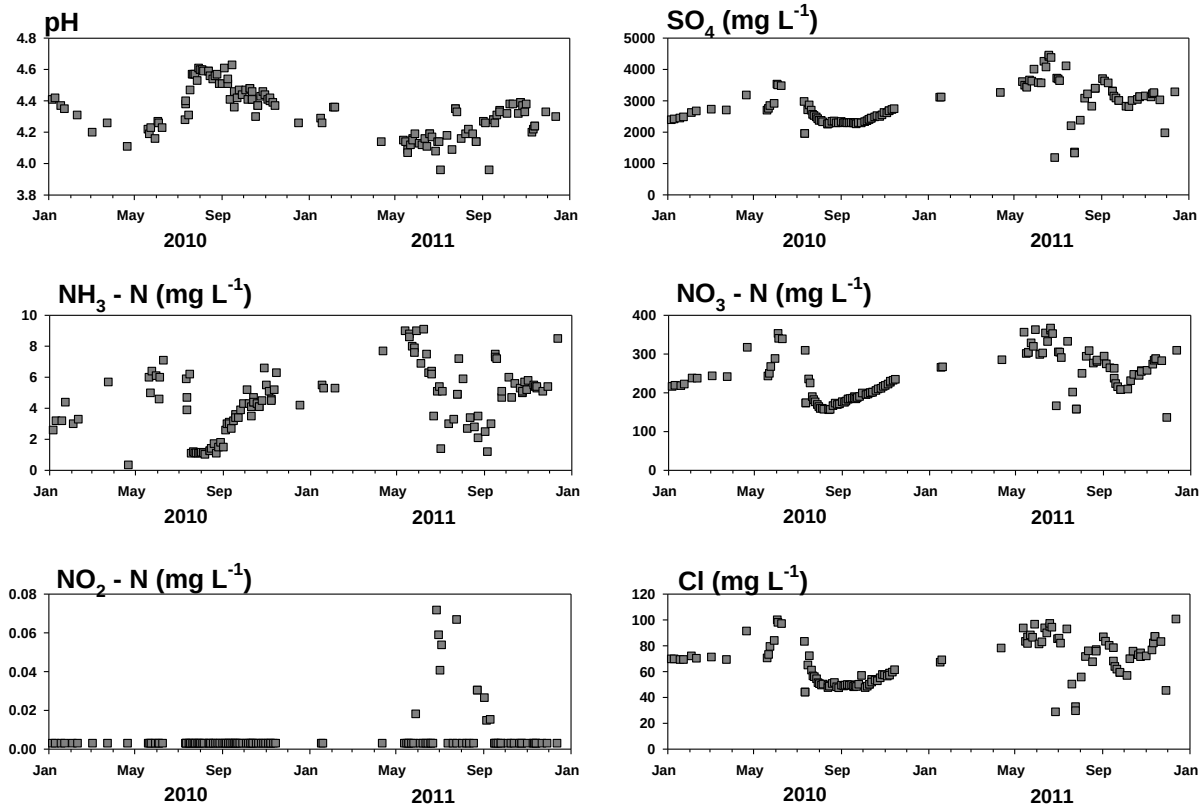

Figure 2-12: Time-series of SO_4^{2-} and sulfide oxidation products in the Covered test pile.

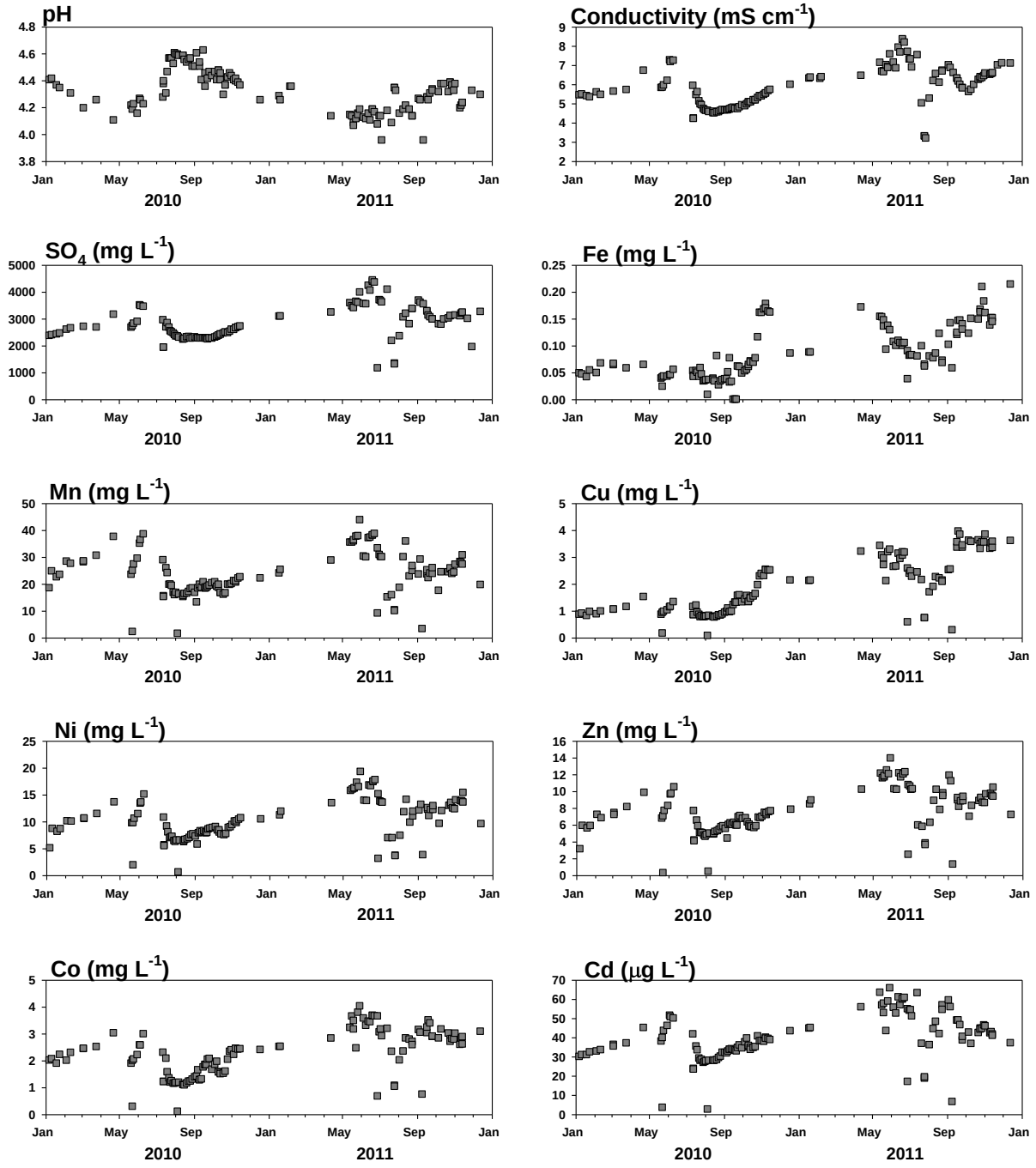

Figure 2-13: Time-series of major cations in the Covered test pile.

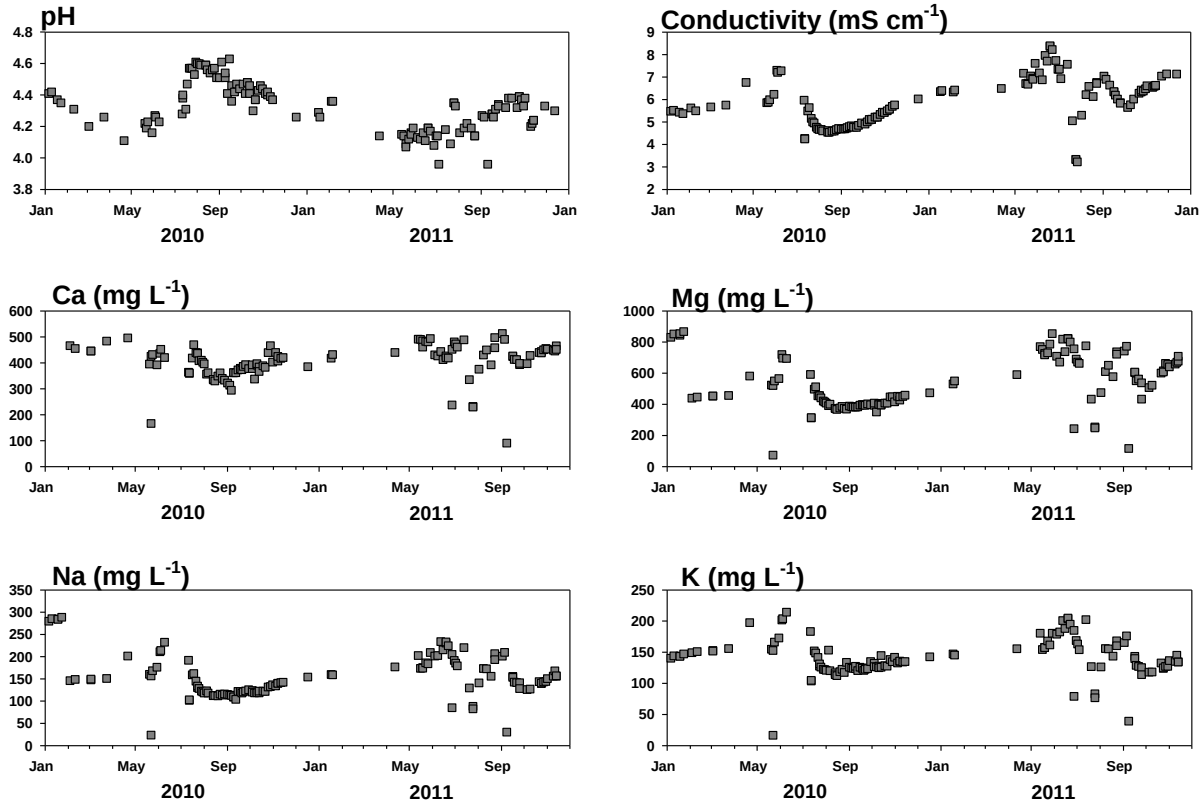

Figure 2-14: Time-series of pH buffering reactions with modeled saturation indices in the Covered test pile.

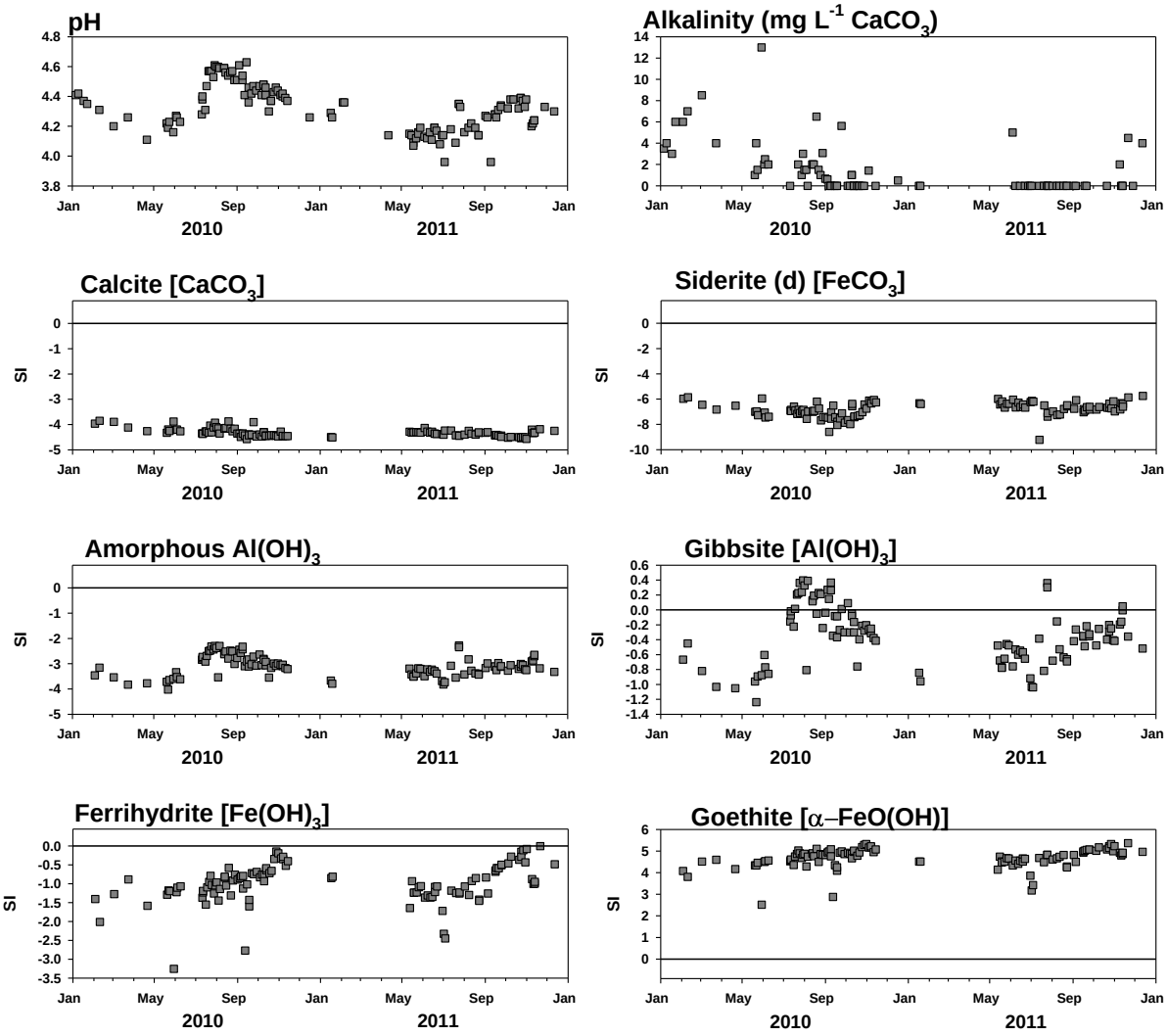

Chapter 3

Mineralogical and geochemical studies of a waste rock stockpile and experimental test pile in the Arctic

3.1 Introduction

Mine wastes containing sulfide minerals have the potential to generate low-quality drainage when exposed to atmospheric conditions, as infiltrating water can mobilize sulfide oxidation products to the surrounding environment. Many studies have been conducted exploring the environmental impact of mine tailings and the mineralogy associated with oxidation of sulfide minerals (Blowes & Jambor 1990; Jambor 1994; Jambor 2003; Moncur et al. 2005; Gunsinger et al. 2006). Fewer studies focus on the impacts related to surface storage of the large quantities of waste rock that can be generated (Stromberg & Banwart 1999; Lefebvre et al. 2001; Sracek et al. 2006). Waste rock is heterogeneous, with higher air permeability than mill tailings (Ritchie 1994; Amos et al. 2009), which presents a different set of challenges when developing initial mine plans and remediation strategies. Further consideration must be taken in northern environments as mining operations are often conducted in areas that extremely cold temperatures and permafrost. Studies of the effects of subaerial waste-rock

storage under permafrost conditions will be valuable as northern mining operations continue to expand.

A field-based study has been developed at the Diavik Diamond Mine (Diavik), with complementary laboratory studies at the University of Waterloo, examining the physical and geochemical responses of low-sulfide waste rock stored subaerially in the continuous permafrost region of the Northwest Territories, Canada. Although the sulfide content is low, the low neutralization potential of the waste rock requires that steps be taken to evaluate the potential for the generation of poor-quality drainage. Characterization of the early-stage mineralogical conditions within the waste-rock stockpile and the potential effects of permafrost formation on sulfide mineral oxidation processes can assist in evaluating the potential extent of future weathering in the freeze/thaw active zone. Assessing the quality of drainage that could be released to the surrounding environment as a result of sulfide-mineral oxidation is of particular importance due to the sensitivity of the lakes often adjacent or surrounding mines in the North (Pienitz et al. 1997).

Identification of early-stage sulfide mineral oxidation products can be difficult due to their low abundance, and fine-grained or poorly crystalline nature of these solids (Flemming et al. 2005). Identification is particularly difficult when attempting to isolate sulfide alteration products in the low-sulfide Diavik waste rock. Conventional identification techniques such as bulk powder X-ray diffraction (XRD) may not be effective for identification of sulfides or reaction products in Diavik waste rock, as the primary minerals mask the peaks from the

trace constituents (Jambor 2003). Use of advanced techniques such as scanning electron microscopy (SEM), micro x-ray diffraction (μ-XRD) and synchrotron-based analyses provide suitable supplements to optical microscopy when identifying the composition of reaction products generated by a sparse sulfide mineral assemblage. Application of synchrotron-based μ-XRD further assists in direct reaction product identification *in situ* by targeting reaction rims on individual sulfide grains.

3.1.1 Site description

Diavik is located 300 km northeast of Yellowknife, Northwest Territories, Canada, in the continuous permafrost zone, on a 20 km^2 island in the oligotrophic lake Lac de Gras. The mean annual air temperature measured from 1998 to 2007 was -9.1 °C with maximum daily averages of 27 °C in July and minimum temperatures of -44 °C in January/February (Environment Canada, 2012). Precipitation is minimal with an average of 280 mm falling in the region of the mine site, 60 % of which as snow (Environment Canada, 2012). The mine infrastructure includes two open pits and underground workings to mine three kimberlite pipe ore deposits. The kimberlite is hosted in Archaean country rock, which is composed of granite and granite pegmatite (~89%), irregular biotite schist xenoliths (~10%), and contributions from diabase dykes that crosscut the area (~1%) (Jambor 1997; Smith 2009). To access the kimberlite pipes and construct the open pits, significant amounts of country rock were blasted, excavated and dumped to form a waste rock stockpile that is expected to reach up to 120 Mt and a height of up to 80 m by the completion of mining operations.

During operations, the (Smith 2009) the stockpile is built as successive 40 m lifts of waste rock with stockpile slopes at the angle of repose of dumped waste rock (approximately 38°) (Smith et al. 2012a). During mining operations, the waste rock is segregated into three designations based on total S content. Type I waste rock contains < 0.04 wt % S, is composed almost entirely of granite, and is considered non-acid generating. Type II waste rock contains 0.04-0.08 wt % S, composes a very small portion of total waste rock removed, and has uncertain acid-generating potential. Type III waste rock contains > 0.08 wt % S and is considered potentially acid generating due to the sulfide content from the biotite schist contained in this designation. After segregation, waste rock is then dumped into separate locations in the operational stockpile.

For this study, samples of drill cuttings were collected from drill holes installed on the Upper Type III Waste Rock section of the Diavik stockpile (Figure 3-2, Figure 3-3) and made into thin sections for analysis. These samples were studied to determine the extent and nature of sulfide oxidation products occurring as a result of blasting and subsequent exposure to subaerial weathering. Mineralogical characteristics observed in thin sections were compared to water samples collected from an experimental test pile constructed of Type III waste rock (Smith et al. 2012a). The Type III test pile has a lined base measuring 50 by 60 m and is 15 m high constructed of waste rock with an average S content of 0.053 wt % S (Smith et al. 2012a; Smith et al. 2012b). The base of the test pile is graded such that the majority of water flow is discharged through basal drains running along the north and south sides of the

test pile designated the North and South basal drains. The Type III test pile was constructed in 2005 and 2006, and the geochemistry has been continually monitored from the first appearance of flow (Bailey 2012; Bailey et al. 2012; Smith et al. 2012c). The basal drain geochemistry from this test pile is appropriate for comparison to the mineralogical samples from the drill hole on the Upper Type III waste rock dump due to the similarity in S content and the similarity in time of exposure to weathering conditions. The Type III test pile may have undergone higher levels of water-rock interaction than the operational stockpile due to the smaller scale and application of artificial rainfall events (Bailey 2012; Neuner et al. 2012; Smith et al. 2012c). However, until deconstruction of the Type III test pile is conducted, *in-situ* mineralogical samples cannot be examined directly, and the drill-hole samples were used as an alternative.

3.2 Methods

3.2.1 Mineralogical methods

Samples for mineralogical analysis were collected from drill cuttings expelled to the surface of the Upper Type III area of the waste-rock stockpile during borehole drilling in May 2010. Three holes were drilled (designated FD-1, FD-2 and FD-3) to depths of 30-40 m and were located in a close triangular grouping approximately 150 m from the outer edge of the waste rock pile (Figure 3-2, 3-3). All three of the drill holes were instrumented for further characterization of the Upper Type III waste-rock dump. Instruments installed in each drill

hole include gas sampling ports, gas-permeability measurement devices and soil water solution samplers (SWSS) at specific depth intervals (see Appendix B). A centre stock of 5.08 cm diameter PVC pipe was used to support the instrumentation as it was lowered into each borehole. In FD-1, the PVC pipe is used for insertion of a thermal conductivity probe. The probe can be raised and lowered for discrete measurements (Pham et al. 2012). The pipe supporting instruments in FD-2 and FD-3 is equipped with screened intervals allowing for microbiological sampling to be conducted.

The drill cuttings for mineralogical study were collected at 4 m depth intervals from FD-1 (0-32 m) and at 2 m intervals from FD-3 (32-40 m). The drill casing used was 2 m in length, and as it was lowered, cuttings were blown up to the surface. This feature of the drilling allowed for discrete depth sampling. Cuttings were split with a riffle-splitter into sample sizes of less than 60 mL, which were appropriate for mounting in thin section (ASTM 2003). Thin section fractions were then freeze-dried to prevent any mineralogical modifications that could occur due to drying at high temperatures – for example; expansion of micaceous minerals or dehydration of compounds with multiple waters of hydration (ASTM 2010). Four samples from every second depth interval were prepared in three polished and one removable thin section, each by Vancouver Petrographics Inc, Langley, BC. Sections were prepared without the use of water to prevent further oxidation or dissolution of soluble mineral phases.

Polished thin sections were approximately 30 µm in thickness and examined by optical microscopy, SEM and synchrotron µ-XRF. The removable thin sections were approximately 100 µm thick to facilitate synchrotron-based analysis in both transmission and fluorescence modes. Splits of the cuttings samples made into thin section were prepared for bulk XRF and carbon/sulfur analysis. XRF analysis was conducted with a PANalytical Minipal 4 energy dispersive X-ray fluorescence (EDXRF) bench-top spectrometer equipped with an Rh X-ray tube (PANalytical, Quebec, Canada). Samples were pulverized and pressed into pellets for analysis. Calibration of the instrument was conducted using certified reference materials from the Geological Survey of Japan (JG-1a granodiorite, JG-2 granite) and from the China National Analysis Centre (NCS DC73301, NCS DC71303). The C and S concentrations were measured using an Eltra CS-2000 Carbon/Sulfur Determinator (Eltra GmbH, Germany). Samples were pulverized and heated inductively with approximately 1.4 g AR077 Fe chip accelerator and approximately 2.2 g AR008 Alphacell II tungsten flux (Alpha Canada Inc.). Multi-point calibration encompassing the expected concentration range of the waste rock samples was conducted daily using Alpha Steel Pin Standards (Alpha Canada Inc.).

Optical study of the polished thin sections was conducted at the University of Waterloo to examine general mineralogical trends and characterize the sulfide minerals. Identification and location of sulfide minerals exhibiting visible reaction rims was also conducted to identify grains for further study using more advanced techniques. Grains of

interest were examined with a variable-pressure scanning electron microscope (SEM) at CANMET Mining and Mineral Sciences Laboratories, Ottawa, ON to collect back-scatter electron (BSE) images of mineral grains, energy dispersive X-ray (EDX) spectra of minerals, coatings and surrounding features, and EDX element distribution maps. The variable-pressure SEM is designed for environmental samples, such as the thin sections for this study, because it does not require a coating of C or Au to be applied allowing the thin sections to be easily re-examined optically.

All synchrotron analysis was conducted at the Advanced Photon Source at Argonne National Laboratory, Argonne, IL at GSECARS beamline 13-BM-D. Samples for µ-XRD analysis were removed from the glass slides and placed between two layers of Kapton® tape before mounting on the instrument stage. Standard thin sections, used for µ-XRF element mapping and XANES, were mounted directly on the instrument stage with double-sided tape. All standards used for XANES analysis were powdered minerals placed between layers of polyethylene teraphthalate (PET) tape (Scotch® Magic Tape, 3M, St. Paul, MN) and mounted on the stage. For the purpose of µ-XRD analysis, the incident beam energy was refined to 21 keV (0.59040Å) with a sample to detector distance of approximately 500 mm. The beam energy, sample to detector distance, tilt angle and rotation were calibrated with a powdered CeO_2 standard. Resulting Debye-Scherrer XRD patterns were then processed with the fitting program Fit2D™ (Hammersly et al. 1996; Hammersley 1998). The resulting 2θ

plots were analyzed with the commercial software Materials Data Inc. (MDI) Jade and the International Centre for Diffraction Data (ICDD) database.

3.2.2 Geochemical methods

All water samples for geochemical analysis were collected from dedicated sampling cells at each sampling location. Sampling cells dedicated to basal lysimeters and the North Basal Drain were constructed of plexiglass with an approximate volume of 500 mL. The AZL, and Covered, Type I and South Basal Drain cells were open to the atmosphere with a capacity of 550 mL and connected through 3.18 cm PVC connectors to subsequent cells. These higher flow-capacity cells were installed between June 2010 and May 2011 to resolve problems associated with losses of flow data due to leaks in the sealed cells. Samples were collected through dedicated 0.635 cm PVC tubing using a new, clean syringe, triple-rinsed with sample water, and dispensed into triple-rinsed 60 mL HDPE wide-mouth bottles. Samples for analysis of dissolved cations, and anions were filtered with 0.45 µm cellulose syringe filters. Samples for analysis of dissolved cations were preserved at pH < 2 with analytical grade HNO_3. Samples for determination of anion concentrations were unpreserved. All samples were kept refrigerated at 4°C. Measurements of pH, E_h, electrical conductivity and temperature were conducted on unfiltered samples from each location on every sampling occurrence. The pH measurements were conducted using a Thermo combination electrode (Orion ROSS Ultra ® 8156, Thermo Scientific, USA). A three-point calibration was conducted with either pH 1.68, 4 and 7, or 4, 7 and 10 buffers, selected to encompass the

anticipated pH range of the sample. E_h was measured with a Thermo Orion platinum redox electrode (Orion 96-78; Thermo Scientific, USA) and checked against both Zobell (Nordstrom 1977) and Light (Light 1972) redox solutions. The redox measurements are presented E_h values with reference to the started hydrogen electrode (SHE). Electrical conductivity and temperature were measured with an Orion 3-Star Plus Conductivity meter calibrated with conductivity solutions in the sample range. Field alkalinity was measured on samples filtered through 0.45 µm cellulose filters using the Hach Digital Titrator with 0.16N H_2SO_4 cartridges and bromcresol green/methyl red indicator packets. Spectrophotometric analysis of water samples for concentrations of NH_3-N (Hach method 10031), Fe^{2+} (Hach method 8146), PO_4^{3-} (Hach method 8048) and H_2S (Hach method 8131) was conducted on filtered samples on site.

Analytical determinations on collected samples were performed at the University of Waterloo. Cation concentrations were determined for the elements Ca, K, Mg, Na, Si, Al, As, Ba, Be, Cd, Co, Cr, Cu, Fe, Mn, Mo, Ni, Pb, Sb, Se, Sr, Ti, U, and Zn. Concentrations were measured using a Thermo Scientific inductively coupled plasma-optical emission spectrometer (ICP-OES, iCAP 6000, Thermo Scientific, USA), for elements present at high concentration, and a Thermo Instruments ICP-mass spectrometer (ICP-MS, X-Series 2, Thermo Scientific, USA) for trace elements, with instrument blanks, sample duplicates and standard analysis included for QA/QC purposes. Concentrations of Br^-, Cl^-, NO_2^-, NO_3^-, and SO_4^{2-} anions were measured using ion chromatography (IC DX600; Dionex, USA).

3.2.3 Geochemical modeling

Interpretation of effluent geochemistry was facilitated by the use of the equilibrium/mass-transfer modeling program PHREEQCI. The WATEQ4F (Ball & Nordstrom 1991) database was used to determine the saturation indices of discrete mineral phases. Field measurements of alkalinity were input in units of mg/L $CaCO_3$ and measured Eh values were converted to pe to ensure compatibility with the PHREEQCI input format.

3.3 Results and discussion

3.3.1 Mineralogical study

The average S content from the two drill holes from which cuttings samples were taken (FD-1 and FD-3) was 0.050 wt % S (σ=0.028, n=24) with single measurements ranging from 0.0041-0.10 wt % S. This places the waste rock under the designation of Type II, similar to the waste rock used to construct the Type III test pile (0.053 wt % S) (Smith et al. 2012b). Although the waste rock falls into the Type II category, it is representative of waste rock that is segregated into the Type III category and placed locations of the stockpile designated for Type III rock deposition. These samples will be referred to as Type III waste rock throughout this chapter. The handling of waste rock over the course of operations, and variability in S content likely resulted in an average below the operational target of > 0.08 wt % S of Type III waste rock. The variability observed within and between samples from the drill hole

reflects the heterogeneity of the waste-rock stockpile, and is a consistent observation throughout the Diavik Waste Rock Project.

Previous studies found that the granite mineralogy is dominated by quartz [SiO_2] and K-feldspar [$KAlSiO_8$] with smaller amounts of albite [$NaAlSi_3O_8$], biotite [$K(Mg,Fe^{2+})_3(Al,Fe^{3+})Si_3O_{10}(OH)_2$] and muscovite [$KAl_2(Si_3Al)O_{10}(OH)_2$]. The biotite schist contains quartz, albite and biotite in varying amounts. The diabase dykes are considered to be volumetrically insignificant within the overall waste rock volume (Jambor 1997). XRF whole-rock analysis conducted on samples collected from FD-1 and FD-3 had oxide abundances consistent with samples of granite and biotite schist examined during initial mineralogical studies (Table 1) (Jambor 1997). Due to the very low overall sulfide content of the waste rock, standard bulk mineral identification methods, such as powder diffraction, cannot be used to determine the quantity and mineralogy of the sulfide minerals or the oxidation products (Jambor 1994). Iron oxides can also be particularly difficult to identify through conventional XRD techniques due to weak diffraction intensity (Herrera et al. 2008). Petrographic studies combined with advanced SEM and synchrotron-based techniques allow for a better understanding of the oxidation processes occurring in the waste rock at Diavik.

3.3.1.1 Optical analysis

Optical analysis focused on the sulfide mineral assemblage in the Type III waste rock collected from drill-hole samples on the Upper Type III portion of the waste-rock stockpile at Diavik. Initial optical analysis of the thin sections from the drill-hole cuttings samples

showed a mineralogical composition that is consistent with previous baseline mineralogical studies of Diavik waste rock (Jambor 1997; Blowes & Logsdon 1998). The samples are composed of a mixture of the granite and the biotite schist, which is consistent with the Type III designation of the waste rock in the drillhole location within the stockpile. In thin sections primarily composed of granite, sulfide minerals were present only in very small amounts and were generally small (20-50 μm), unaltered pyrite grains (Figure 3-5). Non-sulfide minerals were consistent with previous studies of granite samples, consisting primarily of quartz and plagioclase with small amounts of micaceous minerals (Jambor 1997). Similar unaltered grains of pyrite were also seen in thin sections with more heavily altered examples of pyrrhotite. As the samples were collected from drill-hole cuttings, sulfide grains may originate from within boulders, or other areas of the rock that have not been exposed to the atmosphere. This relationship between pyrrhotite and pyrite within a thin section may indicate that exposure to oxidative conditions had only been sufficient at this stage to alter pyrrhotite and not pyrite.

Thin sections containing greater amounts of pyrrhotite contained mineralogical contributions from the biotite schist as well as granite. In general, pyrrhotite grains were larger than pyrite, reaching widths of up to 1 mm in rare cases, with less-defined grain edges and more extensive alteration (Figure 3-6). Baseline studies of biotite schist mineralogy show that fresh samples do not show signs of alteration, but exposure to atmospheric conditions quickly causes oxidation of the pyrrhotite (Jambor 1997). The oxidation exhibited in the

pyrrhotite from the drill-hole thin sections is probably due to exposure to atmospheric conditions after dumping at the stockpile location. The pyrrhotite grains examined exhibited varying degrees of alteration, both along the depth of the drill hole and between samples within a single depth interval (Figure 3-6). There was no indication of sharp zonation designating changes in the extent of oxidation as a result of depth within the waste rock stockpile. Due to the relatively young age of the waste rock pile at the time of sampling, the variability in the extent of oxidation is likely indicative of conditions shortly after dumping. Significant changes within the waste rock stockpile may not be seen until several years after initial blasting and exposure (Ritchie 1994). These samples illustrate an intermediate stage of weathering of sulfide minerals, shortly after waste-rock disposal. As the waste-rock pile matures, the rate of sulfide mineral oxidation would be expected to slow below the depth of permafrost development, and continue seasonally in the upper freeze/thaw active zone. Because the majority of the waste rock in which the borehole was drilled was dumped in a short period of time, the lack of major differences in oxidation between sample depths is not unexpected.

Other occurrences of sulfide minerals in the biotite schist include pyrite as laths along the basal cleavage of biotite (Figure 3-7). There are occurrences of both altered and unaltered pyrite in biotite, usually consistent with the level of weathering observed on the biotite. The concurrent weathering of biotite and pyrite is another indicator of the current extent of alteration within the waste-rock stockpile. This observation is also consistent with

measurements that indicate increasing sulfate concentrations coincide with increased Mg and K concentrations in the Type III test pile basal drain effluent, as discussed in Chapter 2. Waste rock was deposited in the area of the Type III waste-rock dump in which the boreholes were drilled at approximately the same time as the Type III test pile was constructed. As a consequence, it is anticipated that the degree of weathering of the waste rock should be similar. Artificial rainfall events and tracer tests have been conducted on the Type III test pile, exposing it to proportionally larger amounts of flow, potentially resulting in greater water-rock interaction in the test pile than the Upper Type III dump. However, period of exposure to oxygen is similar and it is anticipated that the bore-hole samples act as a useful indicator of the style and extent of weathering prior to deconstruction of the Type III test pile in the final years of the Test Piles Research Project.

3.3.1.2 SEM studies

During the SEM examination of the waste rock samples, BSE images, EDX spectra and elemental maps of the sulfide mineral assemblages were collected to assess variations in the elemental compositions of sulfide minerals and reaction products seen along grain edges and within fractures. Varying degrees of oxidation were seen throughout the grains examined, in a manner that was consistent with the alteration patterns observed during the optical microscopy study. A common alteration pattern observed was shrinking-core alteration, in which the core of a pyrrhotite grain remains intact and Fe-(oxy)hydroxides form in varying thickness around the core (Figure 3-9). Also observed were various surface textures in

samples that exhibited alteration features evenly distributed across the entire grain (Figure 3-9). All of the sulfide-mineral grains examined showed at least minimal evidence of secondary reaction products surrounding the primary sulfide grain, regardless of the overall extent of oxidation. This observation is consistent with observations of rapid weathering of sulfide minerals in the Diavik waste rock assemblage (Jambor 1997).

Figure 3-8 illustrates a grain of pyrrhotite, which developed cracks which may be a result of oxidation followed by subsequent desiccation (Pratt, Nesbitt & Muir 1994), fracturing during drilling, or a result of rock blasting before dumping in the waste rock pile. This texture is common in the vadose zone as it undergoes wet and dry cycling promoting desiccation, which exposes fresh mineral surfaces to oxidative conditions and contributes to the acceleration of sulfide mineral weathering (Jambor 2003). Secondary precipitates have formed both around the edges of the grain and in the fractures. SEM-EDX elemental maps indicate that the alteration extends into many of the cracked areas of the grain, beyond the sharp borders. This observation, in conjunction with the presence of aluminum and silica in the voids, indicates the likelihood of Fe-(oxy)hydroxide formation and incorporation of Al and Si onto the secondary phase (Jambor 1994).

Based on the sulfide alteration index (SAI) developed by Blowes and Jambor (1990), none of the sulfide grains and thin sections examined reached a point in the index higher than 4-5. This index categorizes the extent of sulfide oxidation in a sample on a scale from zero to ten. A sample with a rating of zero would show no oxidation of the sulfide minerals and at

level ten both pyrite and pyrrhotite would be completely obliterated. In the drill hole samples, pyrite was still present and showed little alteration, and pyrrhotite weathering had only progressed to complete oxidation in rare mineral grains from drill-hole samples (Figure 3-6). Similar to the observations from the optical analysis, there was little consistency in weathering between grains within a thin section, within a depth interval, or between the depth intervals examined with the SEM. The absence of consistent trends is a consequence of both the inherent heterogeneity of waste rock stockpiles (Ritchie 1994), and the method of sample collection from drill cuttings, which may have provided sulfides from areas not directly exposed to subaerial weathering.

3.3.1.3 Synchrotron analysis

Several sulfide grains which exhibited visible alteration features were identified with a reflected light microscope for further analysis with synchrotron-based techniques. The goal of the synchrotron study was to characterize the mineralogy of secondary reaction products surrounding sulfide grains, by collecting µ-XRD patterns of small discrete areas, and to examine the distribution of metals using µ-XRF. High-resolution µ-XRF elemental distribution maps were collected for each of the sulfide mineral grains subsequently examined with µ-XRD, in order to specifically determine the distribution of Fe, Ni, Cu and Zn within each grain, and to delineate locations for µ-XRD characterization. The sensitivity of these measurements required precise determination of the location of oxidation and elemental features within each grain, which was provided by the µ-XRF maps. Elemental

maps and μ-XRD transects were collected from six individual sulfide mineral grains. The quality of the resulting Debye-Scherrer rings collected from each of these transects varied between grains and along individual transects themselves. Intensity variations and background interference in some of the patterns made them difficult to analyze and account for deviations quantitatively (Majzlan et al. 2011). In some of these cases, the rings contained bright spots that overpowered lower-intensity cohesive ring patterns, and in others there may have been insufficient randomly oriented crystallites to produce a definitive diffraction pattern (Klug & Alexander 1954; He 2003; Flemming et al. 2005). One of the transects that produced clear Debye-Sherrer patterns is shown in Figure 3-10. The grain is oxidized and the μ-XRD pattern collected near the grain edge shows the presence of marcasite, an early stage oxidation product of pyrrhotite (Blowes & Jambor 1990).

In many cases where reference patterns were successfully matched to the μ-XRD patterns collected at the APS, it can be seen that the reference peak intensities do not match the experimental peak intensities. This occurs because the reference patterns are collected from powder diffraction samples where the minerals have been ground and distributed such that multiple randomized crystal orientations are exposed to the incident X-ray beam (Klug & Alexander 1954; He 2003). In the case of μ-XRD, the sample exposed to the incident beam is much smaller and has not been optimized for multiple random crystal orientations. The preferential orientations exposed give experimental intensities that do not correspond to the reference samples (He 2003). In several instances, μ-XRD analysis produced Debye-

Scherrer ring patterns with high intensity spikes due to monocrystalline contributions along barely discernible rings (Figure 3-11). This pattern was collected from an unaltered grain of pyrite which would have presented few crystal orientations to the small footprint of the synchrotron beam for µ-XRD. Other complications arise from processing XRD patterns with broader humps as opposed to sharp peaks, which occur as a result of amorphous phases in the diffraction area (Klug & Alexander 1954; Courtin-Nomade et al. 2010)

3.3.2 Type III basal drain aqueous geochemistry

Due to the scale of the Upper Type III waste rock pile, the location of the drill holes, and the lack of drainage produced from the full-scale pile; it was not feasible to examine the geochemical and mineralogical properties of this system together. Additionally, deconstruction of the Type III test pile for the purpose of collecting mineralogical samples for comparison to drainage geochemistry was not possible as it would prevent continued monitoring of the Type III test pile evolution. The waste rock used to construct the Type III test pile and the Upper Type III waste rock dump have similar S contents and have been exposed to subariel weathering for similar lengths of time. The geochemistry from the Type III test pile basal drains and the relationship to the mineralogical observations from the Upper Type III dump will be discussed, as the results are most applicable to the waste rock samples from the drill hole. A comprehensive geochemical report of the test piles was previously described in Chapter 2.

3.3.3 Acid neutralization

As discussed in Chapter 2, effluent water samples and PHREEQCI equilibrium calculations suggest that acid generated by sulfide oxidation in the Type III test pile is neutralized by dissolution of Al-(oxy)hydroxides and Fe-(oxy)hydroxides. Mineralogical study by optical and SEM microscopy revealed the presence of secondary reaction products surrounding many of the sulfide grains examined in thin section. SEM-EDX elemental mapping of sulfide grains showed that the phase consistently contained Fe, Al and Si, which are common in amorphous and crystalline phases surrounding oxidized sulfides (Jambor 1994). Many of the non-sulfide grains also showed evidence of accumulation of secondary phases often containing Si, Al, and K, which could be a product of concurrent weathering of micaceous minerals in the waste rock. Presence of these Al- and Fe-(oxy)hydroxide phases is consistent with the results of the equilibrium calculations for the Type III test pile effluent (Figure 3-12). Comparison of dissolved Al and Fe concentrations and saturation indices of (oxy)hydroxides and the accumulation of Al in the secondary phases surrounding the primary sulfide mineral grains indicates that these phases provide secondary mineral controls on metal concentrations in the effluent samples.

3.3.4 Geochemical modeling and secondary reaction products

Results from equilibrium modeling of secondary phases that could possibly form within the waste rock pile were compared to mineralogical observations from the Upper Type III waste rock dump. In general, it would be expected that phases deemed unlikely to form within the

test pile would be less likely to form at the Upper Type III dump, because the amount of water that has contacted the waste rock in the test piles is significantly greater than that which has contacted the rock at various depths of the drill hole.

3.3.4.1 Nickel and Cobalt

The primary source of Ni and Co in the Type III test pile basal drain effluent is the oxidation of pyrrhotite, which has an average elemental composition of $Fe_{0.852}Ni_{0.004}Co_{0.001}S$ in the Diavik waste rock. (Jambor 1997). Peak concentrations of Ni and Co were consistently reached at the end of each field season after the test pile had thawed completely, the rate and extent of sulfide oxidation throughout the test pile reached a maximum, and flow had decreased (Table 3-2, Figure 3-13). Equilibrium calculations with PHREEQCI suggest that there were no secondary mineral precipitates of Ni or Co forming throughout the system (Figure 3-12). This is consistent with mineralogical observations from the Upper Type III waste rock dump location which showed no evidence of Ni or Co concentrations surrounding mineral grains.

3.3.4.2 Copper

Dissolved Cu detected in the effluent from the Type III test pile basal drains was primarily a result of the oxidation of chalcopyrite (Figure 3-14). Copper concentrations also peak at the end of each flow season in 2010 and 2011 (Table 3-2, Figure 3-13). Equilibrium calculations show that the Type III test pile basal drain effluent remained undersaturated with respect to

all secondary Cu phases in the WATEQ4F database. The secondary Cu phases brochantite and malachite approached, but did not achieve saturation in the Type III South basal drain when mid-season pH reached nearly neutral levels (Figure 3-12). Mineralogical investigation showed no traces of secondary precipitates forming from Cu oxidation.

3.3.4.3 Zinc and Cadmium

Oxidation of spahlerite contributes Zn and Cd to the Type III test pile effluent. Traces of sphalerite were seen throughout mineralogical investigations, with one typical example shown in Figure 3-15. Maximum concentrations in the effluent were consistently achieved at the end of each field season, following established historical trends (Table 3-2). Equilibrium calculations using PHREEQCI indicate that the effluent water from both of the Type III test pile basal drains remained undersaturated with respect to secondary minerals containing Zn or Cd (Figure 3-12). In addition, mineralogical investigations did not reveal the presence of secondary Zn or Cd precipitates.

3.4 Summary and conclusions

The waste rock sampled from the Upper Type III waste-rock stockpile at Diavik has undergone oxidative conditions sufficient to cause the formation of early secondary oxidation products surrounding sulfide grains examined in thin section. Advanced techniques including SEM-EDXA and synchrotron-based analysis were utilized in determining the nature and extent of sulfide oxidation occurring within the low-sulfide waste rock. Distinct zonation of

weathering was not observed throughout the 40 m sampling depth, indicating that the formation of permafrost at depth has not yet affected oxidation rates. Oxidation in the stockpile is expected to be equal to or less than what would be observed in the Type III test pile due to the increased water-rock interaction within the test pile. The low concentration of carbonate minerals within the waste rock limits the acid neutralization potential causing a decrease in pore water pH as measured within the Type III test pile as sulfide oxidation increases throughout each thaw season. The acidic effluent generated by sulfide oxidation is neutralized by dissolution of Al and Fe(oxy)hydroxides at a pH below neutral. Geochemical modeling indicates that there are no secondary mineral controls on the dissolved concentrations of Cu, Cd, Ni and Zn, nor was there evidence of secondary phases during mineralogical investigation. Mineralogical analysis during the deconstruction phase of the Type III test pile will also be useful for comparison to weathering rates within the operational waste-rock stockpile.

3.5 Figures

Figure 3-1: Diavik Diamond Mine site in the Northwest Territories, Canada. Location of the Test Piles and drill hole installation indicated.

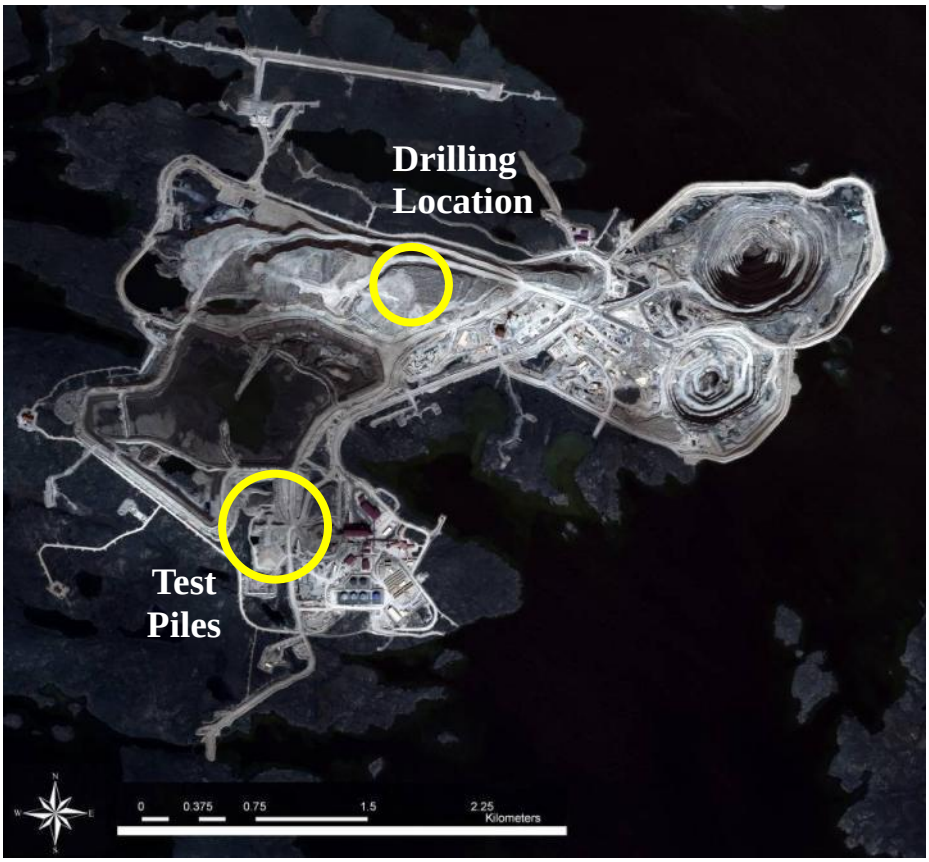

Figure 3-2: Location of FD-1, FD-2 and FD-3 drill holes installed at the Upper Type III waste rock dump in May 2010.

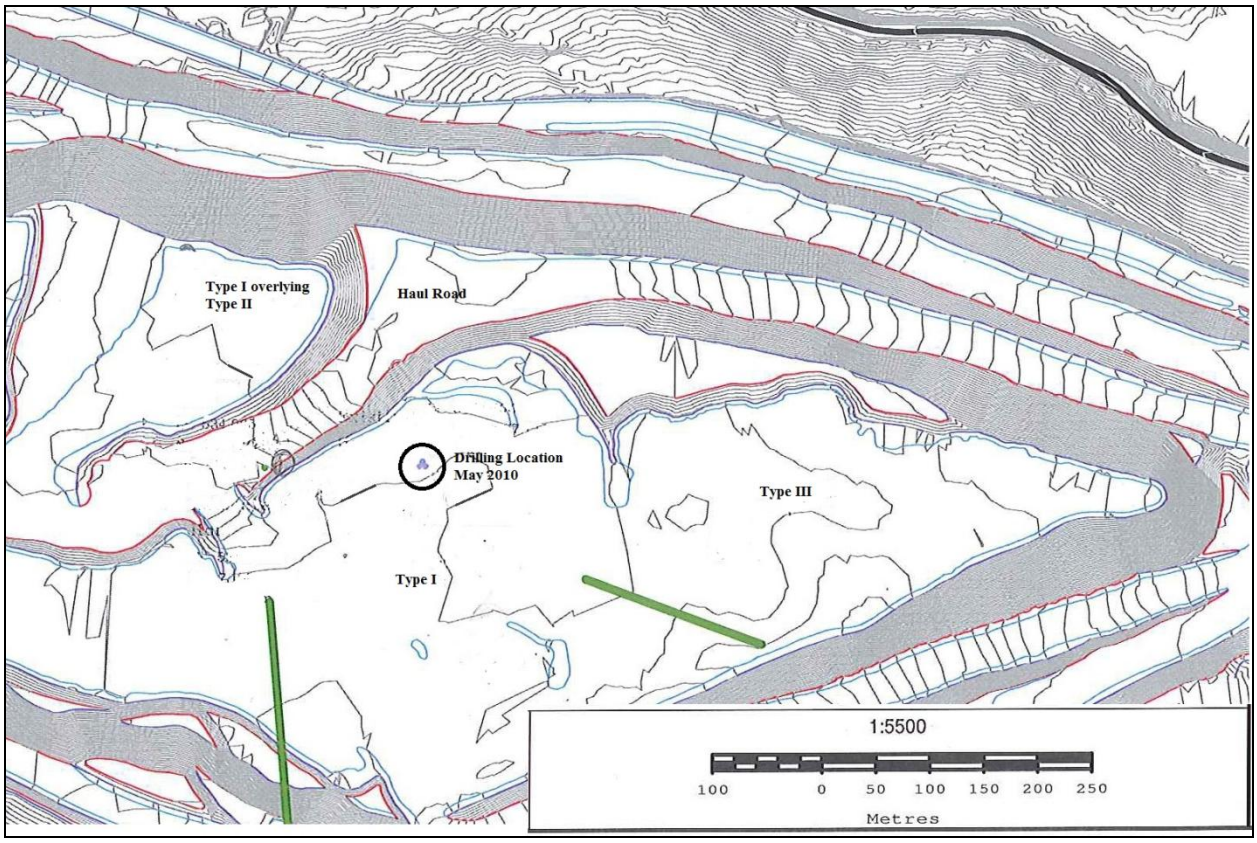

Figure 3-3: Drill hole installation by DNX drilling on the Upper Type III waste rock dump in May 2010.

Figure 3-4: Type III test pile. Waste rock used in construction has similar average S content and exposure time as the drilling location at the Upper Type III waste rock dump.

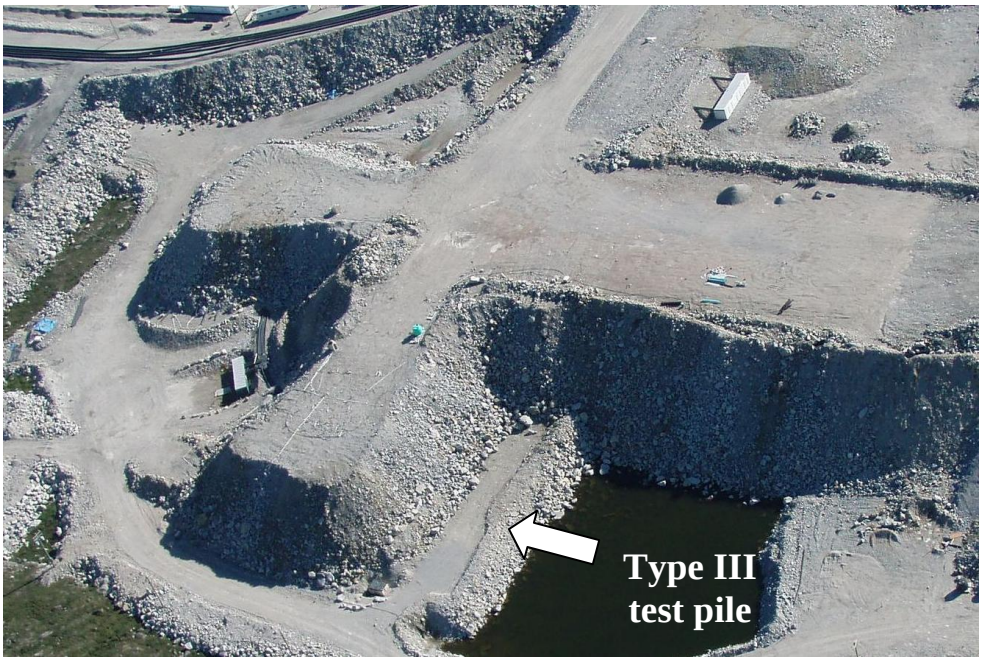

Figure 3-5: Typical examples of small pyrite grains seen throughout mineralogical examination under reflected light. Depth interval origins of each grain, clockwise from upper left are: 8-12 m, 8-12 m, 0-4 m, 16-20 m.

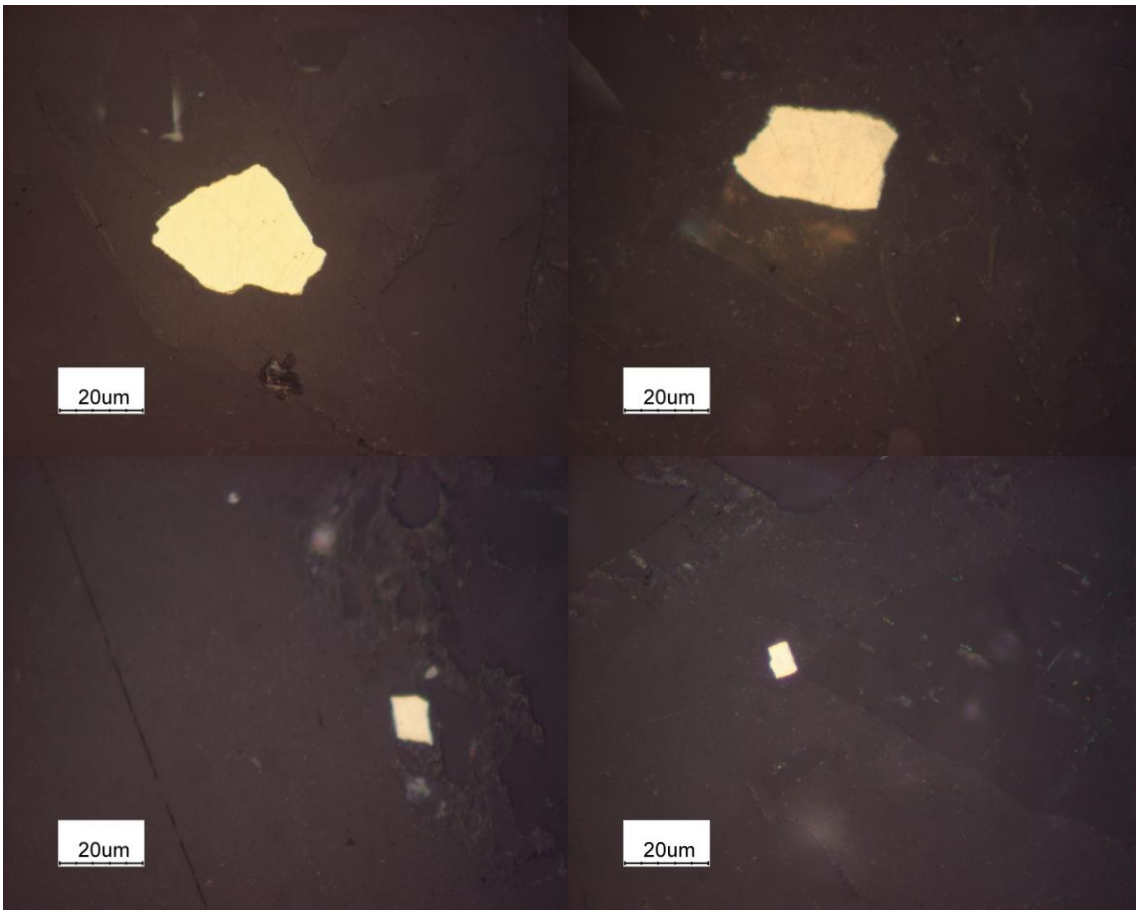

Figure 3-6: Examples of varying oxidation in pyrrhotite from the Type III drill hole installation under reflected light microscopy. Upper left grain shows little oxidation whatsoever, whereas upper right shows oxidation in parallel lineation. The lower two pyrrhotite grains have been almost completely oxidized. Depth interval origins, clockwise from upper left are: 24-28 m, 8-12 m, 16-20 m, 36-38 m.

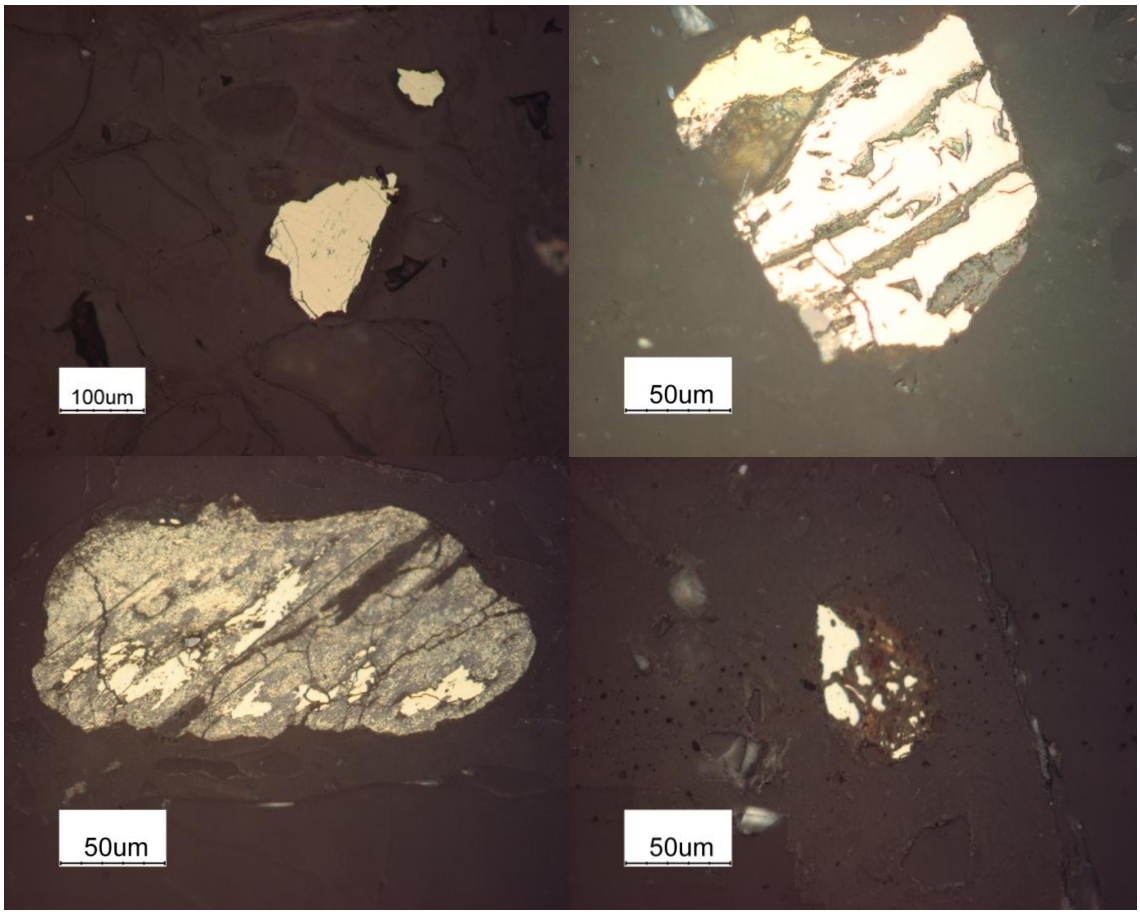

Figure 3-7: Examples of pyrite seen along basal cleavage of biotite. Upper images are reflected light photomicrographs, and lower images are SEM-BSE photos. Depth interval origins, clockwise from upper left are: 24-28 m, 38-40 m, 36-38 m, column sample.

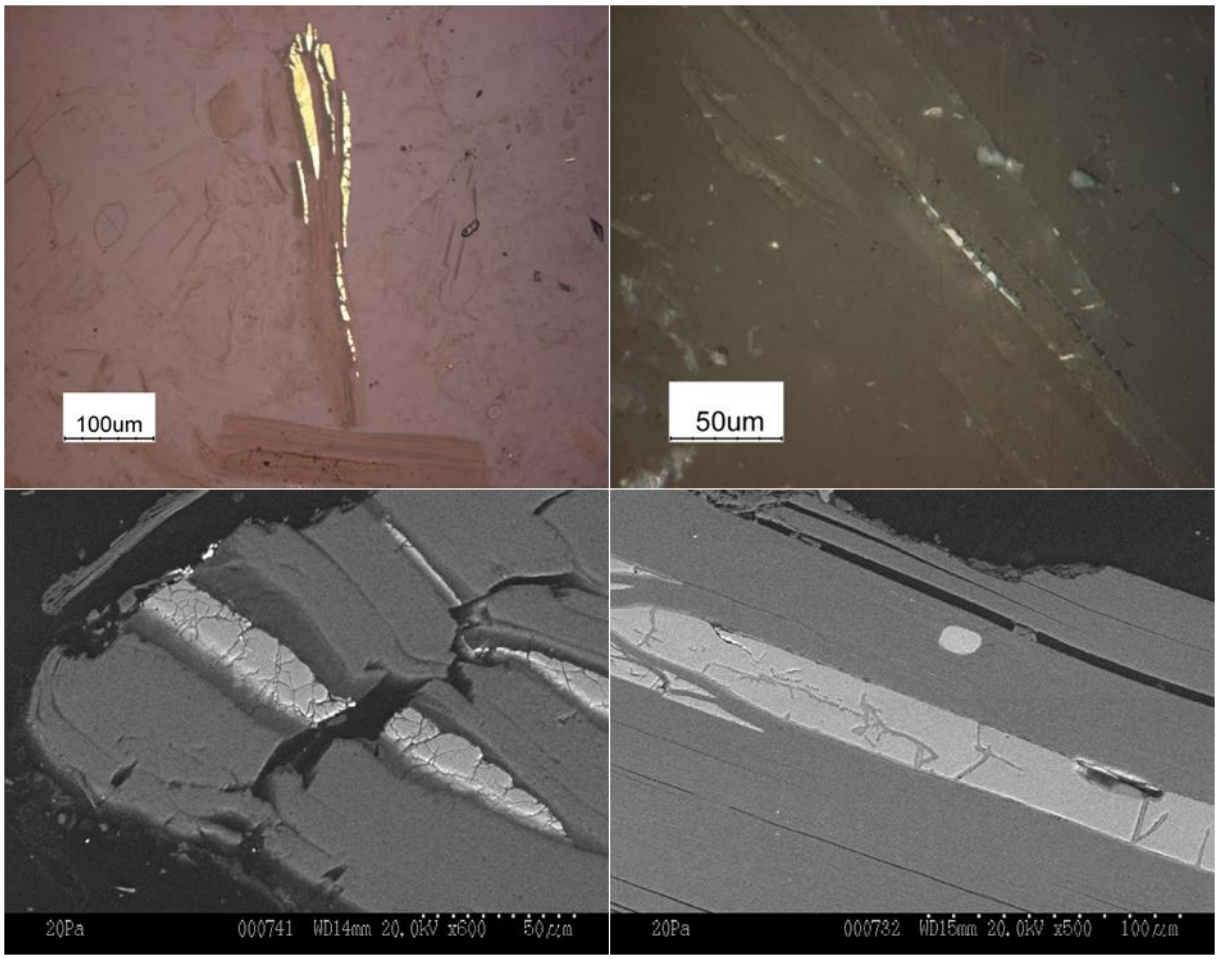

Figure 3-8: Evidence of cracks and oxidation features in a grain of pyrrhotite from the 16-20 m depth interval of the FD-1 drill hole. The upper images are a reflected light photomicrograph and SEM-BSE image of the grain with a closer magnification of the cracks to the right. Lower images are from EDX elemental mapping of the magnified area, where brighter areas indicate higher concentrations of each element.

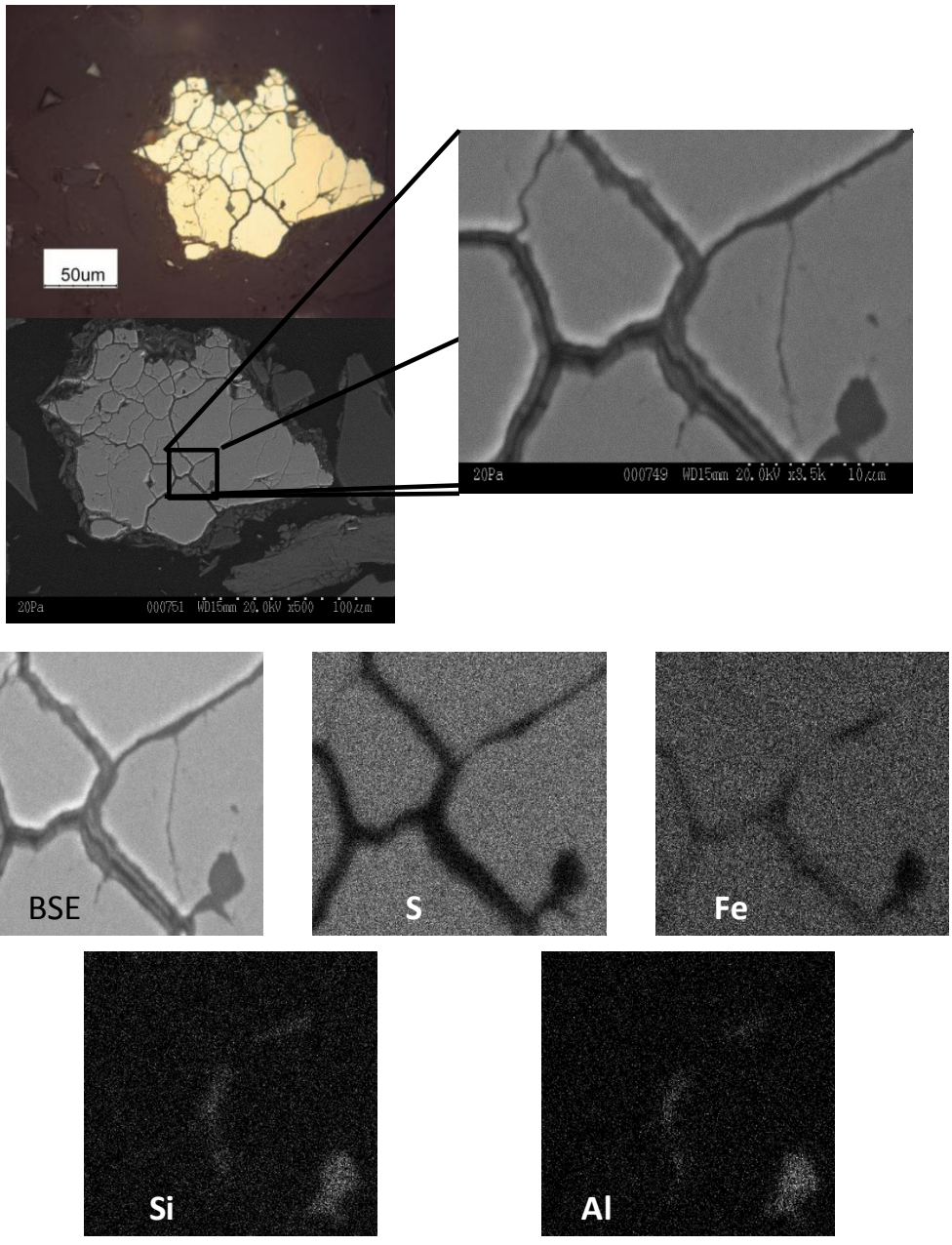

Figure 3-9: The upper SEM-BSE images and elemental maps show a sulfide grain with oxidation features shown across the surface of the grain. The lower SEM images show a pyrrhotite grain with classic shrinking-core weathering patterns. Both grains are from the 16-20 m depth interval.

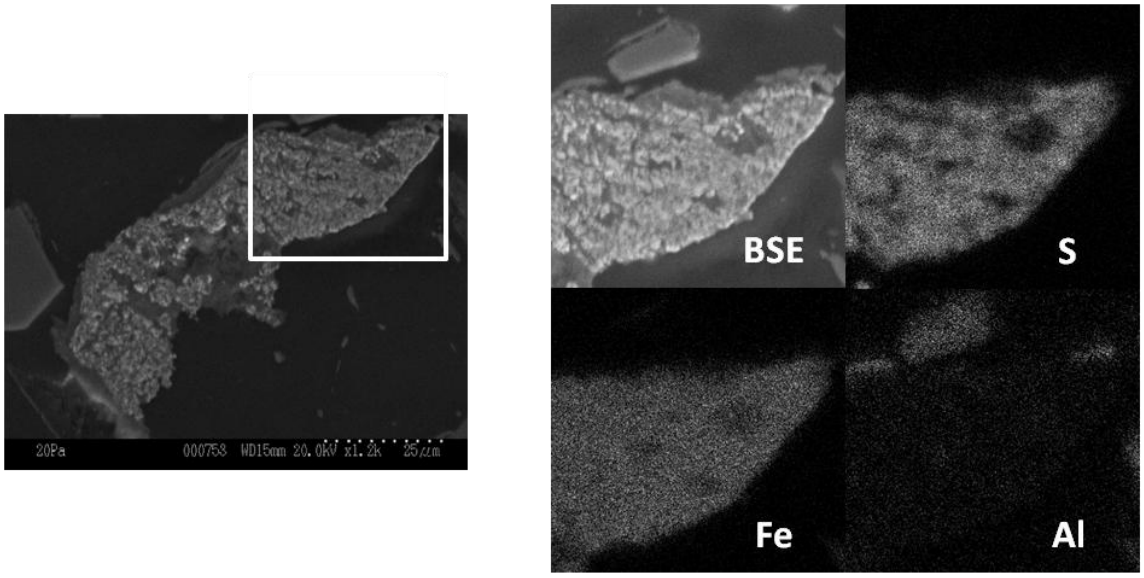

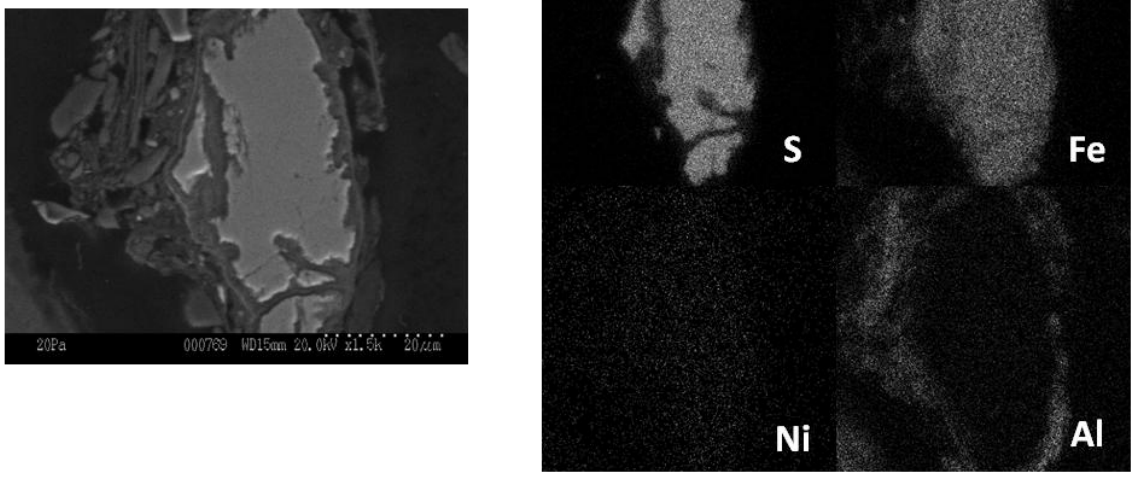

Figure 3-10: Upper images are μ-XRF elemental maps collected at APS. Below is a Debye-Scherrer μ-XRD ring spectrum collected from the edge of the grain showing the presence of marcasite and kaolinite in the corresponding processed two-theta plot.

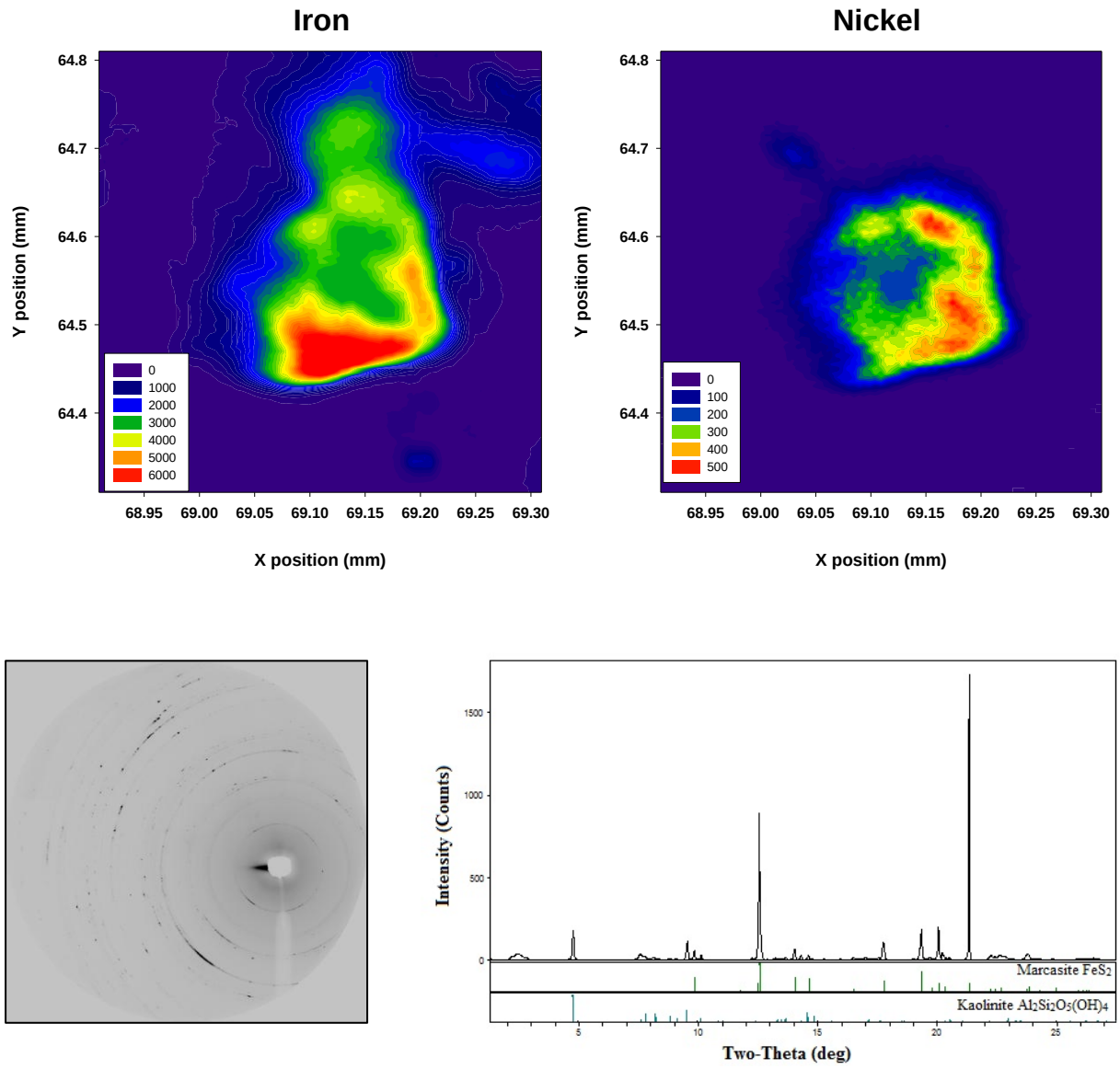

Figure 3-11: Several of the μ-XRD Debye-Scherrer spectra collected contained intensity variations that caused spotty ring patters similar to the spectrum below. Background removal and compensation for these variations was difficult to accomplish in order to process the images into two-theta diffraction plots. In this example, the intensity peaks are due to reflections from pyrite crystals exposing minimal crystal orientations to the synchrotron beam.

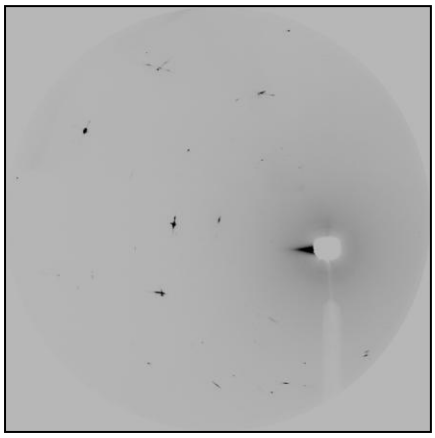

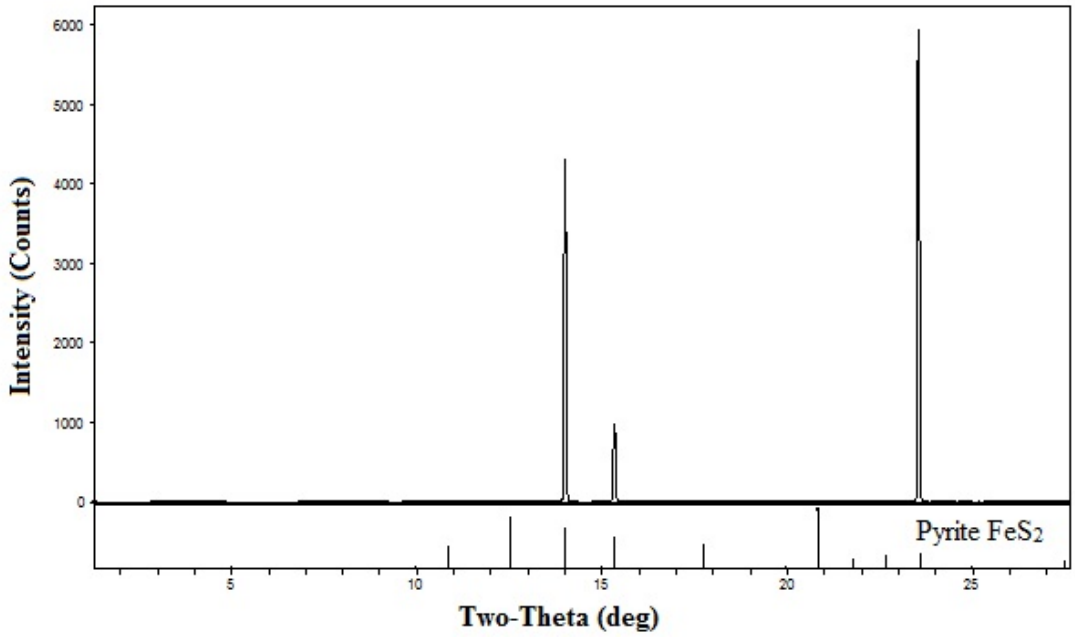

Figure 3-12: Time-series of pH buffering species and potential secondary oxidation products with modeled saturation indices. Open circles represent the Type III test pile north basal drain and closed squares represent the Type III test pile south basal drain.

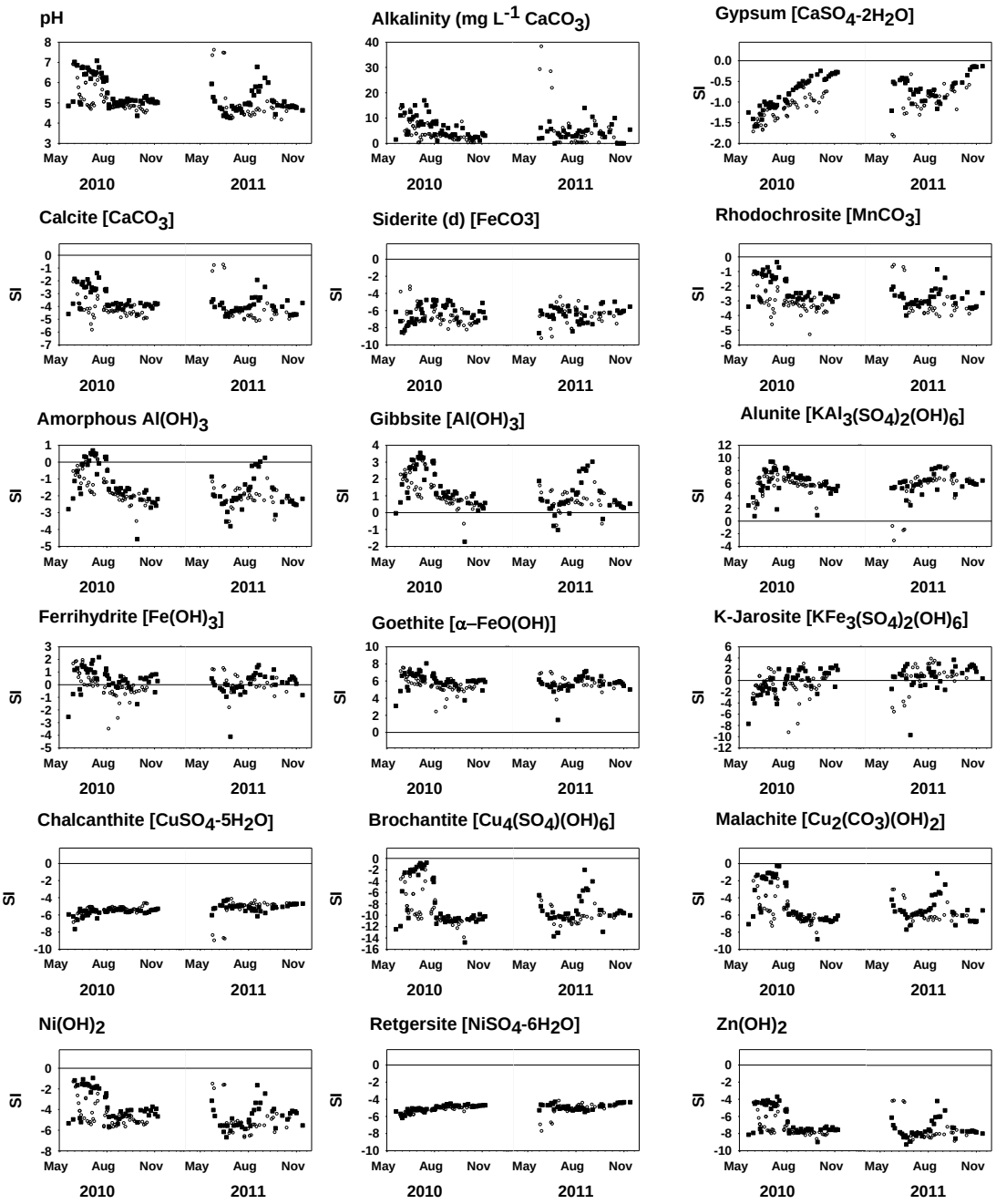

Figure 3-13: Time-series of geochemical parameters and dissolved metals in the Type III test pile. Open circles represent the Type III north basal drain and closed squares represent the Type III south basal drain.

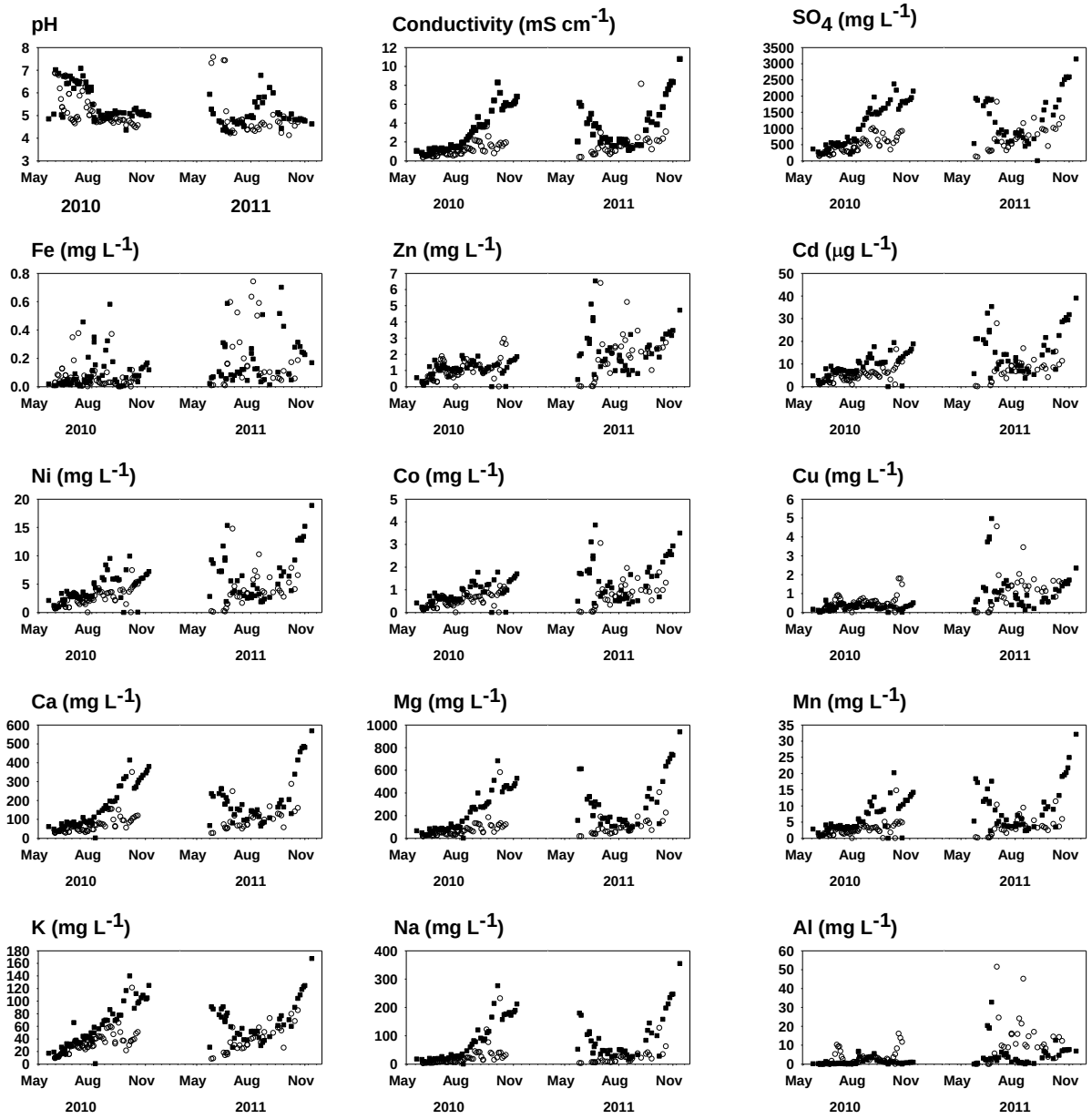

Figure 3-14: SEM-BSE image and EDX elemental map of a sulfide grain at the 16-20 m depth showing the presence of chalcopyrite along the grain edges. Chalcopyrite within the waste rock at Diavik is a source of Cu in the Type III test pile effluent.

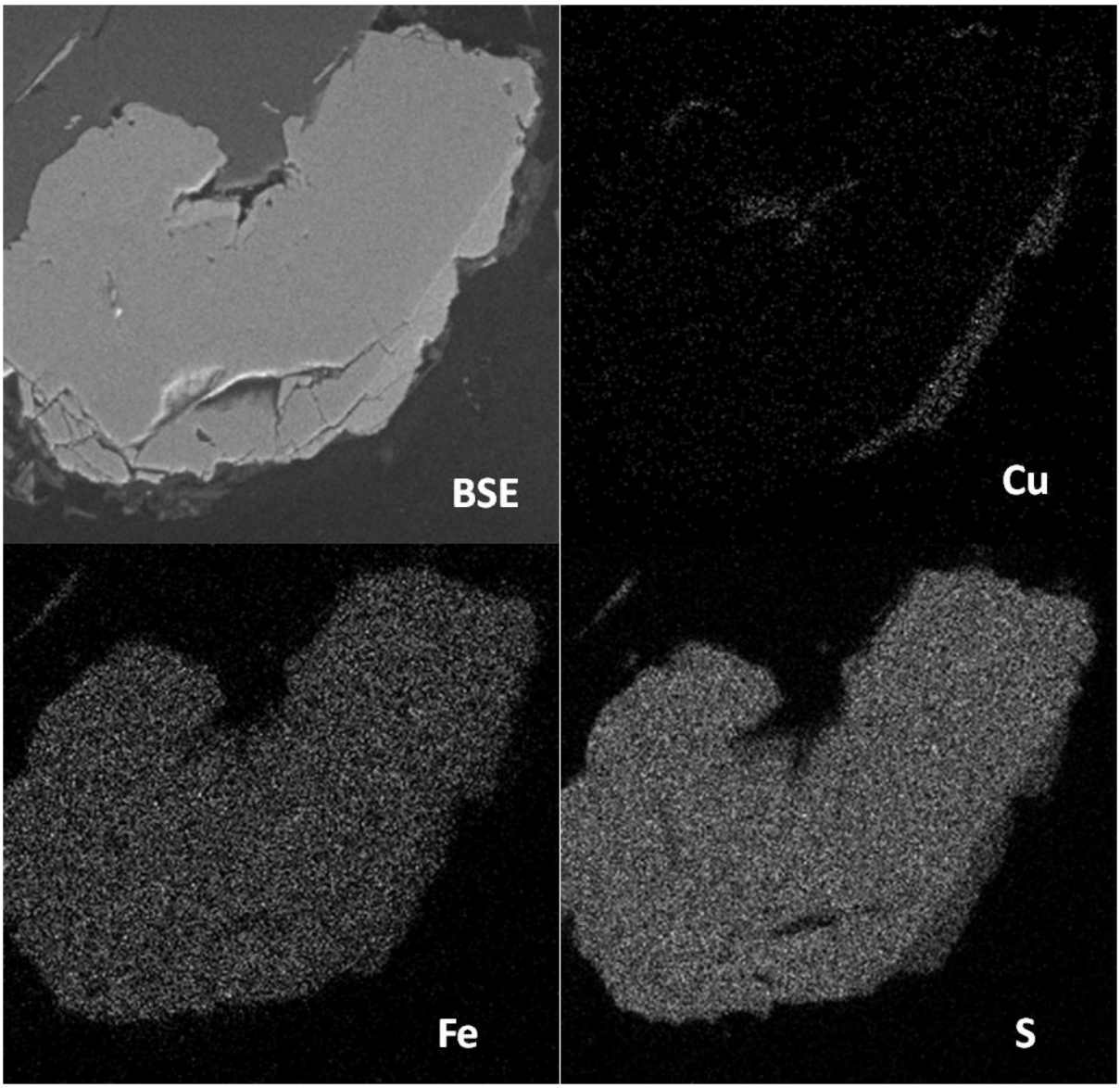

Figure 3-15: Reflected light photomicrograph and SEM-BSE image with corresponding EDX spectra of a grain of mixed sphalerite and pyrite from the 36-38 m depth interval of FD-3. Weathering of sphalerite contributes Zn and Cd to the Type III test pile effluent.

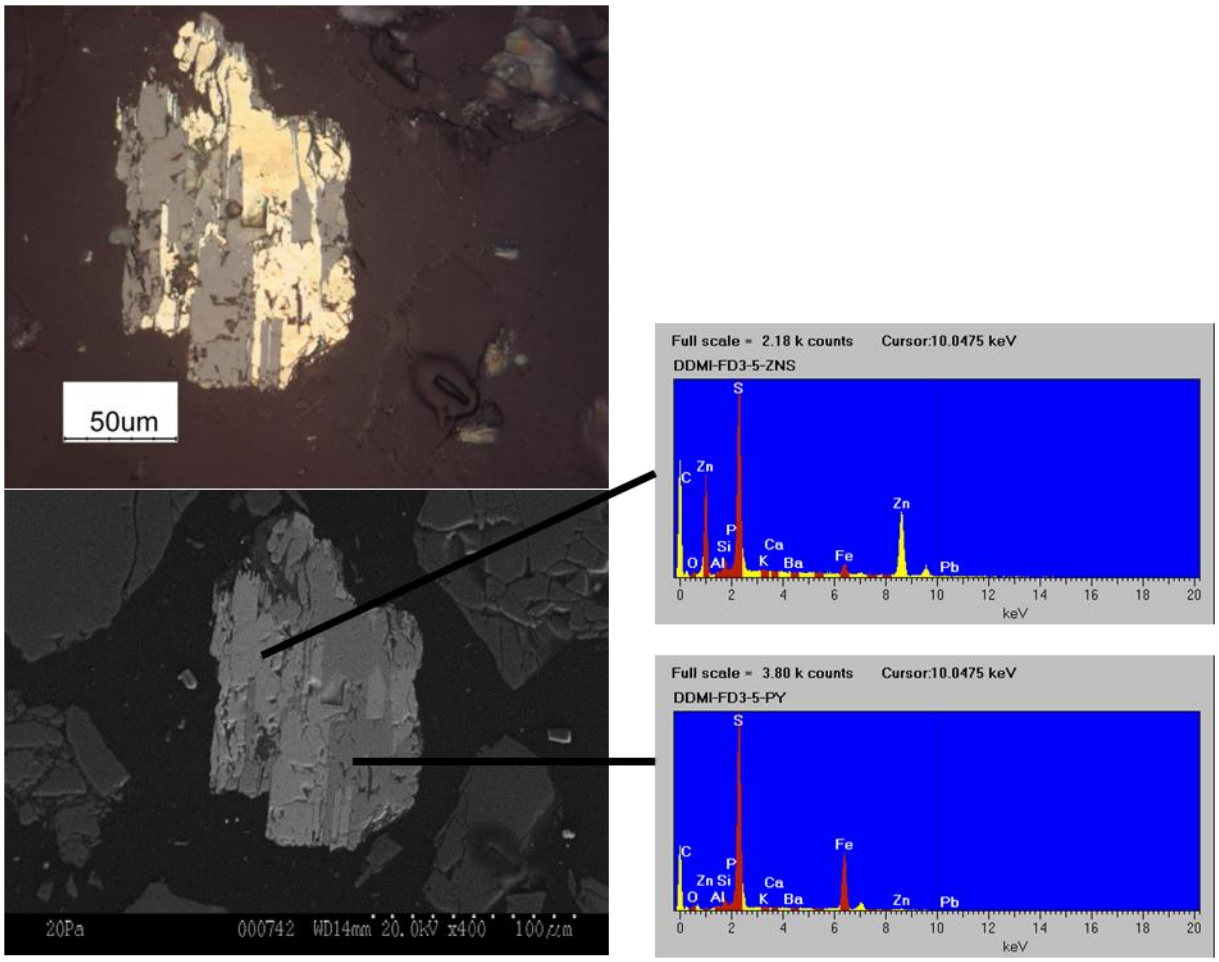

3.6 Tables

Table 3-1: XRF and C/S analysis of the FD-1 and FD-3 drill cuttings samples.

	FD-1 0-4 m	FD-1 8-12 m	FD-1 16-20 m	FD-1 24-28m	FD-3 36-38 m	FD-3 38-40 m
wt%						
Al_2O_3	15.32	15.70	15.99	15.06	15.66	15.01
SiO_2	78.19	77.28	72.44	75.11	75.98	75.46
CaO	0.67	0.80	0.94	1.05	0.94	0.97
TiO_2	0.15	0.18	0.31	0.35	0.26	0.22
MnO	0.02	0.02	0.04	0.04	0.03	0.03
Fe_2O_3	1.85	2.30	3.82	4.25	3.34	2.94
K_2O	4.99	4.75	4.70	4.06	4.40	4.83
Na_2O	4.21	3.35	1.48	1.48	1.90	1.77
MgO	0.33	0.58	1.23	1.31	1.02	0.90
C	0.070	0.063	0.052	0.178	0.070	0.078
S	0.015	0.030	0.062	0.095	0.047	0.049
Sum	105.80	105.06	101.07	103.00	103.65	102.25
ppm						
Sr	99	140	174	189	155	142
Ba	< DL	< DL	< DL	< DL	211	282
Ni	12	21	45	42	35	33
Rb	136	115	125	121	119	119
Pb	39	74	40	62	79	59
Cu	16	30	28	47	33	29
Cr	93	91	107	137	114	92
Co	6	8	14	17	14	11
Zn	53	116	79	113	118	87
As	3	19	5	14	22	13
V	12	23	50	57	40	35
Rh	1251	1228	1143	1120	1170	1185

Table 3-2: Maximum concentrations achieved in the Type III test pile basal drains for elements of interest in geochemical modeling.

Maximum Dissolved Concentrations in the Type III Test Pile North and South Basal Drains				
Element	**2010**		**2011**	
	North	**South**	**North**	**South**
Fe (mg L^{-1})	0.38	0.58	0.74	0.70
Cu (mg L^{-1})	1.8	0.65	3.4	2.4
Ni (mg L^{-1})	5.3	9.9	10	19
Co (mg L^{-1})	1.1	1.8	2.0	3.5
Zn (mg L^{-1})	3.0	1.9	5.2	4.7
Cd (µg L^{-1})	12	19	17	39

Chapter 4

Summary and Conclusions

The Diavik Waste Rock Research Project consists of six active zone lysimeters (AZLs), three, fully instrumented test piles and three sets of drill holes in the operational waste rock pile at the Diavik Diamond Mine site in the Northwest Territories, Canada. The quality of drainage emanating from the three test piles and four of the AZLs has been monitored continually from the first sign of flow and is planned to continue through 2015. General trends in the effluent from the AZLs and uncovered test piles include a decrease in pH and increase in dissolved constituents as temperature increases during the spring and summer. These observations suggest that the rate of sulfide oxidation increases as the temperature increases and that a greater proportion of the test piles contribute to basal drain flow as flowpaths in the central portion of the test piles thaw. During the 2010 and 2011 field seasons, the effluent from the Type I AZLs and Type I test pile remained circum-neutral and had low concentrations of dissolved metals typically associated with sulfide oxidation. The modest decrease in pH in the Type I test pile is attributed to the weathering of the trace amounts of sulfide minerals in the granite component of the Type I waste rock (< 0.04 wt % S). The Type I test pile had a consistently lower pH than the Type I AZLs, which illustrates the influence of heterogeneity inherent in waste rock stockpiles when

compared to smaller, more constrained systems such as the AZLs. Alkalinity remained measureable throughout both field seasons indicating that neutralization potential remained within the Type I waste rock. Contributions from blasting agents had been almost entirely depleted from the Type I AZLs, but persisted in the Type I test pile after reaching maxima in 2010.

The effluent derived from the Type III test pile and AZLs exhibited a lower pH seasonally than the effluent from the Type I installations. The effluent from the Type III test pile basal drains was near neutral pH in the early spring of each year, and then decreased below pH 5 as flow rates slowed in the fall. The Type III AZLs had considerably lower pH, decreasing to levels below pH 3 at times. The lower pH in the Type III AZLs is attributed to their smaller size and higher relative extent of water-rock interaction. Carbonate alkalinity in the Type III AZLs has been depleted, and remained at concentrations less than 20 mg L^{-1} $CaCO_3$ in the Type III test pile throughout 2010 and 2011. The lower pH in the effluent from the Type III installations is attributed to the greater abundance of biotite schist in the Type III waste rock. The weathering of pyrrhotite, present in the biotite schist component of the waste rock at concentrations up to 0.42 wt % S, released higher concentrations of sulfate, and dissolved metals typically associated with sulfide oxidation to the effluent. Equilibrium calculations suggest that acid neutralization proceeds through the dissolution of Al- and Fe-(oxy)hydroxides, which provide controls on dissolved Al and Fe concentrations, and through the dissolution of aluminosilicate minerals, principally biotite. Similar to the Type I AZLs

and test pile, blasting residuals persist in the Type III test pile, but have been almost completely flushed from the Type III AZLs.

The Covered test pile had the lowest average pH of the three test piles and the high rates of sulfate and dissolved metal release typically associated with sulfide oxidation. The Type III waste-rock contained in the core of the Covered test pile contributes to these characteristics of the basal-drain effluent. This test pile does not follow the same seasonal trends as the uncovered test piles due to influences from the cover, which moderates advective air transport in the pile, and the operation of heat trace, which maintained the core of the test pile above 0°C and a portion of the till layer thawed. Sulfide oxidation in the Type III core proceeded throughout the winter, which contributed to stabilizing the pH between approximately pH 4 to 4.7. At this lower pH, equilibrium calculations and dissolved concentrations of Fe and Al suggest that the effluent is neutralized by dissolution of Al- and Fe-(oxy)hydroxides and of aluminosilicate minerals, to a greater extent than the uncovered Type III test pile.

Mineralogical investigations of drill cuttings throughout 40 m of Type III waste rock in the operational stockpile revealed initial oxidation of sulfide minerals had progressed in some areas to partly consume pyrrhotite, but not pyrite. Overall, pyrrhotite grains exhibited early-stage oxidation features such as formation of Fe-(oxy)hydroxides surrounding cores of the primary sulfide mineral. There was no indication of zonation in mineral weathering trends between depths suggesting that permafrost formation has not yet had a significant

effect on oxidation rates during the early evolution of the stockpile. The combination of petrographic, SEM and synchrotron-based mineralogical investigations was useful for analysis of the early stage sulfide-mineral weathering products of Type III waste rock. Due to the low sulfide mineral content of the waste rock at Diavik, characterization of the nature and extent of sulfide weathering products would be difficult without the use of these advanced techniques. Observations of Fe-(oxy)hydroxide formation are consistent with the results of equilibrium calculations conducted using measurements of the composition of the effluent from the Type III test pile, which indicated that the pH is neutralized by dissolution of Al- and Fe-(oxy)hydroxides. These secondary sulfide-mineral oxidation- reaction products also are inferred to contribute to controlling the concentrations of dissolved Al and Fe in the effluent. Continued monitoring of the test piles and use of advanced mineralogical techniques to study the evolution of sulfide mineral weathering *in situ*, will be valuable for current and future mining operations in Northern climates.

References

Chapter 1: Introduction

Al, TA, Blowes, DW, Martin, CJ, Cabri, LJ & Jambor, JL 1997, 'Aqueous geochemistry and analysis of pyrite surfaces in sulfide-rich mine tailings', *Geochimica et Cosmochimica Acta*, vol 61, no. 12, pp. 2353-2366.

Amos, RT, Blowes, DW, Smith, L & Sego, DC 2009, 'Measurement of wind-induced pressure gradients in a waste rock pile', *Vadose Zone Journal*, vol 8, no. 4, pp. 953-962.

Bailey, BL, Smith, LJD, Blowes, DW, Ptacek, CJ, Smith, L & Sego, DC 2012, 'Diavik Waste Rock Project: Persistence of contaminants from blasting agents in waste rock effluent', *Applied Geochemistry*, In press.

Blowes, DW & Jambor, JL 1990, 'The pore-water chemistry and the mineralogy of the vadose zone of sulfide tailings, Waite Amulet, Quebec', *Applied Geochemistry*, vol 5, pp. 327-346.

Chi, X, Amos, RT, Stastna, M, Blowes, DW, Sego, DC & Smith, L 2012a, 'The Diavik Waste Rock Project: Implications of wind-induced gas transport', *Applied Geochemistry*. *Submitted*.

Chi, X, Blowes, DW, Amos, RT, Stastna, M, Sego, DC & Smith, L 2012b, 'The Diavik Waste Rock Project: Particle size analysis using digital image processing', *Applied Geochemistry. Submitted*.

DDMI 2011, 'Interim Closure and Reclamation Plan, Version 3.2, July 2011', Internal Report.

Environment Canada 2012, Monthly data report for Ekati A, Northwest Territories, bulk data 1998-2007, Accessed 2012, <climate.weatheroffice.ec.gc.ca/climateData/canada_e.html>.

Fretz, N, Momeyer, S, Smith, L, Blowes, DW, Sego, D & Amos, R 2011, 'Diavik Waste Rork Project: Unsaturated water flow', *Tailings and Mine Waste 2011 Proceedings*, Vancouver, BC, November 6-9, 2011.

Gunsinger, MR, Ptacek, CJ, Blowes, DW & Jambor, JL 2006, 'Evaluation of long-term sulfide oxidation processes within pyrrhotite-rich tailings, Lynn Lake, Manitoba', *Journal of Contaminant Hydrology*, vol 83, pp. 149-170.

Jambor, JL 1997, 'Mineralogy of the Diavik Lac de Gras kimberlites and host rocks'. Internal Report.

Lefebvre, R, Hockley, D, Smolensky, J & Gelinas, P 2001, 'Multiphase transfer processes in waste rock piles producing acid mine drainage 1: Conceptual model and system characterization', *Journal of Contaminant Hydrology*, vol 52, pp. 137-164.

Moncur, MC, Ptacek, CJ, Blowes, DW & Jambor, JL 2005, 'Release, transport and attenuation of metals from an old tailings impoundment', *Applied Geochemistry*, vol 20, pp. 639-659.

Neuner, M, Smith, L, Blowes, DW, Sego, DC, Smith, LJD & Gupton, M 2012, 'The Diavik Waste Rock Project: Water flow through mine waste rock in a permafrost terrain', *Applied Geochemistry, Submitted.*

Nichol, C, Smith, L & Beckie, R 2005, 'Field-scale experiments of unsaturated flow and solute transport in a heterogeneous porous medium', *Water Resources Research*, vol 41.

Nordstrom, DK & Alpers, CN 1999, 'Negative pH, efflorescent mineralogy, and consequences for environmental restoration at the Iron Mountain Superfund site, California', *Proceedings of the National Academy of Science*, vol 96, pp. 3455-3462.

Pham, NH, Sego, DC, Arenson, LU, Blowes, DW, Amos, RT & Smith, L 2012, 'The Diavik Waste Rock Project: Measurement of the thermal regime of a waste rock pile in a permafrost environment', *Applied Geochemistry, Submitted.*

Ritchie, AIM 1994, 'The Waste-rock Environment', in DW Blowes, JL Jambor (eds.), The *Environmental Geochemistry of Sulfide Mine-wastes*, Short Course Handbook, Mineralogical Association of Canada.

Smith, L & Beckie, R 2003, 'Hydrologic and geochemical transport processes in mine waste rock', in JL Jambor, DW Blowes, AIM Ritchie (eds.), *Environmental Aspects of Mine Wastes*, Short Course Volume 31, Mineralogical Association of Canada.

Smith, LJD, Moncur, MC, Neuner, M, Gupton, M, Blowes, DW, Smith, L & Sego, DC 2012a, 'The Diavik Waste Rock Project: Design, construction, and instrumentation of field-scale experimental waste-rock piles', *Applied Geochemistry, In Press.*

Smith, LJD, Blowes, DW, Jambor, JL, Smith, L, Sego, DC & Neuner, M 2012b, 'The Diavik Waste Rock Project: Particle size distribution and sulfur characteristics of low-sulfide waste rock', *Applied Geochemistry, Submitted.*

Smith, LJD, Bailey, BL,Blowes, DW, Jambor, JL, Smith, L & Sego, DC 2012c, 'The Diavik Waste Rock Project: Initial geochemical response from a low-sulfide waste rock pile', *Applied Geochemistry, Submitted.*

Sracek, O, Gelinas, P, Lefebvre, R & Nicholson, RV 2006, 'Comparison of methods for the estimation of pyrite oxidation rate in a waste rock pile at Mine Doyon site, Quebec, Canada', *Journal of Geochemical Exploration*, vol 91, pp. 99-109.

Stockwell, J, Smith, L, Jambor, JL & Beckie, R 2006, 'The relationship between fluid flow and mineral weathering in heterogeneous unsaturated porous media: A physical and geochemical characterization of a waste-rock pile', *Applied Geochemistry*, vol 21, pp. 1347-1361.

Stromberg, B & Banwart, SA 1999, 'Experimental study of acidity-consuming processes in mining waste rock: some influence of mineralogy and particle size', *Applied Geochemistry*, vol 14, pp. 1-16.

Chapter 2: Chapter 12010-2011 Geochemical trends in experimental waste rock test piles at the Diavik Diamond Mine

Allison, JD, Brown, DS & Novo-Gradac, KJ 1991, 'MINTEQA2/PRODEFA2, A geochemical assessment model for environmental systems: Version 3.0 user's manual', Environmental Research Laboratory Office of Research and Development, US EPA, Athens, Georgia.

Amos, RT, Blowes, DW, Smith, L & Sego, DC 2009, 'Measurement of wind-induced pressure gradients in a waste rock pile', *Vadose Zone Journal*, vol 8, no. 4, pp. 953-962.

Anthonisen, AC, Loehr, RC, Prakasam, TBS & Srinath, EG 1976, 'Inhibition of nitrification by ammonia and nitrous acid', *Journal of the Water Pollution Control Federation,* vol 48, no. 5, pp. 835-852.

Aziz, C, Borch, R, Nicholson, P & Cox, E 2006, 'Alternative Causes of Wide-Spread, Low Concentration Perchlorate Impacts to Groundwater', in B, Gu, Coates, JD (eds.), *Perchlorate: Environmental occurrence, interactions and treatment,* Springer, New York.

Bailey, BL, Smith, LJD, Blowes, DW, Ptacek, CJ, Smith, L & Sego, DC 2012a, 'Diavik Waste Rock Project: Persistence of contaminants from blasting agents in waste rock effluent', *Applied Geochemistry, In press.*

Bailey, BL 2012b, 'Geochemical and microbiological characterization of effluent and pore water from low-sulfide content waste rock', PhD Thesis, University of Waterloo, Canada.

Ball, JW & Nordstrom, KD 1991, 'User's manual for WATEQ4F, with revised thermodynamic database and test cases for calculating speciation of major, trace, and redox elements in natural waters', U.S. Geological Survey.

Blowes, DW & Jambor, JL 1990, 'The pore-water chemistry and the mineralogy of the vadose zone of sulfide tailings, Waite Amulet, Quebec', *Applied Geochemistry*, vol 5, pp. 327-346.

Blowes, DW & Logsdon, MJ 1998, 'Diavik geochemistry baseline report', Report prepared for Diavik Diamond Mines, Inc.

Blowes, DW & Ptacek, CJ 1994, 'Acid-neutralization Mechanisms in Inactive Mine Tailings, Short Course Handbook', in DW Blowes, JL Jambor (eds.), *The Environmental Geochemistry of Sulfide Mine-wastes*, Mineralogical Association of Canada.

Blowes, DW, Ptacek, CJ, Jambor, JL & Weisener, CG 2003, 'The Geochemistry of Acid Mine Drainage', in B Sherwood Lollar, HD Hooland, KK Turekian (eds.), Treatise on Geochemistry, Elsevier.

Chi, X, Amos, RT, Stastna, M, Blowes, DW, Sego, DC & Smith, L 2012a, 'The Diavik Waste Rock Project: Implications of wind-induced gas transport', *Applied Geochemistry*. *Submitted.*

Chi, X, Blowes, DW, Amos, RT, Stastna, M, Sego, DC & Smith, L 2012b, 'The Diavik Waste Rock Project: Particle size analysis using digital image processing', *Applied Geochemistry. Submitted.*

DDMI 2011, 'Interim Closure and Reclamation Plan, Version 3.2, July 2011', Internal Report.

Dubrovsky, NM, Cherry, JA, Reardon, EJ & Vivyurka, AJ 1985, 'Geochemical evolution of inactive pyritic tailings in the Elliot Lake uranium district', *Canadian Geotechnical Journal,* vol 22, no. 1, pp. 110-128.

Environment Canada 2012, Monthly data report for Ekati A, Northwest Territories, bulk data 1998-2007, Accessed 2012, <climate.weatheroffice.ec.gc.ca/climateData/canada_e.html>.

Espana, JS, Pamo, EL, Santofimia, E, Aduvire, O, Reyes, J & Barettino, D 2005, 'Acid mine drainage in the Iberian Pyrite Belt (Odiel river watershed, Huelva, SW Spain): Geochemistry, mineralogy and environmental implications', *Applied Geochemistry*, vol 20, pp. 1320-1356.

Fretz, N, Momeyer, S, Smith, L, Blowes, DW, Sego, D & Amos, R 2011, 'Diavik Waste Rork Project: Unsaturated water flow', *Tailings and Mine Waste 2011 Proceedings,* Vancouver, BC, November 6-9, 2011.

Fretz, N, Smith, L, Blowes, DW & Sego, DC 2012, 'Diavik Waste Rock Project: Preliminary estimates of multi-year net infiltration', *Proceedings of the 9th International Conference on Acid Rock Drainage,* Ottawa, ON, May 20-26, 2012.

Gunsinger, MR, Ptacek, CJ, Blowes, DW & Jambor, JL 2006, 'Evaluation of long-term sulfide oxidation processes within pyrrhotite-rich tailings, Lynn Lake, Manitoba', *Journal of Contaminant Hydrology*, vol 83, pp. 149-170.

Hudson-Edwards, KA, Schell, C & Macklin, MG 1999, 'Mineralogy and geochemistry of alluvium contaminated by metal mining in the Rio Tinto area, southwest Spain', *Applied Geochemistry*, vol 14, pp. 1015-1030.

Jambor, JL 1997, 'Mineralogy of the Diavik Lac de Gras kimberlites and host rocks'. Internal Report.

Janzen, MP, Nicholson, RV & Scharer, JM 2000, 'Pyrrhotite reaction kinetics: Reaction rates for oxidation by oxygen, ferric iron and for nonoxidative dissolution', *Geochimica et Cosmochimica Acta*, vol 64, no. 9, pp. 1511-1522.

Johnson, RH, Blowes, DW, Robertson, WD & Jambor, JL 2000, 'The hydrogeochemistry of the Nickel Rim mine tailings impoundment, Sudbury, Ontario', *Journal of Contaminant Hydrology*, vol 41, pp. 49-80.

Jurjovec, J, Ptacek, CJ & Blowes, DW 2002, 'Acid neutralization mechanisms and metal release in mine tailings: A laboratory column experiment', *Geochimica et Cosmochimica Acta*, vol 66, no. 9, pp. 1511-1523.

Light, TS 1972, 'Standard Solution for Redox Potential Measurements', *Analytical Chemistry*, vol 44, no. 6, pp. 1038-1039.

Moncur, MC, Ptacek, CJ, Blowes, DW & Jambor, JL 2005, 'Release, transport and attenuation of metals from an old tailings impoundment', *Applied Geochemistry*, vol 20, pp. 639-659.

Moore, ML 2009, 'Laboratory column experiments of low sulfide waste rock', M.Sc. Thesis, University of Waterloo, in preparation.

Neuner, M, Smith, L, Blowes, DW, Sego, DC, Smith, LJD & Gupton, M 2012, 'The Diavik Waste Rock Project: Water flow through mine waste rock in a permafrost terrain', *Applied Geochemistry, Submitted.*

Nordstrom, DK 1977, 'Thermochemical redox equilibria of ZoBell's solution', *Geochimica et Cosmochimica Acta*, vol 41, pp. 1835-1841.

Nordstrom, DK & Alpers, CN 1999, 'Negative pH, efflorescent mineralogy, and consequences for environmental restoration at the Iron Mountain Superfund site, California', *Proceedings of the National Academy of Science*, USA.

Pham, N, Sego, DC, Arenson, LU, Blowes, DW, Smith, L, Smith, LJD, Gupton, M, Neuner, M & Amos, RT 2009, 'Diavik Waste Rock Project: Heat transfer in experimental waste rock piles under a permafrost environment', Paper presented at Securing the Future and 8th ICARD, June 23-26, 2009.

Pham, NH, Sego, DC, Arenson, LU, Blowes, DW, Amos, RT & Smith, L 2012, 'The Diavik Waste Rock Project: Measurement of the thermal regime of a waste rock pile in a permafrost environment', *Applied Geochemistry, Submitted.*

Pommen, LW 1983, 'The effect on water quality of explosives use in surface mining Volume 1: Nitrogen sources, water quality, and prediction and management of impacts', British Columbia Ministry of the Environment, Victoria, British Columbia.

Rimstidt, JD & Vaughan, DJ 2003, 'Pyrite oxidation: A state-of-the-art assessment of the reaction mechanism', *Geochimica et Cosmochimica Acta,* vol 67, no. 5, pp. 873-880.

Sawyer, CN & McCarty, PL 1967, Chemistry for Sanitary Engineers, Second Edition, McGraw-Hill Inc., New York, New York, USA.

Smith, LJD, Moncur, MC, Neuner, M, Gupton, M, Blowes, DW, Smith, L & Sego, DC 2012a, 'The Diavik Waste Rock Project: Design, construction, and instrumentation of field-scale experimental waste-rock piles', *Applied Geochemistry, Submitted.*

Smith, LJD, Blowes, DW, Jambor, JL, Smith, L, Sego, DC & Neuner, M 2012b, 'The Diavik Waste Rock Project: Particle size distribution and sulfur characteristics of low-sulfide waste rock', *Applied Geochemistry, Submitted.*

Smith, LJD, Bailey, BL, Blowes, DW, Jambor, JL, Smith, L & Sego, DC 2012c, 'The Diavik Waste Rock Project: Initial geochemical response from a low-sulfide waste rock pile', *Applied Geochemistry, Submitted.*

Williamson, MA & Rimstidt, JD 1994, 'The kinetics and electrochemical rate-determining step of aqueous pyrite oxidation', *Geochimica et Cosmochimica Acta*, vol 58, no. 24, pp. 5443-5454.

Chapter 3: Mineralogical and geochemical studies of a waste rock stockpile and experimental test pile in the Arctic

Amos, RT, Blowes, DW, Smith, L & Sego, DC 2009, 'Measurement of wind-induced pressure gradients in a waste rock pile', *Vadose Zone Journal*, vol 8, no. 4, pp. 953-962.

ASTM 2003, 'Standard Practice for Reducing Samples of Aggregate to Testing Size (Method A 702-98)', American Society for Testing and Materials.

ASTM 2010, 'Standard test methods for laboratory determination of water (moisture) content of soil and rock by mass (Method D2216-10)', American Society for Testing and Materials.

Bailey, BL, Smith, LJD, Blowes, DW, Ptacek, CJ, Smith, L & Sego, DC 2012a, 'Diavik Waste Rock Project: Persistence of contaminants from blasting agents in waste rock effluent', *Applied Geochemistry, In press.*

Bailey, BL 2012b, 'Geochemical and microbiological characterization of effluent and pore water from low-sulfide content waste rock', PhD Thesis, University of Waterloo, Canada.

Ball, JW & Nordstrom, KD 1991, 'User's manual for WATEQ4F, with revised thermodynamic database and test cases for calculating speciation of major, trace, and redox elements in natural waters', U.S. Geological Survey.

Blowes, DW & Jambor, JL 1990, 'The pore-water chemistry and the mineralogy of the vadose zone of sulfide tailings, Waite Amulet, Quebec', *Applied Geochemistry*, vol 5, pp. 327-346.

Blowes, DW & Logsdon, MJ 1998, 'Diavik geochemistry baseline report', Report prepared for Diavik Diamond Mines, Inc.

Courtin-Nomade, A, Bril, H, Beny, J-M, Kunz, M & Tamura, N 2010, 'Sulfide oxidation observed using micro-Raman spectroscopy and micro-X-ray diffraction: The importance of water/rock ratios and pH conditions', *American Mineralogist,* vol 95, pp. 582-590.

Environment Canada 2012, Monthly data report for Ekati A, Northwest Territories, bulk data 1998-2007, Accessed 2012, <climate.weatheroffice.ec.gc.ca/climateData/canada_e.html>.

Flemming, RL, Salzsauler, KA, Sherriff, BL & Sidenko, NV 2005, 'Identification of scorodite in fine-grained, high-sulfide, arsenopyrite mine-waste using micro X-ray diffraction (uXRD)', *The Canadian Mineralogist,* vol 43, pp. 1243-1254.

Gunsinger, MR, Ptacek, CJ, Blowes, DW & Jambor, JL 2006, 'Evaluation of long-term sulfide oxidation processes within pyrrhotite-rich tailings, Lynn Lake, Manitoba', *Journal of Contaminant Hydrology,* vol 83, pp. 149-170.

Hammersley, AP 1998, 'ESRF Internal Report, ESRF98HA01T, FIT2D V9.129 Reference Manual V3.1'.

Hammersly, AP, Svensson, SO, Hanfland, M, Fitch, AN & Hausermann, D 1996, 'Two-Dimensional detector software: From real detector to idealized image or two-theta scan', High Pressure Research, vol 14, pp. 235-248.

He, BB 2003, 'Introduction to two-dimensional X-ray diffraction', *Powder Diffraction*, vol 18, pp. 71-85.

Herrera, LK, Cotte, M, Jimenez de Haro, MC, Duran, A, Justo, A & Perez-Rodriguez, JL 2008, 'Characterization of iron oxide-based pigments by synchrotron-based micro X-ray diffraction', *Applied Clay Science*, vol 42, pp. 57-62.

Jambor, JL 1994, 'Mineralogy of Sulfide-rich Tailings and Their Oxidation Products', in DW Blowes, JL Jambor (eds.), *The Environmental Geochemistry of Sulfide Mine-Wastes,* Short Course Handbook, Mineralogical Association of Canada.

Jambor, JL 1997, 'Mineralogy of the Diavik Lac de Gras kimberlites and host rocks'.

Jambor, JL 2003, 'Mine-waste mineralogy and mineralogical perspectives of acid-base accounting', in JL Jambor, DW Blowes, AIM Ritchie (eds.), *Environmental Aspects of Mine Wastes.*

Klug, HP & Alexander, LE 1954, X-Ray Diffraction Procedures for Polycrystalline and Amorphous Materials, John Wiley & Sons, Inc.

Lefebvre, R, Hockley, D, Smolensky, J & Gelinas, P 2001, 'Multiphase transfer processes in waste rock piles producing acid mine drainage 1: Conceptual model and system characterization', *Journal of Contaminant Hydrology,* vol 52, pp. 137-164.

Light, TS 1972, 'Standard Solution for Redox Potential Measurements', *Analytical Chemistry,* vol 44, no. 6, pp. 1038-1039.

Majzlan, J, Lalinska, B, Chovan, M, Blass, U, Brecht, B, Gottlicher, J, Steininger, R, Hug, K, Ziegler, S & Gesher, J 2011, 'A mineralogical, geochemical, and microbiological assessment of the antimony- and arsenic-rich neutral mine drainage tailings near Pexinok, Slovakia', *American Mineralogist,* vol 96, pp. 1-13.

Moncur, MC, Ptacek, CJ, Blowes, DW & Jambor, JL 2005, 'Release, transport and attenuation of metals from an old tailings impoundment', *Applied Geochemistry,* vol 20, pp. 639-659.

Neuner, M, Smith, L, Blowes, DW, Sego, DC, Smith, LJD & Gupton, M 2012, 'The Diavik Waste Rock Project: Water flow through mine waste rock in a permafrost terrain', *Applied Geochemistry, Submitted.*

Nordstrom, DK 1977, 'Thermochemical redox equilibria of ZoBell's solution', *Geochimica et Cosmochimica Acta,* vol 41, pp. 1835-1841.

Pienitz, R, Smol, J & Lean, DRS 1997, 'Physical and chemical limnology of 24 lakes located between Yellowknife and Contwoyto Lake, Northwest Territories (Canada)', *Canadian Journal of Fisheries and Aquatic Sciences,* vol 54, no. 2, pp. 347-358.

Pratt, AR, Nesbitt, HW & Muir, IJ 1994, 'Generation of acids from mine waste: Oxidative leaching of pyrrhotite in dilute H2SO4 solutions at pH 3.0', *Geochimica et Cosmochimica Acta,* vol 58, no. 23, pp. 5147-5159.

Ritchie, AIM 1994, 'The Waste-rock Environment', in DW Blowes, JL Jambor (eds.), *The Environmental Geochemistry of Sulfide Mine-wastes,* Short Course Handbook, Mineralogical Association of Canada.

Smith, LJD 2009, 'Building and characterizing low sulfide instrumented waste rock piles: Pile design and construction, particle size and sulfur characterization, and initial geochemical response', MSc. Thesis, University of Waterloo, Waterloo, Canada.

Smith, LJD, Moncur, MC, Neuner, M, Gupton, M, Blowes, DW, Smith, L & Sego, DC 2012a, 'The Diavik Waste Rock Project: Design, construction, and instrumentation of field-scale experimental waste-rock piles', *Applied Geochemistry, In Press.*

Smith, LJD, Blowes, DW, Jambor, JL, Smith, L, Sego, DC & Neuner, M 2012b, 'The Diavik Waste Rock Project: Particle size distribution and sulfur characteristics of low-sulfide waste rock', *Applied Geochemistry, Submitted.*

Smith, LJD, Bailey, BL, Blowes, DW, Jambor, JL, Smith, L & Sego, DC 2012c, 'The Diavik Waste Rock Project: Initial geochemical response from a low-sulfide waste rock pile', *Applied Geochemistry, Submitted.*

Sracek, O, Gelinas, P, Lefebvre, R & Nicholson, RV 2006, 'Comparison of methods for the estimation of pyrite oxidation rate in a waste rock pile at Mine Doyon site, Quebec, Canada', *Journal of Geochemical Exploration,* vol 91, pp. 99-109.

Stromberg, B & Banwart, SA 1999, 'Experimental study of acidity-consuming processes in mining waste rock: some influence of mineralogy and particle size', *Applied Geochemistry*, vol 14, pp. 1-16.

Appendix A

Test pile basal drain geochemistry

Geochemical data for the Type I, Covered pile, and Type III North and South basal drains, and the AZLs is included on CD. This data includes analyses in the field, major and minor cations, and anions as described in Chapter 2. The files on disk are labeled as follows:

Appendix A Type I basal drain geochemistry.xlsx

Appendix A Type III north basal drain geochemistry.xlsx

Appendix A Type III south basal drain geochemistry.xlsx

Appendix A Covered drain geochemistry.xlsx

Appendix A Type I East AZL geochemistry.xlsx

Appendix A Type I West AZL geochemistry.xlsx

Appendix A Type III East AZL geochemistry.xlsx

Appendix A Type III West AZL geochemistry.xlsx

If you do not have access to these files, please contact Stacey Hannam by email at seshanna@uwaterloo.ca

Appendix B

Borehole specifications and instrumentation

Table B-1: Instrumentation installed in FD-1.

Hole No.	FD-1		
Description	Upper Type III		
Target Hole Depth (m)	40		
Actual hole depth (m)	32.16		
Comments			
	Target Depth (m)	As-built depth from top (m)	Instrument ID
Thermistors	32	31.86	FD1-T32
	27	26.86	FD1-T27
	22	21.86	FD1-T22
	17	16.86	FD1-T17
	12	11.86	FD1-T12
	7	6.86	FD1-T7
	2	1.86	FD1-T2
Gas lines	32	31.86	FD1-G32
	22	21.86	FD1-G22
	12	11.86	FD1-G12
	22	1.86	FD1-G22
Permeability Balls	22	21.86	FD1-P22
	7	7.16	FD1-P7
Soil-water solution samplers (SWSS)	32	31.86	FD1-S32
	7	6.86	FD1-S7
ECH20 Probes	12	12.16	FD1-E12
	22	22.16	FD1-E22
Centre stock Access for Thermal Conductivity			

Table B-2: Instrumentation installed in FD-2.

Hole No.	FD-2		
Description	Upper Type III		
Target Hole Depth (m)	40		
Actual hole depth (m)	30.66		
Comments			
	Target Depth (m)	As-built depth from top (m)	Instrument ID
Thermistors	31	30.66	FD2-T31
	26	25.66	FD2-T26
	21	20.66	FD2-T21
	16	15.66	FD2-T16
	11	10.66	FD2-T11
	6	5.66	FD2-T6
	1	0.66	FD2-T1
Gas lines	26	25.66	FD2-G26
	16	15.66	FD2-G16
	6	5.66	FD2-G6
		n/a	
Permeability Balls	21	20.66	FD2-P21
	6	5.66	FD2-P6
Soil-water solution samplers (SWSS)	31	30.66	FD2-S31
	21	20.66	FD2-S21
ECH20 Probes	30	29.66	FD2-E30
	21	20.66	FD2-E21
Microbiology screens	21	20.8	FD2-M21
	10	10.1	FD2-M10

Table B-3: Instrumentation installed in FD-3

Hole No.	FD-3		
Description	Upper Type III		
Target Hole Depth (m)	40		
Actual hole depth (m)	40.2		
Comments			
	Target Depth (m)	As-built depth from top (m)	Instrument ID
Thermistors	40	39.5	FD3-T40
	35	34.5	FD3-T35
	30	29.5	FD3-T30
	25	24.5	FD3-T25
	20	19.5	FD3-T20
	15	14.5	FD3-T15
	10	9.5	FD3-T10
Gas lines	40	39.5	FD3-G40
	30	29.5	FD3-G30
	20	19.5	FD3-G20
	10	9.5	FD3-G10
Permeability Balls	40	39.5	FD3-P40
	25	24.5	FD3-P25
Soil-water solution samplers (SWSS)	37	37.3	FD3-S37
	30	29.5	FD3-S30
ECH20 Probes	35	34.5	FD3-E35
	25	14.5	FD3-E15
Microbiology screens	36	36.4	FD2-M36
	22	22.7	FD2-M22
	12	12.0	FD2-M12

Table B-4: Instrumentation installed in FD-4. Continued on next page.

Hole No.	FD-4		
Description	Batter		
Target Hole Depth (m)	40.00		
Actual hole depth (m)	41.00		
Comments			
	Target Depth (m) lead	As-built depth from top (m) lead	Instrument ID
Thermistors	2.25	2.25	
	7.25	7.25	
	12.25	12.25	
	17.25	17.25	
	22.25	22.25	
	27.25	27.25	
	32.25	32.25	
	37.25	37.25	
	39.75	39.75	
	34.75	34.75	
	29.75	29.75	
	24.75	24.75	
	19.75	19.75	
	14.75	14.75	
	9.75	9.75	
	4.75	4.75	
Gas lines	10	11	FD4-G11
	20	21	FD4-G21
	30	31	FD4-G31
	40	41	FD4-G41
Permeability Balls	20	21	FD4-P21
	40	41	FD4-P41

Table B-4: Instrumentation installed in FD-4. Continued from previous page.

Hole No.	FD-4		
Description	Batter		
Target Hole Depth (m)	40.00		
Actual hole depth (m)	41.00		
Comments			
	Target Depth (m) lead	As-built depth from top (m) lead	Instrument ID
Soil-water solution samplers (SWSS)	2.5	2.6	FD4-S3
	7.5	7.5	FD4-S7
	10	10.2	FD4-S10
	12	12	FD4-S12
	20	20.9	FD4-S21
	40	41.2	FD4-S41
ECH20 Probes	2.5	2.9	FD4-E3
	5.0	5.3	FD4-E5
	10	10.5	FD4-E10
	15	16	FD4-E16
	20	21.2	FD4-E21
Microbiology screens	40	39.5 - 41.0	
	30	28.8 - 30.3	
	20	18.1 - 19.7	
	10	7.5 - 9.0	

Table B-5: Instrumentation installed in FD-5. Continued on next page.

Hole No.	FD-5		
Description	Sump		
Target Hole Depth (m)	80		
Actual hole depth (m)	77.4		
Comments	Hit bedrock (quarry bottom) 77.4 m		
	Target Depth (m)	As-built Depth from top (m)	Instrument ID
Thermistors	5	2.4	
	10	7.4	
	15	12.4	
	20	17.4	
	25	22.4	
	30	27.4	
	35	32.4	
	40	37.4	
	45	42.4	
	50	47.4	
	55	52.4	
	60	57.4	
	65	62.4	
	70	67.4	
	75	72.4	
	80	77.4	
Gas lines	10	7.4	FD5-G7.
	20	17.4	FD5-G17
	30	27.4	FD5-G27
	40	37.4	FD5-G37
	50	47.4	FD5-G47
	60	57.4	FD5-G57
	70	67.4	FD5-G67
	80	77.4	FD5-G77

Table B-5: Instrumentation installed in FD-5. Continued from previous page.

Hole No.	FD-5		
Description	Sump		
Target Hole Depth (m)	80		
Actual hole depth (m)	77.4		
Comments	Hit bedrock (quarry bottom) 77.4 m		
	Target Depth (m)	As-built Depth from top (m)	Instrument ID
Permeability Balls	40	37.5	FD5-P37
	80	77.1	FD5-P77
Soil-water solution samplers (SWSS)	2.5	2.5	FD5-S2
	5	5.0	FD5-S5
	10	10.0	FD5-S10
	12	12.0	FD5-S12
	40	37.5	FD5-S37
	80	77.4	FD5-S77
ECH20 Probes	2.5	2.5	FD5-E2
	5	5.0	FD5-E5
	10	10.0	FD5-E10
	20	17.4	FD5-E17
	30	27.4	FD5-E27
Microbiology screens	20	16.4 - 18	
	40	36.2 - 37.8	
	60	56.1 - 57.6	
	80	75.9 - 77.4	

Appendix C

XRF and C/S measurements from boreholes

Table C-1: XRF and C/S analysis of waste rock samples from the 0-4 m depth interval of FD-1.

	1	2	3	4a	4b	Average
wt%						
Al_2O_3	15.13	16.03	15.82	14.59	15.02	15.32
SiO_2	78.32	78.33	78.40	77.57	78.32	78.19
CaO	0.66	0.75	0.74	0.59	0.59	0.67
TiO2	0.18	0.15	0.14	0.14	0.13	0.15
MnO	0.02	0.03	0.02	0.02	0.02	0.02
Fe_2O_3	2.12	1.79	1.80	1.78	1.77	1.85
K_2O	4.96	4.73	4.97	5.15	5.14	4.99
Na_2O	4.24	5.65	4.31	2.82	4.01	4.21
MgO	0.41	0.28	0.33	0.33	0.31	0.33
C	0.076	0.063	0.072	0.068		0.070
S	0.016	0.004	0.013	0.028		0.015
Sum	106.13	107.81	106.61	103.08	105.30	105.80
ppm						
Sr	96	109	92	100	99	99
Ba	< DL	< DL	< DL	< DL	< DL	< DL
Ni	14	12	12	12	10	12
Rb	139	132	135	136	138	136
Pb	37	35	35	42	45	39
Cu	14	16	15	18	18	16
Cr	84	98	99	92	90	93
Co	7	6	7	4	6	6
Zn	55	42	44	64	61	53
As	2	1	1	5	6	3
V	18	9	12	11	10	12
Rh	1230	1256	1249	1265	1254	1251

Table C-2: XRF and C/S analysis of waste rock samples from the 8-12 m depth interval of FD-1.

	1	2	3	4a	4b	Average
wt%						
Al_2O_3	16.25	15.92	15.97	15.20	15.18	15.70
SiO_2	78.62	77.84	77.87	76.14	75.93	77.28
CaO	0.88	0.85	0.76	0.77	0.76	0.80
TiO_2	0.16	0.19	0.17	0.19	0.19	0.18
MnO	0.02	0.02	0.02	0.02	0.02	0.02
Fe_2O_3	2.23	2.27	2.12	2.45	2.44	2.30
K_2O	4.30	4.79	4.85	4.91	4.91	4.75
Na_2O	5.23	4.85	4.45	1.31	0.90	3.35
MgO	0.54	0.63	0.51	0.60	0.61	0.58
C	0.050	0.048	0.055	0.098		0.063
S	0.019	0.037	0.018	0.048		0.030
Sum	108.30	107.45	106.79	101.73	100.95	105.06
ppm						
Sr	148	142	137	138	137	140
Ba	627	< DL	< DL	< DL	< DL	< DL
Ni	19	24	18	23	22	21
Rb	109	116	117	118	117	115
Pb	51	41	51	115	112	74
Cu	21	19	19	46	47	30
Cr	94	85	95	90	91	91
Co	9	8	7	8	8	8
Zn	87	66	66	179	180	116
As	9	4	9	35	35	19
V	26	37	20	13	19	23
Rh	1258	1229	1240	1209	1204	1228

Table C-3: XRF and C/S analysis of waste rock samples from the 16-20 m depth interval of FD-1.

	1	2	3	4a	4b	Average
wt%						
Al_2O_3	16.29	14.67	15.91	16.41	16.66	15.99
SiO_2	69.80	75.36	74.07	66.66	76.29	72.44
CaO	0.87	0.91	1.18	0.87	0.87	0.94
TiO_2	0.42	0.30	0.32	0.27	0.27	0.31
MnO	0.05	0.04	0.04	0.03	0.04	0.04
Fe_2O_3	4.61	3.77	3.96	3.37	3.38	3.82
K_2O	5.14	4.05	4.71	4.81	4.81	4.70
Na_2O	0.87	1.36	1.17	1.99	2.01	1.48
MgO	1.34	1.70	1.27	0.72	1.13	1.23
C	0.047	0.062	0.048	0.050		0.052
S	0.041	0.062	0.076	0.069		0.062
Sum	99.47	102.29	102.74	95.25	105.46	101.07
ppm						
Sr	167	166	178	180	180	174
Ba	< DL	297	185	206	179	< DL
Ni	43	60	40	39	41	45
Rb	147	108	130	120	122	125
Pb	43	34	42	38	42	40
Cu	26	27	30	28	29	28
Cr	96	134	113	96	98	107
Co	18	15	14	12	13	14
Zn	97	77	78	71	73	79
As	5	3	6	6	6	5
V	50	51	51	49	47	50
Rh	1096	1150	1122	1168	1179	1143

Table C-4: XRF and C/S analysis of waste rock samples from the 24-28 m depth interval of FD-1.

	1	2	3	4a	4b	Average
wt%						
Al_2O_3	15.35	14.73	14.37	15.51	15.34	15.06
SiO_2	76.44	74.24	73.69	75.93	75.26	75.11
CaO	1.03	1.16	1.04	1.01	1.01	1.05
TiO_2	0.37	0.31	0.34	0.36	0.36	0.35
MnO	0.04	0.04	0.04	0.04	0.04	0.04
Fe_2O_3	4.44	3.86	4.28	4.35	4.35	4.25
K_2O	4.00	4.25	3.97	4.04	4.04	4.06
Na_2O	1.87	1.47	0.76	1.89	1.42	1.48
MgO	1.42	1.10	1.24	1.39	1.40	1.31
C	0.205	0.151	0.164	0.193		0.178
S	0.093	0.089	0.101	0.098		0.095
Sum	105.26	101.40	100.01	104.82	103.22	103.00
ppm						
Sr	189	184	192	190	192	189
Ba	< DL	< DL	< DL	< DL	< DL	< DL
Ni	43	37	45	44	42	42
Rb	124	121	123	118	118	121
Pb	66	45	48	77	77	62
Cu	52	40	50	45	49	47
Cr	140	127	137	143	139	137
Co	20	16	18	17	16	17
Zn	134	96	106	113	116	113
As	15	7	8	21	20	14
V	59	52	64	60	47	57
Rh	1105	1137	1109	1120	1128	1120

Table C-5: XRF and C/S analysis of waste rock samples from the 36-38 m depth interval of FD-3.

	1a	1b	2a	2b	3a	3b	4a	4b	Average
wt%									
Al_2O_3	16.18	16.51	15.28	15.51	15.40	15.29	15.47	15.60	15.66
SiO_2	74.88	76.34	75.26	75.79	77.59	77.30	75.32	75.41	75.98
CaO	1.00	0.99	0.91	0.92	0.88	0.88	0.96	0.95	0.94
TiO_2	0.27	0.27	0.26	0.26	0.24	0.24	0.26	0.26	0.26
MnO	0.03	0.03	0.04	0.04	0.03	0.03	0.03	0.03	0.03
Fe_2O_3	3.28	3.26	3.45	3.44	3.29	3.32	3.36	3.36	3.34
K_2O	4.42	4.43	4.39	4.39	4.45	4.46	4.33	4.32	4.40
Na_2O	2.57	3.15	1.51	1.57	1.48	1.05	1.86	2.02	1.90
MgO	0.98	1.09	1.01	1.04	1.02	0.95	1.01	1.07	1.02
C	0.068		0.074		0.082		0.055		0.070
S	0.028		0.030		0.059		0.071		0.047
Sum	103.71	106.07	102.20	102.95	104.53	103.54	102.71	103.03	103.65
ppm									
Sr	179	179	139	144	141	138	160	158	155
Ba	330	492	176	136	58	203	50	243	211
Ni	36	35	34	36	36	36	33	31	35
Rb	119	120	123	119	118	119	117	116	119
Pb	76	77	70	70	108	109	63	60	79
Cu	28	29	32	28	40	40	33	31	33
Cr	116	115	111	110	118	120	109	109	114
Co	13	13	14	14	14	15	14	13	14
Zn	110	110	107	106	157	156	100	96	118
As	22	22	17	17	34	34	14	14	22
V	39	41	41	48	33	42	36	42	40
Rh	1189	1188	1174	1158	1163	1175	1161	1153	1170

Table C-6: XRF and C/S analysis of waste rock samples from the 38-40 m depth interval of FD-3.

	1a	1b	2a	2b	3a	3b	4a	4b	Average
wt%									
Al_2O_3	15.43	15.58	14.76	14.82	14.68	15.18	14.93	14.70	15.01
SiO_2	77.18	77.55	67.57	75.99	75.95	77.15	76.47	75.81	75.46
CaO	0.89	0.89	0.92	0.91	0.86	0.86	1.20	1.20	0.97
TiO_2	0.23	0.23	0.21	0.21	0.24	0.25	0.20	0.20	0.22
MnO	0.03	0.03	0.03	0.03	0.03	0.03	0.03	0.03	0.03
Fe_2O_3	3.04	3.02	2.85	2.85	3.13	3.14	2.75	2.75	2.94
K_2O	4.82	4.82	4.73	4.72	4.79	4.80	4.99	4.99	4.83
Na_2O	2.10	2.31	2.08	1.94	1.13	1.42	1.91	1.25	1.77
MgO	0.99	1.09	0.50	0.90	1.01	0.99	0.87	0.87	0.90
C	0.056		0.057		0.063		0.138		0.078
S	0.053		0.040		0.046		0.055		0.049
Sum	104.80	105.53	93.75	102.36	101.93	103.82	103.53	101.78	102.25
ppm									
Sr	142	142	145	146	140	140	141	139	142
Ba	206	108	409	302	18	< DL	684	551	282
Ni	31	34	30	29	38	35	32	32	33
Rb	122	119	112	116	119	121	120	119	119
Pb	51	51	61	61	69	67	53	55	59
Cu	31	28	25	28	33	32	28	27	29
Cr	92	89	95	92	85	90	95	94	92
Co	11	12	11	12	11	13	10	11	11
Zn	91	93	76	80	98	96	80	79	87
As	11	10	14	15	18	16	10	12	13
V	36	39	32	45	44	35	25	23	35
Rh	1184	1193	1187	1183	1184	1173	1192	1186	1185

Appendix D

Supplementary mineralogical analysis

This section is included in CD format. It contains high quality photomicrographs from optical mineralogical analysis of all the thin sections made from the drill cuttings samples. The CD also contains all of the SEM images collected during analysis including BSE images, EDX element maps, and EDX spectra pertaining to specific areas of selected BSE images. Finally XRF elemental maps and XRD data collected from the APS at Argonne National Laboratory conclude the supplementary mineralogical information. If you do not have access to these files, please contact Stacey Hannam by email at seshanna@uwaterloo.ca